

UNIVERSITY OF OKLAHOMA

GRADUATE COLLEGE

HYDROGEN BONDING INTERACTIONS AND CATION COORDINATION  
EFFECTS IN NITROGEN-BASED POLYMER ELECTROLYTES  
AND MODEL SYSTEMS

A DISSERTATION

SUBMITTED TO THE GRADUATE FACULTY

in partial fulfillment of the requirements for the

degree of

Doctor of Philosophy

By

Nathalie M. Rocher

Norman, Oklahoma

2006

UMI Number: 3222152



---

UMI Microform 3222152

Copyright 2006 by ProQuest Information and Learning Company.  
All rights reserved. This microform edition is protected against  
unauthorized copying under Title 17, United States Code.

---

ProQuest Information and Learning Company  
300 North Zeeb Road  
P.O. Box 1346  
Ann Arbor, MI 48106-1346

HYDROGEN BONDING INTERACTIONS AND CATION COORDINATION  
EFFECTS IN NITROGEN-BASED POLYMER ELECTROLYTES  
AND MODEL SYSTEMS

A DISSERTATION APPROVED FOR THE  
DEPARTMENT OF CHEMISTRY AND BIOCHEMISTRY

BY

---

Roger Frech, Chair

---

Wai Tak Yip

---

Charles Rice

---

Daniel Glatzhofer

---

John Moore-Furieux

© Copyright by Nathalie M. Rocher 2006  
All Rights Reserved.

## ACKNOWLEDGEMENTS

**Roger Frech**, thanks for all your help, guidance, and encouragement. I enjoyed sharing the experience in Poland at the ISPE9 conference with you. Thanks for being a great coach in this game of science. You showed me how to look at science as if it were beautiful and alluring. Best wishes to you and to your family in the years ahead.

**John Moore-Furieux**, special thanks for your belief in me and getting me into graduate school. I appreciate the tremendous help with questions, problems and experiments. **Daniel Glatzhofer**, I enjoyed spending one summer in your laboratory, even though I nearly lost my fingers. Thanks for all your answers to my many questions. It was a pleasure collaborating with you and your group. I also would like to thank my committee members, **Ralph Wheeler**, **Wai Tak Yip** and **Charles Rice** for your guidance and support. Special thanks to **Jean Keil** for your technical and mental support.

**Shawna York** and **Rebecca Sanders**, thanks for all your training in the laboratory and friendship. **Chris Burba**, I enjoyed working with you on our project. Your professionalism was always appreciated. **Chris Rhodes**, **Varuni Seneviratne**, **Matt Petrowsky**, **Rachel Mason**, **Gwen Giffin**, **Dilhani Jayathilaka** and **Allison McCoy**, I enjoyed working with you in the laboratory. I will always remember bringing my European ideas to our many discussions. Thanks for your friendship.

And of course, I would like to thank my “French family”, especially my parents, **Alain Rocher**, **Monique Rocher** and **Jacques Bouloton**, my sister **Aline Rocher** and her family. Even though they are far away, they have been tremendous support. Their emails and long phone conversations have kept me going. **Anne Clinton**, thanks for

being there for me. No words can describe how much support you have been. You are the best! All my gratitude to **Solon Clinton**, my significant other, for putting up with me, for making me laugh and helping me find a wonderful world outside of school. Special thanks to his family for taking me as their adopted daughter. And I can't forget my wonderful dog **Daisy** for her unconditional love.

## TABLE OF CONTENTS

<b>Acknowledgements</b> .....	iv
<b>Abstract</b> .....	viii
<b>Preface</b> .....	x
<b>1. Introduction</b> .....	1
<b>2. Polymer electrolytes</b> .....	6
2.1. Polymer electrolytes .....	6
2.1.1. General concepts .....	6
2.1.2. Polymer electrolytes in lithium ion rechargeable batteries .....	7
2.1.3. Thermodynamics of complex formation .....	10
2.1.4. Polymers and salts .....	12
2.1.5. Structure .....	15
2.2. Ionic conductivity .....	18
2.2.1. Models of ionic transport .....	19
2.2.2. Measurements of ionic conductivity .....	21
2.3. Poly(ethylenimine) .....	22
2.3.1. Linear form .....	22
2.3.2. Branched form .....	28
2.4. Poly(N-methylenimine) .....	29
2.5. References .....	30
<b>3. Experimental</b> .....	38
3.1. Sample preparation .....	38
3.2. Spectroscopy .....	40
3.3. X-Ray diffraction .....	42
3.4. Differential scanning calorimetry .....	44
3.5. AC complex impedance .....	45
<b>4. Model compounds, dilution in CCl<sub>4</sub>, and model compounds – salt systems</b> .....	47
4.1. Crystal structures and thermal analysis .....	48
4.1.1. Hexylamine:LiTf .....	48
4.1.2. N,N-DMEDA:LiTf and N,N-DMEDA:NaTf .....	51
4.1.3. Dipropylamine:LiTf .....	60

4.2. Vibrational spectroscopy .....	63
4.2.1. Hexylamine system .....	64
4.2.2. N,N-DMEDA system .....	80
4.2.3. Dipropylamine system .....	102
4.3. Anion – host interactions: HEXA–NaBPh <sub>4</sub> and N,N-DMEDA–NaBPh <sub>4</sub> systems	108
4.3.1. Crystal structures and thermal analysis .....	108
4.3.2. Vibrational spectroscopy .....	115
4.4. Conclusions .....	119
4.5. References .....	121
<b>5. Branched poly(ethylenimine) (BPEI) .....</b>	<b>123</b>
5.1. Comparison of BPEI and the model compounds .....	124
5.1.1. NH stretching region .....	124
5.1.2. NH bending region .....	131
5.2. Cation – host interactions: BPEI-LiTf, BPEI-NaTf, and BPEI-TbaTf systems ..	136
5.2.1. Spectroscopic analysis .....	136
5.2.2. Thermal analysis .....	144
5.2.3. Ionic conductivity .....	145
5.3. Anion – host interactions: BPEI – NaBPh <sub>4</sub> and BPEI – NaTf systems .....	147
5.3.1. Spectroscopic analysis .....	147
5.3.2. Thermal analysis .....	154
5.3.3. Ionic conductivity .....	156
5.4. Conclusions .....	157
5.5. References .....	160
<b>6. Branched poly(N-methylethylenimine) (BPMEI) .....</b>	<b>161</b>
6.1. Thermal analysis .....	161
6.2. Spectroscopic analysis .....	162
6.2.1. Room temperature study .....	162
6.2.2. Temperature dependence study .....	169
6.3. Ionic conductivity .....	172
6.4. Conclusions .....	174
6.5. References .....	175

## ABSTRACT

Polymer-based solid electrolytes have been extensively studied for the past twenty five years for their use in lithium rechargeable batteries. Poly(ethylene oxide)-based materials have been so far the most widely studied systems. However, their low room temperature conductivities due to the high degree of crystallinity present in these materials have stimulated the search for alternative polymer-salt systems that are amorphous.

Branched poly(ethylenimine) (BPEI) is a nitrogen based polymer with primary, secondary, and tertiary amine groups that is totally amorphous at any temperature. The understanding of hydrogen bonding interactions and ion-polymer interactions in BPEI-based electrolytes has been considerably enhanced by considering three small molecules that structurally and functionally mimic parts of the polymer chain. Hexylamine (HEXA), N,N-dimethylethylenediamine (DMEDA), and dipropylamine (DPA) were used to further understand hydrogen bonding interactions and cation – nitrogen interactions in BPEI-based electrolytes.

Results from the model compounds studies were significant, and constitute the biggest contribution to this dissertation. In all the model systems, the infrared and Raman spectra were shown to be sensitive to different populations of hydrogen-bonded molecules. In addition, spectroscopic comparisons of the pure molecules with their dilute solutions in CCl<sub>4</sub> deepened our understanding of these systems by eliminating, to a high degree, hydrogen bonding interactions between the molecules. In DMEDA, the presence of intermolecular and intramolecular hydrogen bonding interactions complicated the

analysis of the spectra. The dilution series in  $\text{CCl}_4$  significantly helped to sort out these interactions.

Studies of the model-salt solutions were considerably aided by the formation of crystalline compounds whose structures were solved by single crystal x-ray diffraction methods. The frequency shifts observed in the NH stretching region were attributed to a combination of two effects: a change in the hydrogen bonding environment upon addition of salt as well as the inductive effect of the cation upon coordination to the nitrogen atom. The combination of Raman and IR experiments allowed a separation, to a certain extent, of the contribution from the two effects. This study was further aided by investigating dilution series of the electrolytes in  $\text{CCl}_4$ .

## PREFACE

This thesis is in part based on the research that led to the following publications:

- I. *Hydrogen bonding and the inductive effect in crystalline and solution phases of hexylamine:LiCF<sub>3</sub>SO<sub>3</sub> and dipropylamine:LiCF<sub>3</sub>SO<sub>3</sub>: application to branched poly(ethylenimine)*. Nathalie M. Rocher, Roger Frech, and Masood Khan, J. Phys. Chem. B 2005, 109, 20697 – 20706.
- II. *Inductive effect and hydrogen bonding in complexes of branched poly(ethylenime) with sodium tetraphenylborate and sodium triflate*. Nathalie M. Rocher and Roger Frech, Macromolecules 2005, 38(25), 10561 – 10565.
- III. *Crystalline and solution phases of N,N-dimethylethylenediamine complexed with lithium triflate and sodium triflate: intramolecular hydrogen bonding interactions*. Nathalie M. Rocher, Roger Frech, and Doug Powell, J. Phys. Chem. B 2006, in press.
- IV. *Hydrogen bonding and cation coordination effects in primary and secondary amines dissolved in carbon tetrachloride*. Nathalie M. Rocher and Roger Frech, in progress.
- V. *Crystalline and solution phases of N,N-dimethylethylenediamine and hexylamine complexed with sodium tetraphenylborate: role of the anion*. Nathalie M. Rocher, Roger Frech, and Masood Khan, in progress.

## 1. INTRODUCTION

Solid polymer electrolytes (solvent-free polymer-salt complexes), have attracted considerable attention for their potential use as electrolytes in secondary high energy density batteries, with a variety of applications such as portable electronic devices and electric vehicles. Extensive research has been done to understand the fundamental factors governing the behavior of these systems and in particular the factors controlling the ionic conductivity. The microscopic mechanism of ionic transport is not well understood, but certainly involves the breaking and reforming of cation – heteroatom bonds and changes in the local conformation of the polymer host. In addition, the nature of the charged species that contribute to the ionic conductivity is a controversial subject and research is still in progress. Poly(ethylene oxide) (PEO) has been the most investigated polymer due to its propensity to solvate and transport ions. More recently, other polymeric systems are being investigated. The objective of my research is to gain further insight into the nature of the ion-polymer and cation-anion interactions, as well as hydrogen-bonding interactions in branched poly(ethylenimine) (BPEI) – salt systems.

### **Research strategy**

The complexity of BPEI-salt complexes makes it difficult to develop even a qualitative, molecular-level understanding of the nature of the ionic conductivity. Cation-polymer and cation-anion interactions, as well as hydrogen-bonding interactions are expected to play a major role in the mechanism of ion transport. Unfortunately, all these factors are interdependent in the BPEI-salt systems. Infrared and Raman

spectroscopy can be used to characterize polymer-salt interactions by analyzing the frequency shifts of the host BPEI modes upon complexation with a salt. Both hydrogen-bonding and inductive effects, originating from the coordination of the cation to the heteroatom of the polymer, shift the vibrational frequencies of the BPEI primary amine functional group.

In order to sort these competing effects, many BPEI – salt systems have been investigated. A comparative spectroscopic study of BPEI complexed with lithium triflate (LiTf), sodium triflate (NaTf), and tetrabutylammonium triflate (TbaTf) offered the opportunity to study the effect of the cation – polymer interactions by choosing a series of salts with the same triflate anion. The lithium and sodium cations are expected to coordinatively interact with the nitrogen atoms of BPEI, although to a different extent because of the difference in their charge density. Tetrabutylammonium is a charge-protected cation because of its bulky butyl groups. Consequently, it cannot undergo a direct coordinative interaction with the nitrogen atoms of BPEI. Comparison of the TbaTf data with the LiTf and NaTf data allowed, to a certain extent, a separation of the cation inductive effect (only present in the LiTf and NaTf complexes) from the effect of the N–H...O hydrogen bonding (expected in all complexes).

In a second part of the study, BPEI was complexed with sodium tetraphenylborate (NaBPh<sub>4</sub>). Sodium tetraphenylborate has a bulky anion that is charge protected by four phenyl groups, rendering cation-anion interactions and anion-polymer interactions minimal. Comparison of these data with BPEI – NaTf allowed a further separation of hydrogen bonding interactions and the inductive effect. The sodium ion of both salts can coordinatively interact with the nitrogen atom of BPEI, although to a different extent

because of the presence of relatively strong cation-anion interactions in the NaTf complexes. However, the lack of heteroatoms in the tetraphenylborate anion precludes the formation of hydrogen bonds with the N-H groups upon complexation, in contrast to the N–H...O hydrogen bonds expected in the NaTf complexes.

The study of the local structure, i.e. local backbone conformation, coordination of the cation to the polymer, ionically associated species, and hydrogen bonding interactions is complicated in branched PEI due to the presence of three different amine groups. Consequently, a thorough interpretation of spectroscopic data has been very limited. It is possible to better understand these interactions in a polymer electrolyte by studying small molecules that structurally mimic small regions of a polymer. This strategy has been successfully used in other PE systems. For example, small molecules called glymes, short for glycol dimethyl ether, have been investigated to better understand the nature of the interactions in PEO systems. Numerous experimental and theoretical studies have been conducted on glyme – salt systems in order to understand the interactions in these materials. Theoretical calculations, x-ray structures and spectroscopic studies have enabled the development of spectra – structure correlations, and provided information about the local structure in these systems. Following the strategy developed for ethylene oxide based systems, N,N'-dimethylethylenediamine (NN'-DMEDA) was studied to further understanding in LPEI based polymer electrolytes.

The branched PEI is a more complicated system due to the presence of three different primary amine groups. The choice of a “good” model compound is not as obvious as in the linear polymers. Three small molecules were selected: hexylamine (HEXA), N,N-dimethylethylenediamine (N,N-DMEDA), and dipropylamine (DPA).

Hexylamine contains a primary amine group attached on a hexane backbone, and is the simplest model for a primary amine group. N,N-DMEDA contains a primary amine group separated from a tertiary amine group by an ethylene backbone; this molecule resembles small regions of BPEI much more closely and is therefore more complicated. Finally, dipropylamine contains a secondary amine group attached to two propyl groups, and is the simplest model for a secondary amine group. Following the same approach as in the BPEI system, many salts were investigated with each of the three compounds: LiTf, NaTf, TbaTf, and NaBPh<sub>4</sub>. During the course of the study, six crystal structures were determined: HEXA:LiTf, DPA:LiTf, DMEDA:LiTf, DMEDA:NaTf, DMEDA:NaBPh<sub>4</sub>, and HEXA:NaBPh<sub>4</sub>. These crystal structures yield further insight into cation-polymer and cation-anion interactions.

The use of small molecules as model compounds has been an efficient strategy to enhance our knowledge of the polymeric electrolytes. However, even in these small molecular weight electrolytes, the simultaneous presence of hydrogen bonding interactions and ion coordinating effects complicates the analysis of the NH stretching vibrations. But by diluting these small molecules in non-polar solvents, such as carbon tetrachloride (CCl<sub>4</sub>), it is possible to minimize or eliminate intermolecular hydrogen bonding interactions and analyze the frequencies of the “free” NH bands. Similarly, by diluting an electrolyte in a non-polar solvent, it is possible to study the effect of the salt on the small molecular host in the absence of intermolecular hydrogen bonding interactions. A comparative study of the infrared and Raman spectra of the pure amines combined with concentration-dependent measurements of their carbon tetrachloride solutions, and amine:LiTf complexes in carbon tetrachloride solutions allowed for an

unambiguous separation of the hydrogen bonding interactions and lithium cation coordinative effects.

To my delight, the results emerging from the model compounds research has been a significant contribution to the understanding of hydrogen bonding interactions and cation coordination effects in amine systems.

## 2. POLYMER ELECTROLYTES

### 2.1. POLYMER ELECTROLYTES

#### 2.1.1. General concepts

Polymer electrolytes are formed when a salt is dissolved into a solid, coordinating, polymeric solvent. Polymer electrolytes can be formed from linear, branched, comb-like or coblock polymers. In rigorous terms, solid polymer electrolytes (SPEs) do not contain any low molecular weight additives. SPEs should be distinguished from polyelectrolytes and gel electrolytes. In a polyelectrolyte, positive or negative charged groups are covalently attached to a polymer chain, and the counterions are solvated by a high dielectric constant solvent (usually water). In a gel electrolyte, the polymer and salt are mixed with a low molecular weight organic liquid; the polymer usually acts as a stiffener. In the past century, most synthetic polymers have been used as structural materials or as electric insulators. However, in the past 30 years, polymers have received attention for their ability to dissolve salts and become ionic conductors. The first measurements of the electrical properties of poly(ethylene oxide) (PEO) – alkali salt complexes were done by Fenton, Parker and Wright and published in 1973.<sup>1</sup> In that paper, the electrical properties were only briefly described in the last paragraph that stated that “the conductivity increases markedly as the degree of crystallinity is reduced”. More detailed conductivity measurements were presented by Peter V. Wright at the Ionic Polymer symposium at Brunel University and published in 1975.<sup>2</sup> This work showed that significant conductivities could be obtained for crystalline polymer electrolytes above their melting temperatures. Michel Armand and co-workers called attention to the

importance of such materials for potential applications as solid-state polymer electrolytes in high energy density batteries. In 1978, at the Second International Conference on Solid Electrolytes held at the University of St Andrews, Armand and his group described how an alkali metal salt could be dissolved in a solvating polymer matrix, and reported conductivities as a function of temperature for multiple salts dissolved in PEO.<sup>3,4</sup> In the following years, intensive amount of research started in this new field. The focus of these studies was primarily directed towards four goals: (i) understanding the interactions associated with the formation of a polymer - salt complex with multiple phases, (ii) understanding the nature of the charge transport mechanism, (iii) developing new polymer electrolytes with better mechanical, electrical and chemical properties, and finally, (iv) investigating the functioning of electrochemical cells based on these materials. However, understanding the structure, interactions and the charge transport mechanism in polymer electrolytes has been a difficult task as these properties differ greatly from those in inorganic compounds.<sup>5-9</sup>

### **2.1.2. Polymer electrolytes in lithium ion rechargeable batteries**

The increasing demand for portable energy sources has led to rapid technological improvements in rechargeable solid-state batteries. Some of the secondary batteries include: lead –acid, nickel-cadmium, nickel-metal hydride, and lithium-ion.<sup>10</sup> Lead-acid batteries are used primarily in automobiles for ignition and lighting, and represent over half of all batteries sales.<sup>11</sup> In 2001, Ni-Cd, Ni-MeH and Li-ion batteries shared the market for portable batteries in proportions of 23%, 14%, and 63%, respectively.<sup>11</sup> These batteries are widely used for high power applications and for portable devices such as

laptops, cellular phones, and digital cameras.<sup>12</sup> Lithium batteries that use lithium metal have safety disadvantages when used as secondary energy sources, and are not commercially available. A new promising approach is that of the “rocking chair” battery, where the lithium metal anode is replaced by a lithium ion source.<sup>13</sup> The lithium ions “rock” back and forth during charge and discharge between the two electrodes; however, they are not reduced to neutral lithium metal during the cycle. In such batteries, the anode material is a lithium-carbon intercalation compound, and the cathode material is a lithium-metal oxide intercalation compound. The current battery technology uses organic solvents; however, there are many safety advantages of using solid state batteries over those liquid electrolytes. Organic solvents are volatile, extremely flammable and can easily leak. Also, liquid electrolytes have been found to intercalate and react with the cathode because of the high oxidation potential of the cathode material.<sup>13,14</sup> An increasing use of polymer electrolytes in such batteries is therefore expected. The lithium ion polymer battery provides high energy density with versatile fabrication methods, is safer, and has a longer lifespan than comparable battery technologies.<sup>15</sup>

The polymer electrolyte plays two important roles in a solid-state battery; it is the medium through which ions are transported between the anode and the cathode during charge and discharge cycles, and it acts as a physical separator between the electrodes.<sup>13,16</sup> A schematic diagram of a rocking chair battery is represented in Figure 2.1.

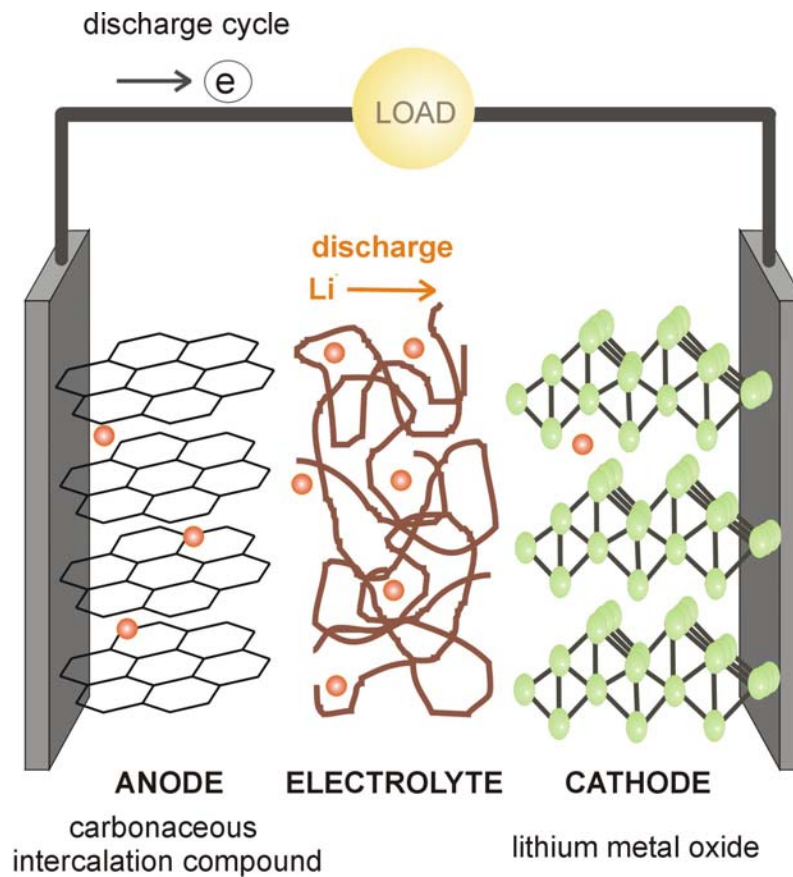


**Figure 2.1.** Schematic representation of a lithium ion “rocking chair” cell in the discharge mode. A graphene structure is used as the anode and a transition metal oxide is used as the cathode material.

Polymer electrolytes are very flexible and can be formed into very thin film of large surface area, giving overall higher energy densities. The flexible nature of these materials allows for designs of more space-efficient batteries of shapes and forms that are easily fabricated and processed. Also, since no metal battery cell casing is needed, the battery can be lighter. For electrochemical applications, the flexibility of the material is important because it can accommodate volume changes in the cell as the battery is cycling, without physical degradation of the interfacial contact with the electrodes. Lithium ion polymer batteries are environmentally friendlier than other batteries; they

contain no toxic metals such as nickel, mercury, cadmium, or lead that are all extremely harmful to the environment. All the materials used in these batteries, including the metal oxide in the cathode, are considered benign.<sup>10,17</sup>

Before batteries made out of a dry polymer electrolyte with no plasticizer or inorganic filler can be commercially available, a number of technological goals need to be met. The ionic conductivity needs to be higher than  $10^{-4}$  S cm<sup>-1</sup> in the temperature range from -20°C to 60°C. The thermal, electrochemical and mechanical stability needs improvement, and finally, production costs must be low.<sup>18</sup>

### **2.1.3. Thermodynamics of complex formation**

Polymers that contain polar groups could be considered as high molecular weight solvents that can dissolve salts to form stable salt – polymer complexes.<sup>19</sup> However, a salt dissolves in a solvent, either liquid or solid, only if the energy and entropy changes associated with the dissolution lead to an overall reduction in the free energy of the system.<sup>5,6,20</sup> Therefore, the thermodynamics of dissolution can be described by the change in the Gibbs free energy  $\Delta G$ , at constant pressure and temperature.  $\Delta G$  of dissolution is a function of three components: change in enthalpy of dissolution ( $\Delta H$ ), change in entropy of dissolution ( $\Delta S$ ), and temperature (T), as shown in Equation 2.1.

$$\Delta G = \Delta H - T\Delta S \qquad \text{Eqn. 2.1}$$

So, for  $\Delta G$  to be negative, we need to consider the two terms  $\Delta H$  and  $\Delta S$ . The overall entropy change arises from two parts: an increase in entropy due to the destruction of the salt crystal lattice as it dissolves into the polymer matrix, and a negative entropy change brought by short range interactions between the ions and the

polymer, causing local ordering and a stiffening of the chains. Due to the two competing factors, the overall entropy change can be positive or negative. However, in many polymer systems, the overall entropy change of dissolution is negative because the loss of entropy of the polymer chains due to the restriction of the polymer chains to specific conformations is greater than the gain in entropy due to the disordering of the ions.<sup>6</sup> This restriction is also reflected experimentally by an increase in the glass transition temperature.<sup>21</sup> As shown in Equation 1.1, the effect of  $\Delta S$  on  $\Delta G$  is temperature dependent; as the temperature increases, the  $T\Delta S$  term dominates the equation. In a number of polymer electrolytes, salt precipitation will occur with increasing temperature, which indicates that the overall entropy of dissolution is negative in these systems.<sup>22</sup> In general, the individual entropy changes of the salt and polymer are not expected to vary greatly between different salt - polymer combinations, and therefore the enthalpy change of dissolution seems to be the main factor controlling the dissolution process.

The enthalpy of dissolution varies greatly for different systems, and is dependent on a number of factors:<sup>23-27</sup> (1) the lattice energy of the salt, (2) the presence of suitable coordinating sites on the polymer, (3) the formation of coordinate bonds between the cation and the polymer, and (4) electrostatic interactions between cations and anions. It is believed that the anions are primarily solvated in the polymer because of their attraction to the cation, but not by interactions with the polymer. However, in protic media, anion solvation may occur via hydrogen bonding interactions with the polymer<sup>28</sup> or they can be solvated by polymers containing Lewis acids. Despite these cases, the solvation enthalpy depends primarily on the strength of the coordinative bond between the cation of the salt and the polymer chain.<sup>8</sup>

#### 2.1.4. Polymers and salts

The thermodynamics point of view provides a general understanding of dissolution. A more specific description of the types of salts and the types of polymers compatible for complex formation can now be considered. The main interest in polymer electrolytes is their possible use in power sources and other devices. The majority of the studies have involved lithium and to a lesser extent sodium salts due to their high energy density. The choice of these cations was based on solubility, conductivity, and redox stability requirements for polymer electrolytes in rechargeable batteries. Most of all, the choice of lithium and sodium salts for the electrolyte was based on the advanced development of electrodes based on insertion or intercalation compounds.<sup>17,18,29</sup> As discussed above, the solubility of the salt in polymers is largely dependent on the lattice energy of the salt and the solvation energy of the cation. However, because the solvation of the anions is weak, large anions with low ion – dipole stabilization energy and with delocalized charge, such as the conjugated bases of strong acids, are preferable.<sup>30,31</sup> Such anions are likely to have relatively low lattice energies and have little tendencies to form tight ion pairs which were shown to decrease the ionic conductivity in most polymer electrolytes.<sup>32-36</sup> Some of the most widely studied anions are:  $\Gamma^-$ ,  $\text{ClO}_4^-$ ,  $\text{SCN}^-$ ,  $(\text{CF}_3\text{SO}_2)\text{N}^-$ ,  $\text{CF}_3\text{SO}_3^-$ ,  $\text{B}(\text{C}_6\text{H}_5)_4^-$ ,  $\text{BF}_4^-$ ,  $\text{AsF}_6^-$ ,  $\text{PF}_6^-$ , and  $\text{SbF}_6^-$ .

Since the solvation energy of the cation is one of the terms which dominate the energetics of solvation, dissolution occurs only if the polymer chains contain atoms that are capable of coordinating the cations. For a polymer to be a good medium for ion solvation, a few characteristics are necessary. The coordinating atoms that belong to the polymer chain should have sufficient electron donor power to coordinate with the cation.

The strength of the interactions between a cation and the coordinating group on the polymer chain can be described according to the hard/soft acid base theory.<sup>37,38</sup> Hard Lewis acids and bases are small, highly electronegative, of low polarizability, and hard to oxidize; i.e. they hold their electrons very tightly. Soft Lewis acids and bases, on the other hand, are large, highly polarizable, with low electronegativity, and easy to oxidize. In a polymer electrolyte, the polymer acts as a Lewis base and the cation acts as a Lewis acid. The strongest interactions occur between hard acid and bases or soft acid and bases; for example a polyether is expected to form very stable complexes with  $Mg^{2+}$  (hard), whereas it would only have very weak interactions with  $Hg^{2+}$  (soft).<sup>31,39</sup> Some of the electron donating atoms and groups found widely in polymer electrolytes are O, NH, NR, and S. The order of stability for coordination of alkali or alkali earth ions with the different heteroatoms is:  $O > NR > NH > S$ , following the trend of the electron donating power of the groups.<sup>7</sup>

The solvation of the cation also depends on the number of coordinating sites readily available. In high molecular weight polymers, a suitable distance between the coordinating sites is important as the cations may be coordinated by atoms on the same chain. For example, polyethers with the repeat unit  $(-CH_2-CH_2-O-)_n$  (PEO) seem to have a favorable arrangement for effective interaction with alkali metal cations in particular; on the other hand, polyethers with  $(-CH_2-CH_2-CH_2-O-)_n$  or  $(-CH_2-O-)_n$  repeat units do not form homogeneous polymer-salt mixtures, even though they also have an ether oxygen as the coordinating site.<sup>4,39</sup> Because of the spacing between the oxygen atoms, the PEO chain has the ability to adopt conformations which accommodate the salt without exerting excessive strain of the polymer. In general, to provide enough coordinating sites, a

polymer chain needs to adopt conformations where several intra-polymer and/or inter-polymer cation bonds are possible. For that reason, the atoms of the main chain have to have low energy barriers of rotation to ensure flexibility.

Besides considering polymers that are capable of dissolving salts, the choice of the polymer host is also highly dependent on the ionic conductivity of the polymer electrolyte. Significant ionic conductivity has been found to be highly dependent on the presence of an amorphous phase.<sup>26,40-42</sup> Consequently, ionic conductivity is generally restricted to the amorphous phase above the glass transition temperature ( $T_g$ ), where the polymer chains are in rapid motion due to bond rotations; these large amplitude internal modes are called *segmental motion*.<sup>5</sup> The motion of ions in a polymer electrolyte is coupled to that of the polymer. Segmental motion has been shown to promote ion transport by making the environment of the cation more liquid-like.<sup>24,43</sup> The mobility and therefore the ionic conductivity of ions in a polymer matrix can be increased with the use of amorphous polymer hosts having low glass transition temperature (well below ambient temperatures). At the operating temperatures of batteries, a material with a low  $T_g$  has highly flexible chains that can promote ionic transport; such materials will be more likely to have higher conductivities than a crystalline material or more rigid material. For that reason, amorphous materials with low glass transition temperatures are the best candidates for use in solid state batteries.<sup>44</sup> The polymer poly[bis-((methoxyethoxy)ethoxy)phosphazene] or MEEP is a good example of such electrolyte as it is a single phase polymer that is highly amorphous ( $T_g = -84^\circ\text{C}$ ).<sup>45</sup> However, the good ionic conductivity of electrolytes based on MEEP is offset by poor mechanical properties.<sup>46-48</sup>

### 2.1.5. Structure

The structure of polymer electrolytes exists at two different levels: (1) a macroscopic level, which corresponds to the macroscopic identity of the phases present (crystalline and amorphous), their morphology, and their arrangement respective to each other, and (2) a microscopic level, which corresponds to the arrangements of the atoms in the polymer – salt complex.

**Macroscopic structure.** On a macroscopic scale, a number of distinct phases are present in a polymer electrolyte. The nature of these phases is dependant on the intrinsic properties of the polymer and the salt, on the concentration of the salt and the temperature of observation. In many cases, a polymer – salt mixture can form a crystalline phase or several crystalline phases of different compositions. In addition, a polymer that is able to dissolve a salt can yield an amorphous phase.

Many different techniques have been used in an effort to characterize polymer salt complexes. Optical microscopy<sup>49,50</sup> can identify the presence of amorphous and crystalline phases. Anisotropic crystals are observed under a polarizing microscope. NMR can be used to determine the numbers of nuclei with magnetic spins (<sup>1</sup>H, <sup>7</sup>Li, <sup>19</sup>F, <sup>23</sup>Na) in each phase due to the differences in their relaxation time in different phases.<sup>40,51,52</sup> Short relaxation times are attributed to crystalline phases, and longer relaxation times are attributed to amorphous phases. X-ray diffraction has been used for crystalline complexes; although large unit cells with low symmetry makes the indexing difficult.<sup>49,53,54</sup> Finally, differential scanning calorimetry (DSC) provides information on the presence and thermal stability ranges of the different phases.<sup>55-57</sup>

Using the techniques described above, phase diagrams of polymer electrolytes have been constructed. However, this process is not straightforward since polymer electrolytes do not always obey the Gibbs phase rule because metastable states are often present.<sup>39</sup> Kinetics of crystallization can be very slow because of slow structural reorganization, which can lead to systems that have not fully reached chemical equilibrium. Moreover, the method of preparation and the thermal history have been found to affect phase distributions and compositions.<sup>7,56,58,59</sup> For these reasons, some scientists refer to polymer electrolytes phase diagrams as “pseudophase diagrams”.<sup>57</sup> Numerous PEO – alkali metal salts phase diagrams have been constructed driven by the potential technological applications of polymer electrolytes in high energy density batteries.<sup>41,60-62</sup> However, no phase diagrams involving other polymer hosts such as polyethylenimine (PEI) can be found in the literature, although DSC and X-ray diffraction studies of PEI with NaI<sup>63</sup> and NaTf<sup>64</sup> have been reported.

It is now recognized that significant ionic conductivity in SPEs primarily takes place in the amorphous regions. However, a recent study on PEO – LiSbF<sub>6</sub> has shown that in this system, the crystalline phase has a higher ionic conductivity than the amorphous phase.<sup>65,66</sup> Nevertheless, the construction of pseudophase diagrams provides a descriptive approach that has been very useful in the understanding of conductivity, stability and mechanical properties of SPEs.

***Microscopic structure.*** To understand the mechanism of ionic transport and its relationship with the structure of the material, knowledge of the structure at the microscopic level is necessary. Many different techniques have been used to study the structure of polymer electrolytes: X-ray diffraction<sup>67,68</sup>, extended X-ray fine structure

analysis (EXAFS)<sup>69-72</sup>, and spectroscopic methods such as infrared, Raman<sup>25,26,73,74</sup> and NMR<sup>75</sup>. In polymer electrolytes, the local structure is determined by the interactions between ions and the host polymer, by the interactions between cations and anions, and by the interactions between polymer chains, such as *hydrogen bonding interactions*.

The interactions between the host polymer and the cation are important for ionic conductivity because ionic transport is believed to be closely related to segmental motions of the polymer. Segmental motions involve changes in the conformation of the polymer and breaking and reforming of cation – polymer bonds, allowing the cation to diffuse in the polymer matrix under the influence of an electric field.<sup>5,8</sup> Specific interactions between polymer host and dissolved electrolytes have been evidenced by infrared and Raman spectroscopy. In PEO and related comb polymer systems (polymers with short side chains), cation polymer interactions have been observed by the Raman CH<sub>2</sub> rocking bands.<sup>26</sup> Also, far infrared studies have shown the “solvent cage” vibrations, corresponding to the vibration of the cation in its coordination sphere. Vibrational spectroscopy has also been very useful to study the conformation changes of the polymer backbone. The conformation of the polymer is directly related to the O-C-C-O torsional angles in PEO<sup>76-84</sup>, and the respective N-C-C-N torsional angle in PEI.<sup>85-87</sup> The CH<sub>2</sub> rocking and C-O (or C-N) stretching modes between 800 and 1000 cm<sup>-1</sup> are particularly sensitive to the changes in the conformation, and have been extensively studied.<sup>88-91</sup>

Ionic association in polymer electrolytes has been evidenced by various static techniques such as vibrational spectroscopy<sup>92,93</sup>, EXAFS and X-ray diffraction, and by dynamic techniques, such as measurements of the molar conductivity and transference

numbers.<sup>94-96</sup> The formation of associated ionic species results from the low permittivity of polymers. In such media, the oriented dipoles associated with the heteroatoms of the polymer chain are not strong enough to reduce the effective field of the ions. The attractive electrostatic potential energy of the ions becomes greater than thermal motion, and ionic association keeps the system stable.<sup>34</sup> The ionic species present in a polymer electrolyte have been classified as “free” ions or solvent separated ion pairs, contact ion pairs and aggregates. For a salt MX consisting of  $M^+$  and  $X^-$  ions, contact ion pairs are written  $[MX]^0$ , and aggregates species can take the form of  $[M_2X]^+$ ,  $[MX_2]^-$  or other larger aggregates.<sup>97</sup> Vibrational spectroscopy has been extensively used to study the degree of ionic association in some polymer – salt systems by observing the shifts or the splitting in the vibrational bands of a polyatomic anion. Specifically, for non-degenerate modes, multiple bands are observed and can be assigned to different ionic species. The assignment of vibrational frequencies for modes of the  $CF_3SO_3^-$  and  $ClO_4^-$  anions especially, has been widely developed.<sup>92,98-100</sup> The type and amount of the ionic species are highly dependent on the polymer – salt system and are also a function of the molecular weight, salt concentration, kinetic, and temperature.<sup>101-104</sup> The nature of the ionic species present in a polymer electrolyte is thought to have an important effect on the ionic conductivity.<sup>105,106</sup> However, the contribution of the different ionic species to the ionic conductivity has been controversial and research is still very active in this area.

## 2.2. IONIC CONDUCTIVITY

The measurement of ionic conductivity in polymer electrolytes is relatively easy; however, understanding the mechanisms of ionic conduction has proven to be more

difficult. One of the main tasks is to identify the types of ionic species that are carrying the charge, and then understand the role of each species in their contribution to the total current. This task requires accurate measurements of the transport and transference numbers of the ionic species present in the polymer electrolyte.

### 2.2.1. Models of ionic transport

**Macroscopic model.** The dc conductivity of any material, at temperature T and pressure P, can be expressed by the Kohlrausch summation

$$\sigma(T, P) = \sum_i n_i |q_i| \mu_i \quad \text{Eqn. (2.2)}$$

where  $n_i$  is the concentration of charge carriers of type  $i$ ,  $q_i$  is their charge, and  $\mu_i$  is their mobility. In polymer electrolytes, the charge carriers include all the charged species, i.e. single cations and anions, as well as ion clusters. As the salt concentration is increased, the number and the type of charge carriers changes, along with their mobility, and this model fails to describe the experimental conductivity of polymer electrolytes.<sup>43,107</sup>

**Empirical models: VTF and WLF equations.** The ionic conductivity of polymer electrolytes is usually plotted in an Arrhenius type plot, which consists of  $\log \sigma(T)$  vs.  $T^{-1}$ . When a straight line is observed, it can be fit to the Arrhenius equation:

$$\sigma(T) = \sigma_o \exp(-E_a/kT) \quad \text{Eqn. (2.3)}$$

where  $E_a$  is the activation energy, and  $k$  the Boltzmann constant. If an abrupt change in the slope of the line is observed, it is generally attributed to a phase change. Below  $T_g$ , the activation energy is usually larger, and the curve has the biggest slope.

When a curved line is observed<sup>3,4,108-111</sup>, it can be fit to the semi-empirical Vogel, Tamman, Fulcher equation (VTF) written in the following form:<sup>112-114</sup>

$$\sigma(T) = \sigma_0 \exp [-B/(T-T_0)] \quad \text{Eqn. (2.4)}$$

where  $\sigma_0$  is a pre-exponential factor proportional to  $T^{1/2}$ ,  $B$  is a constant with the dimensions of energy, and  $T_0$  is normally called the equilibrium glass transition temperature, and is related to the measured glass transition temperature by  $T_0 \approx T_g - 50$ . The form of this equation is consistent with the idea that above  $T_0$ , thermal motion contributes to transport processes, and that for low  $T_g$ , faster segmental motions should occur. The VTF equation, used to characterize viscoelastic properties of polymeric systems, relates the viscosity of polymeric materials with the conductivity and shows that structural motions of the polymer are required for diffusive motions of the ions.<sup>115-119</sup>

The VTF equation can be readily transformed into the Williams, Landel, Ferry (WLF) equation<sup>120</sup> that has been widely used to describe the relaxation and transport processes of amorphous polymeric materials in the vicinity of the glass transition temperature. This equation expresses a characteristic property in terms of a shift factor,  $a_T$ , which is the ratio between any mechanical relaxation process at temperature  $T$ , and its value at a reference temperature  $T_S$ . The temperature dependence of the conductivity can be written in the WLF form:<sup>23,111</sup>

$$\log \frac{\sigma(T)}{\sigma(T_S)} = \frac{C_1(T - T_S)}{C_2 + (T - T_S)} \quad \text{Eqn. (2.5)}$$

where  $\sigma(T_S)$  is the conductivity at a reference temperature  $T_S$ , and  $C_1$  and  $C_2$  are constants that may be obtained experimentally. The reference temperature  $T_S$  is arbitrary, but it is often taken to be 50K above  $T_g$ .

The VTF and WLF models are useful to describe the temperature dependence of all transport or relaxation properties: diffusion, viscosity and conductivity. In both models, the similarity between the temperature dependence of the ionic conductivity and the viscosity or relaxation properties of the polymer indicates that the dynamic of the polymer chain is linked to the charge transport process. Local motions of the polymer host are largely responsible for ionic transport in the electrolyte. However, these models are empirical generalizations based on experimental observations, rather than the product of theoretical treatments.

### **2.2.2. Measurements of ionic conductivity**

In polymer electrolytes, the conductivity is due to the migration of ions in the polymer, which only serves as a host. The measurement of the ionic conductivity is usually done by ac impedance spectroscopy. The polymer electrolyte is sandwiched between two electrochemically inert electrodes, usually stainless steel; a sinusoidal potential excitation is applied and the magnitude and phase shift of the current are measured in response. This measurement is repeated at a series of frequencies that can range from  $10^{-4}$  Hz to 10 MHz. From these data, the conductivity of the bulk electrolyte can be calculated using an analysis proposed by Cole and Cole<sup>121</sup> and further developed by Macdonald.<sup>122,123</sup> The ac current signal,  $I$ , and the ac potential,  $E$ , can be written in terms of real and imaginary parts. The ac impedance,  $Z=E/I$  can also be expressed in terms of a real ( $Z'$ ) and imaginary part ( $Z''$ ) as follows:  $Z = Z' + jZ''$  with  $j=\sqrt{-1}$ . In an impedance spectrum plot,  $Z'$  is plotted against  $-Z''$  for data collected at a series of

frequencies. The bulk resistance  $R_b$  of the electrolyte can be deduced from such a plot as shown on Figure 2.2.

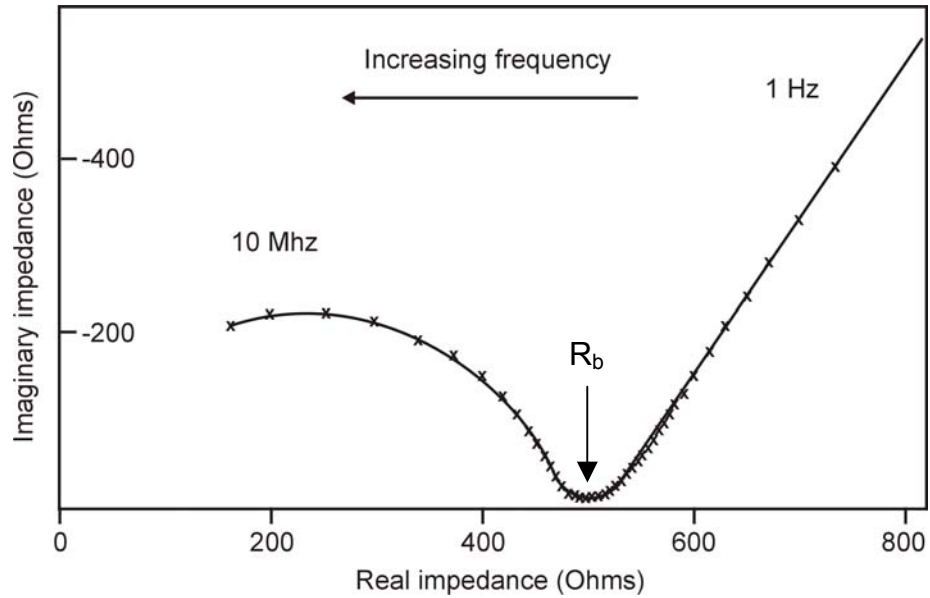


**Figure 2.2.** Impedance spectrum.

The conductivity  $\sigma$ , of a sample can then be calculated using the relation:

$$\sigma = \frac{d}{R_b A} \quad \text{Eqn. (2.6)}$$

where  $d$  is the separation between the electrodes of the cell, and  $A$  is their surface area.

## 2.3. POLY(ETHYLENIMINE)

### 2.3.1. Linear form

Linear poly(ethylenimine) or LPEI is a structural analogue of poly(ethylene oxide) with a NH secondary amine group in place of the ether oxygen. The presence of the unshared electron pair on the nitrogen atom makes LPEI a good host polymer for the dissolution of various electrolytes. Upon addition of alkali metal salts, many of the

phenomena observed in the imine polymer are similar to those occurring in PEO – salt systems. For example, the addition of sodium iodide to either PEO or LPEI first reduces the crystallinity of the polymer and increases the ionic conductivity, but at higher salt concentrations a crystalline complex forms in which conductivity is reduced.<sup>63,124</sup> Moreover, LPEI dissolves many of the same alkali metal salts as PEO, as evidenced by the absence of X-ray diffraction patterns from the pure salt, a loss of crystallinity of the polymer, and an increase in the glass transition temperature.

Linear PEI can be prepared by two different methods. Low molecular weight material ( $< 10^4$  MW) is synthesized by ring-opening polymerization of 2-methyloxazoline.<sup>125,126</sup> High molecular weight LPEI ( $\sim 100,000$  MW) is prepared by the acidic hydrolysis of  $\sim 200,000$  MW commercial poly(2-ethyl-2-oxazoline).<sup>127,128</sup> The melting temperature of LPEI has been reported around  $58^\circ\text{C}$ , and some papers also report a glass transition temperature around  $-23^\circ\text{C}$ .<sup>126</sup> The value of the  $T_g$  is not easily obtained due to the very high crystallinity and low amorphous content of the polymer.

***LPEI crystalline structure.*** Chatani et al. solved the crystal structure of anhydrous LPEI by X-ray structure analysis of a uniaxially oriented sample.<sup>129</sup> This analysis revealed that the polymer chains form double-stranded helices with each polymer chain having five monomeric units per turn (i.e. a  $5/1$  helical form). The double strand is formed by two chains that are rotated  $180^\circ$  about the chain axis with no translation and turning in the same direction. Chatani attributed the formation of a double strand to the presence of interchain bridging N-H  $\cdots$  N hydrogen bonds. The crystals form an orthorhombic unit cell in the  $D_{2h}^{24}$ -Fddd space group with cell

dimensions  $a = 2.98$  nm,  $b = 1.72$  nm, and  $c = 0.479$  nm which is along the fiber axis. A representation of the crystal structure is shown in Figure 2.3.

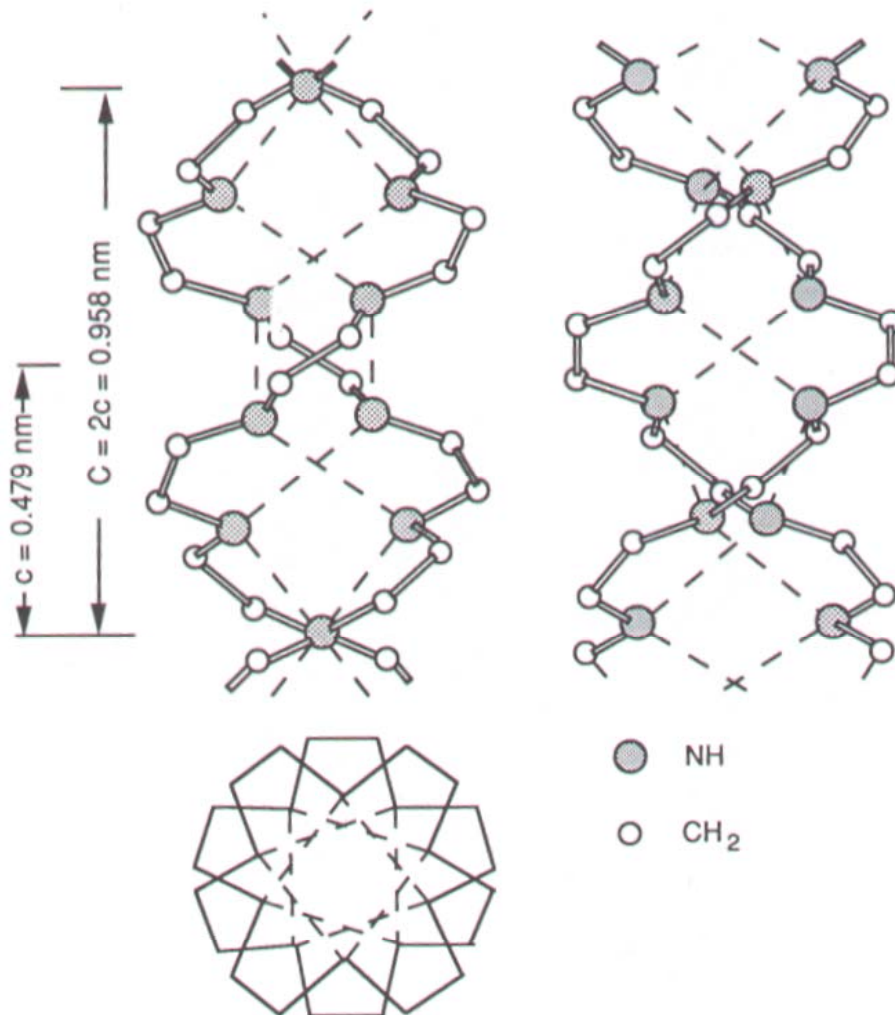


**Figure 2.3.** Double stranded helical chains of anhydrous LPEI viewed in three perpendicular directions. The dashed lines represent N-H  $\cdots$  N hydrogen bonds.<sup>129</sup>

This analysis shows to have some inconsistencies in the observed fiber period, which was determined to be only half of the identity period of the double helix fitted in the cell. The problems emerging from the analysis of the data came from the small number of observable reflections, which impeded a more accurate structural analysis, and required the use of assumptions.

**LPEI hydrates.** LPEI is a very hygroscopic material and forms crystalline hydrates. Chatani et al. also reported the structure of three different hydrates of LPEI: a hemihydrate<sup>130</sup>  $(-\text{CH}_2\text{CH}_2\text{NH}\cdot 0.5\text{H}_2\text{O})_n$ , a sesquihydrate<sup>131</sup>  $(-\text{CH}_2\text{CH}_2\text{NH}\cdot 1.5\text{H}_2\text{O})_n$ , and a dihydrate<sup>131</sup>  $(-\text{CH}_2\text{CH}_2\text{NH}\cdot 2\text{H}_2\text{O})_n$ . In all the hydrates, the polymer chains are fully extended in a planar zigzag form. There are no N-H  $\cdots$  N hydrogen bonds as in the anhydrous form, but in all three hydrates there are N-H  $\cdots$  O and O-H  $\cdots$  N hydrogen bonds. The sesquihydrate and dihydrate also form O-H  $\cdots$  O hydrogen bonds. In the three crystalline hydrates, the nitrogen atom coordinates two water molecules, but the environment of the water molecules is different in each crystal. The melting temperatures of these compounds (80 – 85°C) are higher than for anhydrous LPEI, which is probably due to the existence of stronger hydrogen bonds. The presence of water in a polymer electrolyte is detrimental for practical application in a lithium ion battery. For that reason research efforts have concentrated on anhydrous PEI based electrolytes.

**LPEI:salt complexes.** Besides these crystalline hydrates, Chatani et al. have reported the crystalline structure of LPEI with hydrogen chloride<sup>132</sup> (HCl) and acetic acid<sup>133</sup> ( $\text{CH}_3\text{COOH}$ ). Both compounds crystallize with molar ratios (N:acid) of 1:1. Similarly to the crystalline hydrates, the polymer chains are essentially in a planar zigzag conformation. In the LPEI – HCl complex, the very close N  $\cdots$  Cl distance (3.05 Å) indicates the formation of strong hydrogen bonds between NH groups and Cl ions. The melting temperature of 265°C approaches the thermal decomposition of pure LPEI (~290°C), and can be attributed to those strong interactions. In the LPEI –  $\text{CH}_3\text{COOH}$  complex the polymer chain and the acetic acid molecules are linked by N-H  $\cdots$  O and O-H  $\cdots$  N hydrogen bonds to form a polymeric two dimensional structure. The melting

temperature of this complex is  $\sim 135^{\circ}\text{C}$ , which is still higher than those of the LPEI hydrates.

LPEI has been shown to dissolve a variety of alkali metal salts, such as NaTf, LiTf, LiClO<sub>4</sub>, LiBF<sub>4</sub>, LiSbF<sub>6</sub>, LiF, LiCl, LiBr, LiI, and LiSCN.<sup>64,134-141</sup> Chiang et al. reported the formation of a crystalline complex of LPEI (MW = 2000) with NaI.<sup>63</sup> X-ray and DSC studies revealed a decrease in LPEI crystallinity with addition of NaI. At a 0.15 mole ratio of electrolyte no X-ray pattern due to pure LPEI or pure NaI could be observed indicating full dissolution of the salt. For mole ratios  $\geq 0.3$  a new melting transition was observed in the DSC data and the X-ray diffraction pattern showed the presence of a new crystalline phase attributed to the PEI-NaI complex. Also for these concentrations, X-ray patterns show the presence of a discrete phase of pure NaI. Unfortunately a more structural detailed analysis was not possible because no oriented fiber of the crystalline material could be prepared. LPEI (MW = 100,000) also forms a crystalline complex with NaTf.<sup>64</sup> Again, as the electrolyte is added, the crystallinity of LPEI is destroyed and for higher salt concentrations, X-ray diffraction patterns indicate the formation of a partly crystalline complex with a stoichiometry of (PEI)<sub>4</sub>-NaCF<sub>3</sub>SO<sub>3</sub>. For higher salt concentrations, reflections from pure NaTf are observed in the X-ray diffraction pattern.

When alkali metal salts are added, the crystallinity of LPEI decreases greatly for salt molar ratios usually higher than 10:1.<sup>134,136</sup> The disordering of the crystalline phase is due to the breaking of the intermolecular hydrogen bonds upon addition of salt. It is evidenced in the DSC data by the loss of the melting transition of crystalline LPEI and an increase in the glass transition temperature of the amorphous phase. The increases in  $T_g$  can be attributed to the stiffening of the polymer chains upon coordination to the alkali

metal ion. Spectroscopically, the loss of crystallinity is evidenced by an increase of the infrared and Raman bandwidths. In particular, the NH stretching region contains two different peaks attributed to the crystalline and amorphous regions of the polymer.<sup>136</sup>

The ionic conductivity of the LPEI – alkali salt systems are very poor in general. Tanaka et al. compared LPEI-LiTf and LPEI-LiClO<sub>4</sub>; they reported the highest conductivity value of  $2 \times 10^{-6} \text{ S cm}^{-1}$  at 60°C for the LPEI-LiTf system at a N:Li ratio of 15:1.<sup>135</sup> In general, PEI-LiTf systems are more conductive than PEI-LiClO<sub>4</sub> at comparable salt concentration and temperature. In addition, for concentrations above 15:1 the conductivity was lower in both systems. Chiang et al. reported conductivity values for PEI-LiClO<sub>4</sub> and PEI-LiBF<sub>4</sub> at 10:1 molar ratios between room temperature ( $\sim 10^{-8} \text{ S cm}^{-1}$ ) and 150°C ( $\sim 10^{-3} \text{ S cm}^{-1}$ ).<sup>134</sup> For both systems, they concluded that the conductivity values are similar to those of the respective PEO-salt systems for comparable levels of salts. The PEI-NaI system exhibit a conductivity of  $1.5 \times 10^{-6} \text{ S cm}^{-1}$  at 60°C for the 10:1 sample.<sup>63</sup> An abrupt change in the slope of the conductivity plot as a function of reciprocal temperature is observed around 60°C, with represent the melting temperature of the semi-crystalline PEI phase. In the 3:1 crystalline complex, there is no evidence of a phase change in the conductivity values going through the melting temperature of the complex at 150°C. Only for temperatures above 120°C, the conductivity values for the crystalline compound exceed that of pure PEI. Harris et al. reported conductivity values for the PEI-NaTf system.<sup>64</sup> At 41°C, the 5:1 and 6:1 complexes have similar conductivity values ( $3.1 \times 10^{-6}$  and  $2.4 \times 10^{-6} \text{ S cm}^{-1}$ , respectively) while the conductivity of the semicrystalline 4:1 compound is almost one order of magnitude lower ( $5.6 \times 10^{-6} \text{ S cm}^{-1}$ ).

### 2.3.2. Branched form

Under normal conditions of synthesis, the ring-opening cationic polymerization of aziridine yields highly branched poly(ethylenimine) or BPEI.<sup>125,126,142,143</sup> One of the advantages of using BPEI over LPEI as a polymer host is that it forms homogeneous amorphous polymer salt complexes. As mentioned previously, the ionic conductivity is thought to occur primarily in the amorphous phase. Such a conducting amorphous structure is obtained only above the glass transition temperature, so one way (maybe) to increase the conductivity is to decrease  $T_g$ , which facilitates relaxation processes and therefore, transport. BPEI is fully amorphous due to its high degree of branching and has a  $T_g$  reported as  $-47^\circ\text{C}$ .<sup>144,145</sup> A commercial BPEI contains in average 25% primary amines, 50% secondary amines, and 25% tertiary amines<sup>146-148</sup>, although a study conducted by Pierre *et al.* have found a different result by  $^{13}\text{C}$  NMR.<sup>149</sup> They report 38% of primary, 36% of secondary and 26% of tertiary amines.

There have been only a few reports on branched PEI used as a host for polymer electrolytes. Harris *et al.* investigated BPEI with NaTf and compared the results with analogous complexes made with LPEI.<sup>144</sup> They reported glass transition temperature values and conductivity data for salt concentration between 20:1 and 6:1 nitrogen to salt ratio. In the branched PEI, as the salt concentration increases, the  $T_g$  values increases and the ionic conductivity decreases. At a 20:1 composition, BPEI is a better ionic conductor than LPEI, which is directly related to the fact that the BPEI complex is amorphous whereas the LPEI complex contains a crystalline phase. At a 6:1 composition, the conductivity of LPEI:NaTf is higher than that of BPEI:NaTf. At this composition, both complexes are amorphous but the  $T_g$  value of the linear complex is lower.

Paul et al. conducted a similar study of BPEI, only with the lithium triflate salt instead of the sodium salt.<sup>145</sup> The conductivity and calorimetric data they obtained for the BPEI:LiTf system follow the same trends of those of the BPEI:NaTf system. As in the NaTf system, the highest conductivity value is obtained at low salt concentrations (N:Li = 20) and is on the order of  $10^{-6}$  S cm<sup>-1</sup> at 20°C. The authors also reported the existence of a semi-crystalline phase of 4:1 composition, indicated by the presence of an endotherm peak of melting at 49°C. No x-ray data were reported. Because of the high degree of branching, the presence of this semi-crystalline phase is somewhat disturbing. In fact, during the course of my research on the BPEI – NaTf system, a crystalline phase was observed by x-ray diffraction. It was attributed to a NaTf – MeOH crystalline phase, where methanol was the solvent used in the polymer electrolyte preparation.

#### **2.4. POLY(N-METHYLETHYLENIMINE)**

Poly(N-methylethylenimine) or PMEI is a methyl-substituted derivative of the poly(ethylenimine) polymer. The linear form and the branched form have been synthesized from LPEI and BPEI, respectively. Both polymers are completely amorphous at room temperature, with  $T_g$  values around -91°C.<sup>135,150</sup> LPMEI has been previously investigated with LiClO<sub>4</sub>, LiTf, and NaTf, and characterized by infrared spectroscopy, differential scanning calorimetry, and complex impedance.<sup>135,151,152</sup> In general, the addition of salt to LPMEI increased the  $T_g$  values in all the systems. Temperature dependence conductivity measurements showed that LPMEI is a poor ionic conductor. The LPMEI:LiTf 15:1 sample showed the highest ionic conductivity at all temperatures between 20°C and 120°C, and is on the order of  $10^{-6}$  S cm<sup>-1</sup> at 60°C.<sup>135</sup>

Infrared temperature dependence studies of LPMEI:LiTf showed particularly interesting behavior of the ionic speciation when increasing the temperature.<sup>152</sup> Unlike poly(ethylene oxide) and poly(propylene oxide) – salt systems, the ionic speciation decreases, i.e. shift from contact ion pair to “free” ions, when increasing temperature. In addition, LPMEI with NaTf has been found to form a crystalline phase, evidenced by the presence of an endothermic transition in the DSC thermogram, and strong reflections in the powder x-ray diffraction.<sup>150</sup> There are no data available on the branched methylated polymer, since it has never been studied.

## 2.5. REFERENCES

- (1) Fenton, D. E.; Parker, J. M.; Wright, P. V. *Polymer* **1973**, *14*, 589.
- (2) Wright, P. V. *Br. Polymer J.* **1975**, *7*, 319.
- (3) Armand, M. D.; Chabagno, J. M.; Duclot, M. J. “Polymeric Solid Electrolytes”; Sec. Int. Conf. on Solid Electrolytes, 1978, St. Andrews, Scotland.
- (4) Armand, M. B.; Chabagno, J. M.; Duclot, M. J. Polyethers as Solid Electrolytes. In *Fast Ion Transport in Solids*; Vashista, P., Mundy, J. M., Shenoy, G. K., Eds.; North-Holland: Amsterdam, 1979; pp 131.
- (5) Shriver, D. F.; Bruce, P. G. Polymer electrolytes I: General principles. In *Solid State Electrochemistry*; Bruce, P. G., Ed.; Cambridge University Press: Cambridge, 1995; pp 95.
- (6) MacCallum, J. R.; Vincent, C. A. Ion-molecule and ion-ion interactions in polymer electrolytes. In *Polymer Electrolyte Reviews 1*; MacCallum, J. R., Vincent, C. A., Eds.; Elsevier Applied Science: New York, 1987; Vol. 1; pp 23.
- (7) Vincent, C. A. *Prog. Solid State Chem.* **1987**, *17*, 145.
- (8) Bruce, P. G.; Gray, F. M. Polymer Electrolytes II: Physical Principles. In *Solid State Electrochemistry*; Bruce, P. G., Ed.; University Press: Cambridge, 1995; pp 119.
- (9) Baril, D.; Minchot, C.; Armand, M. *Solid State Ionics* **1997**, *94*, 35.

- (10) Dell, R. M. *Solid State Ionics* **2000**, 139.
- (11) Tarascon, J.-M.; Armand, M. *Nature* **2001**, 414, 359.
- (12) Oman, H. *MRS Bulletin* **1999**, 33.
- (13) Meyer, W. H. *Adv. Mater.* **1998**, 10, 439.
- (14) Wright, P. V. *Electrochim. Acta* **1998**, 43, 1137.
- (15) Vincent, C. A. *Solid State Ionics* **2000**, 134, 159.
- (16) Abraham, K. M.; Alamgir, M. *Solid State Ionics* **1994**, 70/71, 20.
- (17) Xu, K. *Chem. Rev.* **2004**, 104, 4303.
- (18) Winter, M.; Brodd, R. J. *Chem. Rev.* **2004**, 104, 4245.
- (19) Armand, M.; Gauthier, M. Polymeric Solid Ion Conductors - The Immobile Solvent Concept. In *High Conductivity Solid Ionic Conductors*; Takahashi, T., Ed.; World Scientific Press: New Jersey, 1989; pp 114.
- (20) Armand, M. B. Current state of PEO-based electrolytes. In *Polymer Electrolytes Reviews I*; MacCallum, J. R., Vincent, C. A., Eds.; Elsevier applied science: New York, 1987; Vol. 1; pp 1.
- (21) Stevens, J. R.; Schantz, S. *Polym. Commun.* **1988**, 29, 330.
- (22) Cameron, G. G.; Ingram, M. D. Liquid Polymer Electrolytes. In *Polymer Electrolyte Reviews 2*; MacCallum, J. R., Vincent, C. A., Eds.; Elsevier Applied Science: New York, 1989; Vol. 2; pp 157.
- (23) Ratner, M. A.; Shriver, D. F. *Chem. Rev.* **1988**, 88, 109.
- (24) Ratner, M. A. Aspects of the Theoretical Treatment of Polymer Solid Electrolytes: Transport Theory and Models. In *Polymer Electrolyte Reviews*; MacCallum, J. R., Vincent, C. A., Eds.; Elsevier Applied Science: New York, 1987; Vol. 1; pp 173.
- (25) Papke, B. L.; Ratner, M. A.; Shriver, D. F. *J. Phys. Chem. Solids* **1981**, 42, 493.
- (26) Papke, B. L.; Ratner, M. A.; Shriver, D. F. *J. Electrochem. Soc.* **1982**, 129, 1694.
- (27) Shriver, D. F.; Papke, B. L.; Ratner, M. A.; Dupont, R.; Wong, T.; Brodwin, M. *Solid State Ionics* **1981**, 5, 83.
- (28) Armand, M. B. *Ann. Rev. Mater. Sci.* **1986**, 16, 245.
- (29) Whittingham, M. S. *Chem. Rev.* **2004**, 104, 4271.

- (30) Owen, J. R. Ion Conducting Polymers. In *Electrochemical Science and Technology of Polymers I*; Linford, R. G., Ed.; Elsevier Applied Science: New York, 1987; pp 45.
- (31) Gray, F. M. *Solid Polymer Electrolytes: Fundamentals and Technological Applications*; VCH Publishers, Inc.: New York, 1991.
- (32) Munshi, M. Z. A.; Owens, B. B. *Polymer J.* **1988**, *20*, 577.
- (33) Killis, A.; LeNest, J. F.; Gandini, A.; Cheradame, H. *Macromolecules* **1984**, *17*, 63.
- (34) Bruce, P. G.; Vincent, C. A. *J. Chem. Soc. Faraday Trans.* **1993**, *89*, 3187.
- (35) Schantz, S. *J. Chem. Phys.* **1991**, *94*, 6296.
- (36) Torell, L. M.; Jacobsson, P.; Petersen, G. *Polymers for Advanced Technologies* **1993**, *4*, 152.
- (37) Pearson, R. G. *J. Am. Chem. Soc.* **1963**, *85*, 3533.
- (38) Bruce, P. G.; Krok, F.; Vincent, C. A. *Solid State Ionics* **1988**, *27*, 81.
- (39) Cowie, J. M. G.; Cree, S. H. Electrolytes dissolved in polymers. In *Annu. Rev. Phys. Chem.*; Strauss, H. L., Babcock, G. T., Moore, C. B., Eds.; Annual Reviews Inc.: Palo Alto, 1989; Vol. 40; pp 85.
- (40) Berthier, C.; Gorecki, W.; Minier, M. *Solid State Ionics* **1983**, *11*, 91.
- (41) Stainer, M.; Hardy, L. C.; Whitmore, D. H.; Shriver, D. F. *J. Electrochem. Soc.* **1984**, *131*, 784.
- (42) Watanabe, M.; Oohashi, S.; Sanui, K.; Ogata, N.; Kobayashi, T.; Ohtaki, Z. *Macromolecules* **1985**, *18*, 1945.
- (43) Ratner, M. A.; Nitzan, A. *Faraday Discuss. Chem. Soc.* **1989**, *88*, 19.
- (44) Dillon, R. E.; Shriver, R. F. *Chem. Mater.* **2001**, *13*, 1369.
- (45) Blonsky, P. M.; Shriver, D. F.; Austin, P.; Allcock, H. R. *J. Am. Chem. Soc.* **1984**, *106*, 6854.
- (46) Blonsky, P. M.; Shriver, D. F.; Austin, P.; Allcock, H. R. *Solid State Ionics* **1986**, 258.
- (47) Allcock, H. R.; Napierala, M. E.; Olmeijer, D. L.; Best, S. A.; Merz, K. M., Jr. *Macromolecules* **1999**, *32*, 732.

- (48) Allcock, H. R.; O'Connor, S. J. M.; Olmeijer, D. L.; Napierala, M. E.; Cameron, C. G. *Macromolecules* **1996**, *29*, 7544.
- (49) Robitaille, C. D.; Fauteux, D. *J. Electrochem. Soc.* **1986**, *133*, 315.
- (50) Lee, C. C.; Wright, P. V. *Polymer* **1982**, *23*, 681.
- (51) Minier, M.; Berthier, C.; Gorecki, W. *J. Physique* **1984**, *45*, 739.
- (52) Gorecki, W.; Andreani, R.; Berthier, C.; Armand, M.; Chabagno, J. M.; Rigaud, D. *Solid State Ionics* **1986**, *18/19*, 295.
- (53) Hibma, T. *Solid State Ionics* **1983**, *9-10*, 1101.
- (54) Parker, J. M.; Wright, P. V.; Lee, C. C. *Polymer* **1981**, *22*, 1305.
- (55) Fauteux, D.; Lupien, M. D.; Robitaille, C. D. *J. Electrochem. Soc.* **1987**, *134*, 2761.
- (56) Gray, F. M.; MacCallum, J. R.; Vincent, C. A. *Solid State Ionics* **1986**, *18/19*, 282.
- (57) Zahurak, S. M.; Kaplan, M. L.; Rietman, E. A.; Murray, D. W.; Cava, R. J. *Macromolecules* **1988**, *21*, 654.
- (58) Ferloni, P.; Chiodelli, G.; Magistris, A.; Sanesi, M. *Solid State Ionics* **1986**, *18/19*, 265.
- (59) Minier, M.; Berthier, C.; Gorecki, W. *Solid State Ionics* **1983**, *9/10*, 1125.
- (60) Besner, S.; Vallée, A.; Bouchard, G.; Prud'homme, J. *Macromolecules* **1992**, *25*, 6480.
- (61) Weston, J. E.; Steele, B. C. H. *Solid State Ionics* **1982**, *7*, 81.
- (62) Vallée, A.; Besner, S.; Prud'homme, J. *Electrochim. Acta* **1992**, *37*, 1579.
- (63) Chiang, C. K.; Davis, G. T.; Harding, C. A.; Takahashi, T. *Macromolecules* **1985**, *18*, 825.
- (64) Harris, C. S.; Shriver, D. F.; Ratner, M. A. *Macromolecules* **1986**, *19*, 987.
- (65) Gadjourova, Z.; Andreev, Y. G.; Tunstall, D. P.; Bruce, P. G. *Nature* **2001**, *412*, 520.
- (66) Gadjourova, Z.; Marero, D. M.; Andersen, K. H.; Andreev, Y. G.; Bruce, P. G. *Chem. Mater.* **2001**, *13*, 1282.
- (67) Andreev, Y. G.; Bruce, P. G. *J. Physic.:Condens. Matter* **2001**, *13*, 8245.
- (68) Andreev, Y. G.; Bruce, P. G. *Electrochim. Acta* **2000**, *45*, 1417.

- (69) Catlow, C. R. A.; Chadwick, A. V.; N., G. G.; Moroney, L. M.; Worboys, M. R. *Solid State Ionics* **1983**, 9/10, 1107.
- (70) Catlow, C. R. A.; Mills, G. E. *Electrochim. Acta* **1995**, 40, 2057.
- (71) Chadwick, A. V.; Worboys, M. R. NMR, EXAFS and radiotracer techniques in the characterization of polymer electrolytes. In *Polymer Electrolytes Reviews I*; MacCallum, J. R., Vincent, C. A., Eds.; Elsevier Science Publishing: New York, 1987; Vol. 1; pp 275.
- (72) Linford, R. G. *Chem. Soc. Rev.* **1995**, 24, 267.
- (73) Kasatani, K.; Sato, H. *Chem. Soc. Jpn. Lett.* **1986**, 6, 991.
- (74) Nazri, G.-A.; MacArthur, D. M.; O'Gara, J. F. *Mat. Res. Soc. Symp. Proc.* **1991**, 210, 163.
- (75) Greenbaum, S. G.; Pak, Y. S.; Adamic, K. J.; Wintersgill, M. C.; Fontanella, J. J. *Mat. Res. Soc. Symp. Proc.* **1991**, 210, 237.
- (76) Liu, K.; Parsons, J. L. *Macromolecules* **1969**, 2, 529.
- (77) Machida, K.; Miyazawa, T. *Spectrochim. Acta* **1964**, 20, 1865.
- (78) Matsuura, H.; Fukuhara, K. *J. Polym. Sci. B* **1986**, 24, 1383.
- (79) Matsuura, H.; Fukuhara, K.; Tamaoki, H. *J. Sci. Hiroshima Univ., Ser. A* **1985**, 49, 89.
- (80) Matsuura, H.; Miyazawa, T. *J. Polym. Sci., Pt. A-2* **1969**, 7, 1735.
- (81) Matsuura, H.; Miyazawa, T.; Machida, K. *Spectrochim. Acta* **1973**, 29A, 771.
- (82) Maxfield, J.; Shepherd, I. W. *Polymer* **1975**, 16, 505.
- (83) Yang, X.; Su, Z.; Wu, D.; Hsu, S.; Stidham, H. *Macromolecules* **1997**, 30, 3796.
- (84) Yoshihara, T.; Tadokoro, H.; Murahashi, S. *J. Chem. Phys.* **1964**, 41, 2902.
- (85) York, S. S.; Boesch, S. E.; Wheeler, R. A.; Frech, R. *Macromolecules* **2003**, 36, 7348.
- (86) Sanders, R. A.; Frech, R.; Khan, M. A. *J. Phys. Chem. B* **2004**, 108, 2186.
- (87) Boesch, S. E.; York, S.; Frech, R.; Wheeler, R. A. *PhysChemComm(1)* **2001**.
- (88) Bernson, A.; Lindgen, J.; Huang, W.; Frech, R. *Polymer* **1995**, 36, 4471.
- (89) Dissanayake, M. A. K. L.; Frech, R. *Macromolecules* **1995**, 28, 5312.
- (90) Frech, R.; Huang, W. *Macromolecules* **1995**, 28, 1246.

- (91) Yoon, S.; Ichikawa, K.; MacKnight, W. J.; Hsu, S. L. *Macromolecules* **1995**, *28*, 4278.
- (92) Huang, W.; Frech, R.; Wheeler, R. A. *J. Phys. Chem.* **1994**, *98*, 100.
- (93) Schantz, S.; Sandahl, J.; Borjesson, L.; Torell, L. M.; Stevens, J. R. *Solid State Ionics* **1988**, *28-30*, 1047.
- (94) Doeff, M. M.; Georen, P.; Qiao, J.; Kerr, J.; De Jonghe, L. C. *J. Electrochem. Soc.* **1999**, *146*, 2024.
- (95) Ferry, A.; Doeff, M. M.; DeJonghe, L. C. *Electrochim. Acta* **1998**, *43*, 1387.
- (96) Ma, Y.; Doyle, M.; Fuller, T. F.; Doeff, M. M.; Jonghe, L. C. D.; Newman, J. J. *Electrochem. Soc.* **1995**, *142*, 1859.
- (97) Bruce, P. G.; Vincent, C. A. *Solid State Ionics* **1990**, *40-41*, 607.
- (98) Battisti, D.; Nazri, G. A.; Klassen, B.; Aroca, R. *J. Phys. Chem.* **1993**, *97*, 5826.
- (99) Klassen, B.; Aroca, R.; Nazri, G. A. *J. Phys. Chem.* **1996**, *100*, 9334.
- (100) Klassen, B.; Aroca, R.; Nazri, M.; Nazri, G. A. *J. Phys. Chem. B* **1998**, *102*, 4795.
- (101) Frech, R.; Huang, W. *J. Solution Chem.* **1994**, *23*, 469.
- (102) Frech, R.; Huang, W.; Dissanayake, M. A. K. L. *Mat. Res. Soc. Symp. Proc.* **1995**, *369*, 523.
- (103) Kakihana, M.; Shantz, S.; Torell, L. M. *J. Chem. Phys.* **1990**, *94*, 6271.
- (104) Kakihana, M.; Schantz, S.; Torell, L. M. *Solid State Ionics* **1990**, *40/41*, 641.
- (105) Frech, R.; York, S.; Allcock, H.; Kellam, C. *Macromolecules* **2004**, *37*, 8699.
- (106) Papke, B. L.; Dupon, R. W.; Ratner, M. A.; Shriver, D. F. *Solid State Ionics* **1981**, *5*, 685.
- (107) Ratner, M. A.; Johansson, P.; Shriver, D. F. *MRS Bulletin* **2000**, *25*, 31.
- (108) Cheradame, H. In *IUPAC Macromolecules*; Benoit, H., Rempp, P., Eds.; Pergamon Press.: New York, 1982; pp 251.
- (109) Killis, A.; Le Nest, J. F.; Cheradame, H. *Makromol. Chem. Rapid Commun.* **1980**, *1*, 595.
- (110) Killis, A.; Le Nest, J. F.; Gandini, A.; Cheradame, H. *J. Polym. Sci., Polym. Phys. Ed.* **1981**, *19*, 1073.
- (111) Armand, M. *Solid State Ionics* **1983**, *9/10*, 745.
- (112) Fulcher, G. S. *J. Am. Chem. Soc.* **1925**, *8*, 339.

- (113) Tamman, G.; Hesse, W. *Z. Anorg. Allg. Chem.* **1926**, *165*, 245.
- (114) Vogel, H. *Phys. Z.* **1921**, *22*, 645.
- (115) Angell, C. A. *Solid State Ionics* **1986**, *18/19*, 92.
- (116) McLin, M.; Angell, C. A. *J. Phys. Chem.* **1988**, *92*, 2083.
- (117) Cheradame, H.; Le Nest, J. F. Ionically Conducting Polyether Networks. In *Polymer Electrolytes Reviews I*; MacCallum, J. R., Vincent, C. A., Eds.; Elsevier Applied Science: New York, 1987; Vol. 1; pp 103.
- (118) Killis, A.; Le Nest, J. F.; Cheradame, H.; Gandini, A. *Makromol. Chem.* **1982**, *183*, 2835.
- (119) Angell, C. A. *Ann. Rev. Phys. Chem.* **1992**, *43*, 693.
- (120) Williams, M. L.; Landel, R. F.; Ferry, J. D. *J. Am. Chem. Soc.* **1955**, *77*, 3701.
- (121) Cole, K. S.; Cole, R. H. *J. Chem. Phys.* **1941**, *9*, 341.
- (122) MacDonald, J. R. *J. Chem. Phys.* **1973**, *58*, 4982.
- (123) MacDonald, J. R. Superionic Conductors; Mahan, G. D., Roth, W. L., Eds.; Plenum Press: New York, 1976; pp 81.
- (124) Wright, P. V. Morphology and Thermal Properties of Crystalline Complexes of Poly(ethylene oxide) and Alkali Salts. In *Polymer Electrolytes Reviews 2*; MacCallum, J. R., Vincent, C. A., Eds.; Elsevier Applied Science: New York, 1989; Vol. 2; pp 61.
- (125) Saegusa, T.; Ikeda, H.; Fujii, H. *Polym. J.* **1972**, *3*, 35.
- (126) Saegusa, T.; Ikeda, H.; Fujii, H. *Macromolecules* **1972**, *5*, 108.
- (127) Ludwick, A. G.; Overberger, C. G. *J. Poly. Sci., Poly. Chem. Ed.* **1982**, *20*, 2123.
- (128) Tanaka, R.; Ueoka, I.; Takaki, Y.; Kataoka, K.; Saito, S. *Macromolecules* **1983**, *16*, 849.
- (129) Chatani, Y.; Kobatake, T.; Tadokoro, H.; Tanaka, Y. *Macromolecules* **1982**, *15*, 170.
- (130) Chatani, Y.; Kobatake, T.; Tadokoro, H. *Macromolecules* **1983**, *16*, 199.
- (131) Chatani, Y.; Tadokoro, H.; Saugus, T.; Ikede, H. *Macromolecules* **1981**, *14*, 315.
- (132) Chatani, Y.; Irie, T. *Polymer* **1988**, *29*, 2126.
- (133) Chatani, Y.; Yakura, Y.; Ishioka, T. *Polymer* **1990**, *31*, 208.

- (134) Chiang, C. K.; Davis, G. T.; Harding, C. A.; Takahashi, T. *Solid State Ionics* **1986**, *18/19*, 300.
- (135) Tanaka, R.; Fujita, T.; Nishibayashi, H.; Saito, S. *Solid State Ionics* **1993**, *60*, 119.
- (136) York, S.; Frech, R.; Snow, A.; Glatzhofer, D. *Electrochim. Acta* **2001**, *46*, 1533.
- (137) York, S. R. S. Local Structures and Conductivity in Polyethylenimine and Polyphosphazene Polymer Electrolytes. Dissertation, University of Oklahoma, 2002.
- (138) Buckner, M.; York, S. S.; Frech, R.; Glatzhofer, D. T. *Polym. Prepr.* **2003**, *44*, 1085.
- (139) Tanaka, R.; Sakurai, M.; Sekiguchi, H.; Mori, H.; Murayama, T.; Ooyama, T. *Electrochim. Acta* **2001**, *46*, 1709.
- (140) Kobayashi, S.; Shirasaka, H.; Suh, K.-D.; Uyama, H. *Polym. J.* **1990**, *22*, 442.
- (141) York, S.; Buckner, M.; Frech, R. *Macromolecules* **2004**, *37*, 994.
- (142) Hauser, M. *Ring-Opening Polymerization*; Marcel Dekker: New York and London, 1969.
- (143) Goethals, E. J. *Adv. Polym. Sci.* **1977**, *23*, 103.
- (144) Harris, C. S.; Ratner, M. A.; Shriver, D. F. *Macromolecules* **1987**, *20*, 1778.
- (145) Paul, J.-L.; Jegat, C.; Lassegues, J.-C. *Electrochim. Acta* **1992**, *37*, 1623.
- (146) Dick, C. R.; Ham, G. E. *J. Macromol. Sci., Chem.* **1970**, *A4*, 1301.
- (147) Jones, G. D.; MacWilliams, D. C.; Braxton, N. A. *J. Org. Chem.* **1965**, *30*, 1994.
- (148) Ham, G. E. *Polymeric Amines and Ammonium Salts*; Pergamon: Oxford, 1980.
- (149) Pierre, T. S.; Geckle, M. *J. Macromol. Sci., Chem.* **1985**, *A22 (5-7)*, 877.
- (150) Sanders, R. A.; Snow, A. G.; Frech, R.; Glatzhofer, D. T. *Electrochim. Acta* **2003**, *48*, 2247.
- (151) Sanders, R. A.; Boesch, S. E.; Snow, A. G.; Hu, L. R.; Frech, R.; Wheeler, R. A.; Glatzhofer, D. T. *Polym. Prepr.* **2003**, *44*, 996.
- (152) Frech, R.; Giffin, G. A.; Castillo, F. Y.; Glatzhofer, D.; Eisenblatter, J. *Electrochim. acta* **2005**, *50*, 3963.

### 3. EXPERIMENTAL

#### 3.1. SAMPLE PREPARATION

Hexylamine (HEXA), N,N-dimethylethylenediamine (DMEDA), dipropylamine (DPA), branched poly(ethylenimine) (BPEI, number average molecular weight=10,000), anhydrous acetonitrile, tetrabutylammonium trifluoromethane sulfonate (TbaTf), lithium trifluoromethane sulfonate (LiTf), sodium trifluoromethane sulfonate (NaTf), and sodium tetraphenylborate (NaBPh<sub>4</sub>) were obtained from Aldrich. LiTf and NaTf were heated at 120°C under a vacuum of 1 bar for about 48 hours before use. Methanol was dried by distilling over sodium metal. Carbon tetrachloride (CCl<sub>4</sub>) was obtained from Fisher Scientific (99.9%, A.C.S. reagent) and distilled before use. Branched poly(methylethylenimine) (BPMEI) was synthesized by Lieyu (Richard) Hu and Frank Yopez Castillo using previously reported methods.<sup>1,2</sup> All the chemicals were stored and used in a dry argon glove box (VAC, ≤ 1ppm H<sub>2</sub>O) at room temperature.

#### *Polymer electrolytes*

All the BPEI – salt solutions were prepared by dissolving weighed amounts of polymer and salt in dry methanol and stirring for approximately 24 hours to insure a homogeneous solution before casting as films. The BPMEI – salt solutions were prepared in a similar manner, using anhydrous acetonitrile instead of methanol. The compositions of the samples are reported as a nitrogen to cation molar ratio (N:M<sup>+</sup>).

#### *Model compound – salt complexes*

All the model compound – salt solutions were prepared by mixing weighed amounts of salt and solvent. The solutions were stirred for a minimum of 24 hours before

use. The compositions of the samples are reported as the nitrogen to cation molar ratio (N:M<sup>+</sup>). The model compound – salt solutions were prepared with compositions ranging from 40:1 to 3:1.

### *Crystalline samples*

The HEXA:LiTf crystals formed by leaving solutions in the glove box at room temperature for a long period of time (~6 months). The crystals were white (clear under the microscope) and grainy, and seemed to form out of the highly concentrated solutions first (3:1 to 10:1). The entire sample was composed of crystals with no solution left in the vial.

The DPA:LiTf crystals formed in about 3 months out of solutions left in a glove box at room temperature. The DPA:LiTf crystals grew as thin and clear needles that formed more rapidly in the low concentrated solutions (30:1, 40:1). After the crystals appeared, no solution was present in the vial.

The DMEDA:LiTf and DMEDA:NaTf crystals formed by slow evaporation of solutions of various concentrations in the glove box. The crystals were clear thin plates that formed first out of the highly concentrated solutions (3:1); these solutions also produced the highest quality crystals. In general, the sodium complex formed more rapidly than the lithium complex. In both systems, a thin clear “crust” appeared at the surface of the solution after a couple of months. A few months later, thin crystalline plates were floating in the solution.

In the DMEDA:NaBPh<sub>4</sub> solutions with composition of 10:1 and higher, both a liquid and a gel-like phase formed almost immediately after mixing the starting compounds. The solutions were left in the glove box at room temperature, and crystals

appeared after a short period of time ranging from a couple of days for the highly concentrated solutions to a couple weeks for the 10:1 and 20:1 samples. The DMEDA:NaBPh<sub>4</sub> crystals were slightly pink with a brown tone and chunky.

The HEXA NaBPh<sub>4</sub> solutions were clear at all salt compositions. The crystals formed within a couple of weeks in the highly concentrated solutions and within months for lower concentrations. The HEXA:NaBPh<sub>4</sub> crystals also have a pink brown tint and were chunky.

#### *Carbon tetrachloride dilution samples*

The amine – CCl<sub>4</sub> solutions were prepared by mixing weighed amounts of amines and CCl<sub>4</sub>. The compositions of these samples are reported as a CCl<sub>4</sub> to nitrogen molar ratio (CCl<sub>4</sub>:N). Similarly, the electrolytes – CCl<sub>4</sub> solutions were prepared by mixing weighed amounts of the components. The compositions of these samples are also reported as CCl<sub>4</sub> to nitrogen molar ratio.

### **3.2. SPECTROSCOPY**

#### *Fourier Transform infrared spectroscopy*

Infrared data were collected using a Bruker IFS66V FT-IR spectrometer (KBr beam splitter) under vacuum (11 mbar) for the polymeric and crystalline samples and under dry air purge for the liquid samples. The data were recorded over a range of 500-4000 cm<sup>-1</sup> with a spectral resolution of 1 cm<sup>-1</sup>.

The polymer - salt samples for FT-IR studies were made by casting the solutions directly onto zinc selenide windows and drying at room temperature under argon for 24 hours. The samples were then dried under vacuum (1 bar) at room temperature for an

additional 24 hours to insure solvent removal. All the model compounds – salt solutions were placed between zinc selenide windows in a sealed sample holder, and the crystalline samples were ground with potassium bromide and pressed into thin pellets. The model – CCl<sub>4</sub> and electrolytes – CCl<sub>4</sub> samples were recorded using a sealed liquid cell equipped with a potassium bromide window.

Curve-fitting analysis of the N–H stretching bands, and some of the triflate bands, was done using commercially available software Thermo Galactic (Grams / AI 7.00). The spectral bands were fitted using a mixed Gaussian / Lorentzian product function and a straight baseline.

#### ***Fourier Transform Raman spectroscopy***

The FT Raman data were recorded at 2 cm<sup>-1</sup> resolution using a Bruker Equinox 55 equipped with a FRA 106/S system. The 1064 nm line of a Nd:YAG laser was used for excitation. There was a significant amount of fluorescence emitted in the BPMEI and BPMEI –LiTf system, therefore suitable Raman spectra could not be obtained. The pure BPEI, model compounds, model compound – salt samples (solution and crystalline), and all the CCl<sub>4</sub> dilution samples were sealed in a thin NMR tube under an argon atmosphere. The BPEI – salt samples were cast directly onto little mirrors and dried at room temperature under argon for 24 hours. The samples were then dried under vacuum (1 bar) at room temperature for an additional 24 hours to insure solvent removal.

#### ***Raman spectroscopy***

The Raman data were recorded with a Jobin Yvon T64000 spectrometer in the triple subtractive mode with a CCD detector. The 532 nm line of a doubled diode-pumped Nd:YAG laser was used for excitation with a power of 200 mW measured at the

laser head. All the data were collected in a 180° backscattering geometry. The Raman samples were sealed in a thin NMR tube under argon atmosphere.

### 3.3. X-RAY DIFFRACTION

All the data were collected on a Bruker Apex diffractometer using MoK $\alpha$  radiation ( $\lambda=0.71073$  Å). The structures were solved by the direct method using SHELXTL system, and refined by full-matrix least squares on F<sup>2</sup> using all reflections. All the non-hydrogen atoms were refined anisotropically. All the hydrogen atoms were included with idealized parameters.

Single crystals of HEXA:LiTf were isolated for x-ray analysis from a 3:1 solution. The data were collected at 86(2) K. The final R1 = 0.050 is based on 2374 “observed reflections” [ $I>2\sigma(I)$ ], and  $wR^2 = 0.155$  is based on all reflections (2600 unique reflections). The C1, C2 and C3 carbon atoms at the end of the hexylamine molecule were modeled using two components with 50% occupancy for each component due to the presence of some static disorder.

The best DPA:LiTf crystals suitable for x-ray analysis were isolated out of the 30:1 solution. The data were collected at 100(2) K. The final R1 = 0.088 is based on 2198 “observed reflections” [ $I>2\sigma(I)$ ], and  $wR^2 = 0.268$  is based on all reflections (2642 unique reflections). The dipropylamine ligand is extensively disordered and was modeled with two components (50% occupancy). However, there are additional minor components that could not be modeled due to unstable refinement. The R1 value of 0.088 and the large peaks in the final difference map are due to the disorder of the

dipropylamine ligand. Despite the extensive disorder, the geometry of the molecule is reasonable and the coordination of the lithium cation is unambiguously determined.

Single crystals for x-ray analysis were isolated from the 3:1 DMEDA:LiTf and DMEDA:NaTf solutions. Data from the DMEDA:LiTf crystal were collected at 103(2) K. The final  $R_1 = 0.039$  is based on 2074 “observed reflections” [ $I > 2\sigma(I)$ ], and  $wR^2 = 0.108$  is based on all reflections (2506 unique reflections). The triflate ion was modeled using two components with 50% occupancy for each component due to the presence of some static disorder. For the DMEDA:NaTf crystal, the data were collected at 90(2) K. The final  $R_1 = 0.063$  is based on 1584 “observed reflections” [ $I > 2\sigma(I)$ ], and  $wR^2 = 0.182$  is based on all reflections (2197 unique reflections).

Single crystals were isolated from the 5:1 DMEDA:NaBPh<sub>4</sub> solution and the 5:1 HEXA: NaBPh<sub>4</sub> solution for x-ray analysis. The DMEDA:NaBPh<sub>4</sub> crystal data were collected at 95(2) K; the final  $R_1 = 0.042$  is based on 6216 “observed reflections” [ $I > 2\sigma(I)$ ], and  $wR^2 = 0.114$  is based on all reflections (7918 reflections). The HEXA: NaBPh<sub>4</sub> crystal data were collected at 100(2) K; the final  $R_1 = 0.086$  is based on 26930 “observed reflections” [ $I > 2\sigma(I)$ ], and  $wR^2 = 0.246$  is based on all reflections (30612 reflections). The high value of the R factors in the latter structure is due to the disorder in one of the molecules of the asymmetric unit. The hexylamine ligand and the sodium ion are disordered and were modeled with two components (50% occupancy). Despite the disorder, the geometry of the disordered molecule is reasonable and the coordination of the sodium cation is unambiguously determined.

### 3.4. DIFFERENTIAL SCANNING CALORIMETRY

Differential scanning calorimetry (DSC) thermograms were collected using a Mettler DSC 820 calorimeter under a dry nitrogen flow of 87mL/min at heating and cooling rates of 5°C/min. The thermograms were then analyzed using a STAR<sup>e</sup> v.6.10 software from Mettler Toledo.

BPEI and BPMEI electrolytes were cast on Teflon, dried under argon for 24 hours, and placed under vacuum at room temperature for at least 48 hours. BPEI – LiTf and BPEI – NaTf samples with compositions  $\leq 10:1$  were translucent with a light yellow tint. Low concentration BPEI – NaBPh<sub>4</sub> ( $\leq 10:1$ ) samples were also translucent, but with a light pink tint. For higher salt compositions, all the samples appeared lighter in color and more brittle. BPMEI and BPMEI – LiTf samples were dark brown in color. For concentrations above 15:1, the samples appeared stiffer with no change in color. After drying, 20-30 mg samples were sealed in 40  $\mu$ L aluminum pans under argon atmosphere. Each BPEI sample was cycled three times, with the first cycle from room temperature to 150 and then to -100°C. The next two cycles were from -100 to 100°C and back to -100°C. Each BPMEI sample was cycled three times, with the first cycle from room temperature to 150°C and then to -150°C. The next two cycles were from -150 to 50°C and back to -150°C. The reported data corresponds to an average of the second heating cycle of at least three different samples.

For HEXA:LiTf and DPA:LiTf, a 3 – 5 mg amount of crystalline material was sealed in 40  $\mu$ L aluminum pans under argon atmosphere. Each sample was cycled two times between 0 and 200°C. For DMEDA:LiTf and DMEDA:NaTf, an 8 – 15 mg amount of crystalline material was sealed in 40  $\mu$ L aluminum pans under argon

atmosphere. DMEDA:NaTf samples were cycled between 0 and 100°C. Experimental procedures for the DMEDA:LiTf crystals are not straightforward and are discussed in section 4.1.2, along with the results. For DMEDA:NaBPh<sub>4</sub> and HEXA:NaBPh<sub>4</sub>, 10 – 15 mg amounts of crystalline material were sealed in 40 μL aluminum pans under argon atmosphere. The DMEDA:NaBPh<sub>4</sub> crystals were cycled two times between 0 and 100°C and the HEXA: NaBPh<sub>4</sub> crystals were cycled two times between -50 and 90°C. Samples of both crystals were also taken to 200°C in previous experiments.

### **3.5. AC COMPLEX IMPEDANCE**

All polymer electrolytes samples were cast directly onto a 12.5 mm diameter stainless steel electrode in an argon atmosphere. The samples were allowed to dry 24 hours in the glove box and 48 hours under vacuum at room temperature before testing. The film thickness was measured using a micrometer built into the conductivity cell. Conductivity measurements were made over the frequency range 0.005-10000 kHz using a Hewlett-Packard 4192A LF impedance analyzer with Labview 5.1 software (National Instruments). All the BPEI conductivity data were measured using a heating cycle ranging from room temperature to 80°C in 10°C increments. After the first heating cycle, the sample was allowed to cool down to room temperature overnight and a second heating cycle was performed. For the BPMEI samples, the reproducibility of the conductivity data was checked by cycling the sample between room temperature and 80°C at least three times, collecting data at room temperature and 80°C only. Then data were collected in a heating cycle ranging from room temperature to 160°C in 20°C increments. Finally, measurements at room temperature and 160°C were repeated. For

BPEI - NaTf, LiTf, and NaBPh<sub>4</sub> systems, and BPMEI - LiTf system, the conductivities were not measured for compositions of 5:1 and above, due to interfacial contact problems between the electrodes and the electrolyte. The impedance plots were curve fitted using commercially available software Solartron Instruments LTD, Levm 7.1v.

### 3.6. REFERENCES

- (1) Sanders, R. A.; Boesch, S. E.; Snow, A. G.; Hu, L. R.; Frech, R.; Wheeler, R. A.; Glatzhofer, D. T. *Polym. Prepr.* **2003**, *44*, 996.
- (2) Sanders, R. A.; Snow, A. G.; Frech, R.; Glatzhofer, D. T. *Electrochim. Acta* **2003**, *48*, 2247.

## 4. MODEL COMPOUNDS, DILUTIONS IN CARBON TETRACHLORIDE, AND MODEL COMPOUNDS – SALT SYSTEMS

Model compounds are small organic molecules that structurally mimic small regions of a polymer. When complexed with a salt, their vibrational signatures can provide significant insight in the understanding of the polymer electrolytes at a molecular level. In these small molecular hosts, vibrational spectroscopy is a powerful tool for analyzing cation – host interactions, although the presence of ion-coordinating sites that are also hydrogen bonded presents a challenge. This is a particularly effective strategy for studying ionic coordination in polymers when both the polymer and the small molecule have the functional groups that coordinate in a similar manner. Polymer – cation interactions, polymer – anion interactions, and anion – cation interactions affect the local structure of a polymer electrolyte. These interactions are of primary interest in polymer electrolyte research for solid-state batteries as they are important factors in controlling the ionic conductivity.

Three small molecules were studied to further the investigation of branched polyethylenimine: hexylamine, N,N-dimethylethylenediamine, and dipropylamine. Additionally, many different salts were studied in an attempt to sort out the effect of the cation and anion: LiTf, NaTf, TbaTf, and NaBPh<sub>4</sub>. Some of the model salt complexes formed crystalline compounds whose structures were solved by x-ray diffraction. Unambiguous knowledge of local structures present in the crystalline compounds allowed a more precise set of spectral – (local) structure correlations to be developed. These

correlations were used with some degree of confidence to study interactions in the solution phases and in BPEI complexed with various salts.

#### 4.1. CRYSTAL STRUCTURES AND THERMAL ANALYSIS

##### 4.1.1. Hexylamine:LiTf

The compound hexylamine:LiTf crystallizes in an orthorhombic unit cell in the *Pbca* space group, with four (HEXA:LiTf) asymmetric units in the cell. The packing forms a polymeric two-dimensional network in the *a* and *b* directions as illustrated in Figure 4.1, with each lithium ion coordinated to one nitrogen atom from the hexylamine molecule and three triflate oxygen atoms from three different triflate ions (Figure 4.2). The structural data are summarized in Table 4.1. DSC measurements showed an onset of melting at 75°C with a midpoint at 80°C and an onset of recrystallization at 47°C with a midpoint at 44°C.

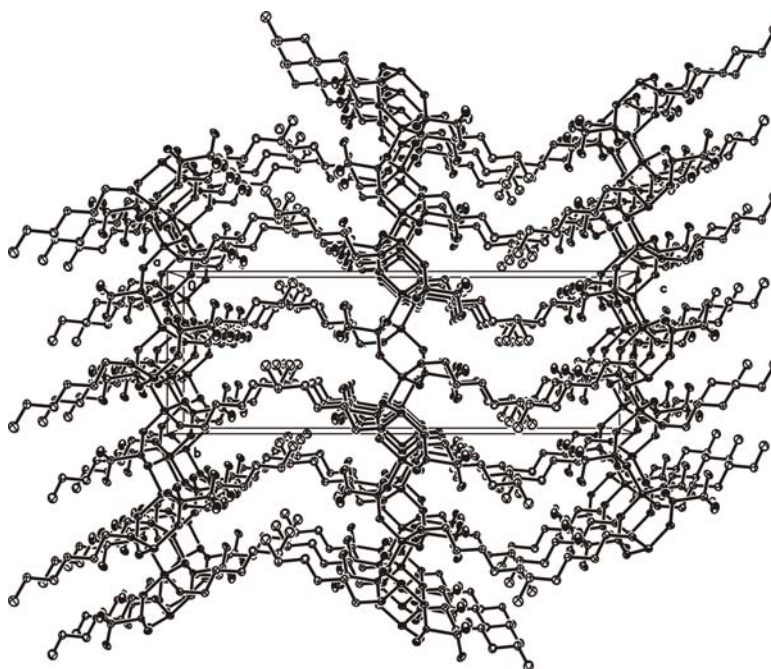


**Figure 4.1.** Packing diagram of the hexylamine:LiTf crystal projected down the crystallographic *a* axis. The crystal forms a 2D polymeric structure in the *ab* plane.

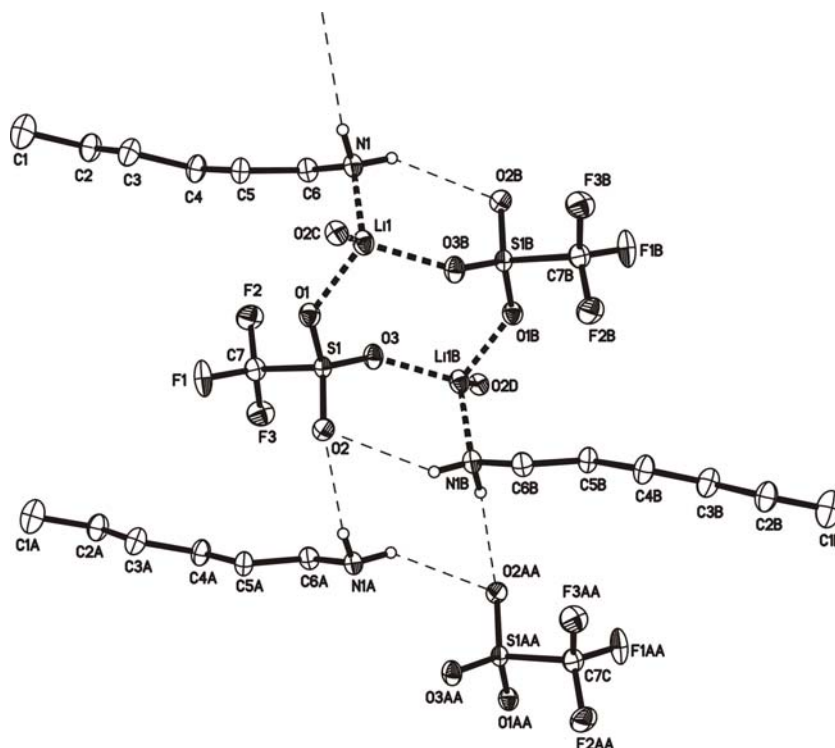


**Figure 4.2.** Crystal structure of hexylamine:LiTf showing the four-fold coordination of lithium and the hydrogen bonding environment of the primary amine group. The disordered part of the hexylamine molecule (atoms C1', C2', and C3') is not shown for the purpose of clarity.

**Table 4.1.** Structural data of the HEXA:LiTf crystal.

Crystal system	Orthorhombic
Space group	Pbca
Temperature	86(2)
a (Å)	8.6035(19)
b (Å)	10.008(2)
c (Å)	28.521(6)
Volume (Å <sup>3</sup> )	2455.7(9)
Z	4
Density (Mg/m <sup>3</sup> )	1.391
R1	0.0501
Crystal size (mm <sup>3</sup> )	0.38 x 0.32 x 0.22

The lithium - oxygen coordination bond distance lies between 1.94 and 1.96 Å, while the corresponding lithium – nitrogen distance is 2.049 Å (Table 4.2).

**Table 4.2.** Coordination bond distances for the lithium cation.

Bond	Bond length (Å)
O(1) – Li(1)	1.945(5)
O(2) – Li(1)	1.940(5)
O(3) – Li(1)	1.959(5)
N(1) – Li(1)	2.049(5)

Other nitrogen compounds such as N,N-dimethylethylenediamine, N,N,N',N'-tetramethylethylenediamine and hexamethyltriethylenetetramine also form complexes with lithium triflate.<sup>1,2</sup> The Li-O and Li-N bond distances in those complexes compare very well with those found in the hexylamine:LiTf compound. The two hydrogen atoms of the NH<sub>2</sub> group in hexylamine form hydrogen bonds with triflate oxygen atoms as illustrated in Figure 4.2. Each hydrogen atom bonds with an oxygen atom belonging to a different triflate ion. Each oxygen atom of a given triflate ion is coordinated to a different lithium ion. In this crystal structure, the distances between the two hydrogen atoms of the amine group and the two triflate oxygen atoms (d (NH<sup>+</sup>...O)) are 2.49 and 2.51 Å (Table 4.3), and the N-H-O angles significantly less than 180° (162.9 and 141.1 °), suggesting that hexylamine and lithium triflate form weak hydrogen bonds. The structural details of the hydrogen bonds are shown in the Table 4.3.

**Table 4.3.** Hydrogen bond parameters for the HEXA:LiTf crystal.

N-H ... O	d (N-H)	d (H ... O)	d (N ... O)	< (NHO)
N(1)-H(1E) ... O(2)	0.92	2.49	3.376(3)	162.9
N(1)-H(1D) ... O(2)	0.92	2.51	3.274(3)	141.1

**4.1.2. N,N-DMEDA:LiTf and N,N-DMEDA:NaTf**

**Crystal structures.** The N,N-DMEDA:LiTf crystals form a monoclinic unit cell in the P2(1)/c space group, with four (DMEDA:LiTf) asymmetric units in the cell. A summary of the structural data is shown in Table 4.4.

**Table 4.4.** Structural data for crystalline phases of DMEDA:LiTf and DMEDA:NaTf.

	DMEDA:LiTf	DMEDA:NaTf
Crystal system	Monoclinic	Monoclinic
Space group	P2(1)/c	P2(1)/c
Temperature (K)	103(2)	90(2)
a (Å)	6.5375(15)	11.477(12)
b (Å)	18.518(4)	9.717(10)
c (Å)	9.440(2)	11.283(12)
$\beta$	93.479(3)	117.01(2)
Volume (Å <sup>3</sup> )	1140.7(5)	1121(2)
Z	4	4
Density (Mg/m <sup>3</sup> )	1.422	1.542
R1	0.0387	0.0634
Crystal size (mm <sup>3</sup> )	0.58 x 0.34 x 0.02	0.46 x 0.40 x 0.16

The packing forms a polymeric one-dimensional network along the crystallographic *c* axis, as shown in Figure 4.3. In this network, lithium coordinates both nitrogens from a single DMEDA molecule and two oxygen atoms from different triflate

anions (Figure 4.4). The polymeric chain is basically composed of alternate triflate ions and DMEDA molecules, both coordinated by lithium ions. The different polymeric chains are held together by hydrogen bonding interactions between the hydrogen atoms of the primary amine group of DMEDA and one triflate oxygen from an adjacent chain (Table 4.5). The crystal structure shows some static disorder, which is accommodated by splitting the triflate group into two distinct positions of 52.5% and 47.7% occupancy for the unprimed and primed atoms, respectively. Only one position of the triflate ion is shown on the figures for purposes of clarity.

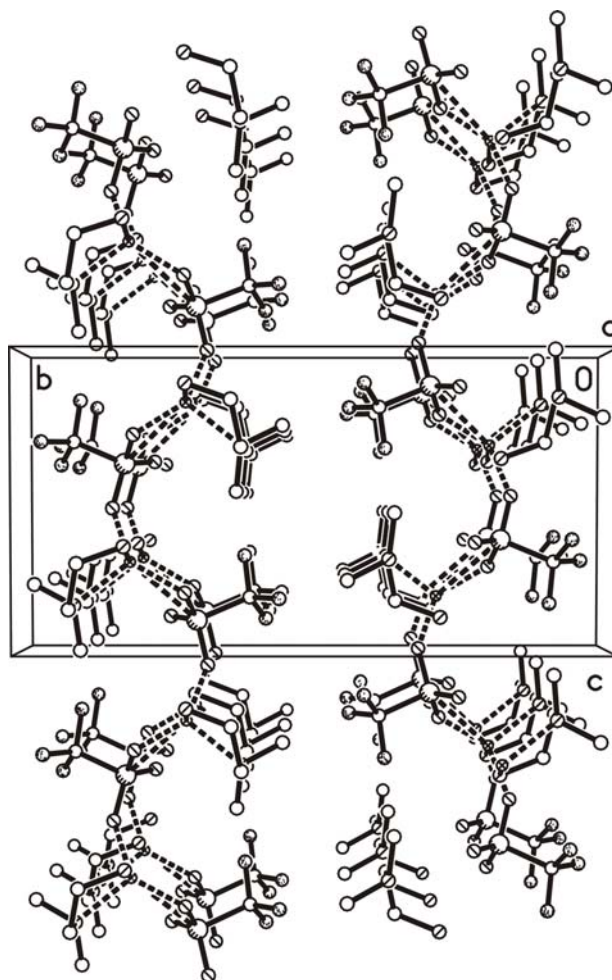


**Figure 4.3.** Packing diagram of the DMEDA:LiTf crystal projected down the crystallographic *a* axis. The crystal forms a polymeric one-dimensional network along the crystallographic *c* axis.

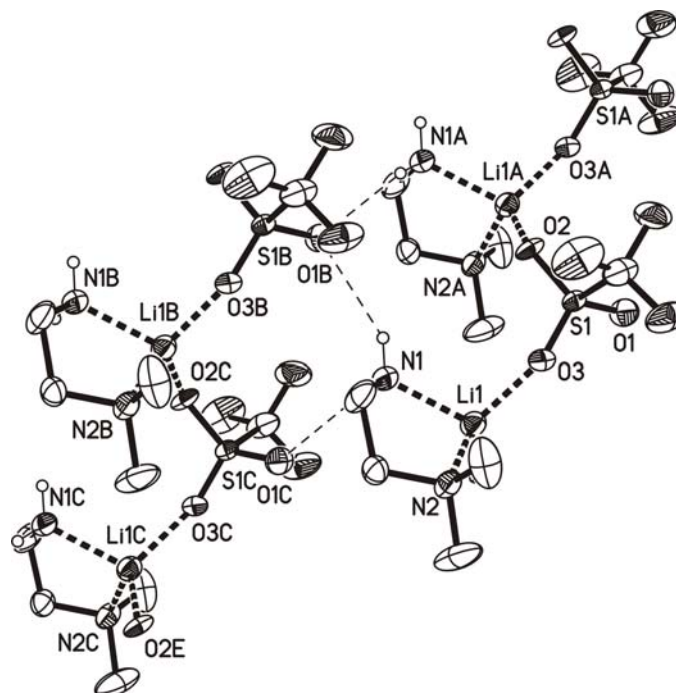


**Figure 4.4.** Crystal structure of DMEDA:LiTf showing the four-fold coordination of lithium and the hydrogen bonding environment of the primary amine groups.

The N,N-DMEDA:NaTf crystal also forms a monoclinic unit cell in the  $P2(1)/c$  space group, with  $Z=4$  (DMEDA:NaTf) asymmetric units in the cell. Crystal data is also presented in Table 4.4. The packing diagram (Figure 4.5) shows the formation of a two-dimensional network parallel to the  $bc$  crystallographic plane. A detailed picture of the coordination in Figure 4.6 shows that each sodium ion is bonded to two nitrogen atoms from one DMEDA molecule, and three oxygen atoms from different triflate anions. One of the primary amine hydrogen atoms forms a hydrogen bond with a triflate oxygen atom, while the other hydrogen atom forms a hydrogen bond with a fluorine atom of a different triflate anion (Table 4.5). The structure forms dimers in which one sodium ion coordinates to O1A and O2AA from two different triflate anions and the other sodium ion coordinates to O2A and O1AA of the same two triflate ions. The third oxygen atom of

the two triflate ions, O3A and O3AA, coordinates to a sodium ion and extends the dimers into a network (Figure 4.6).

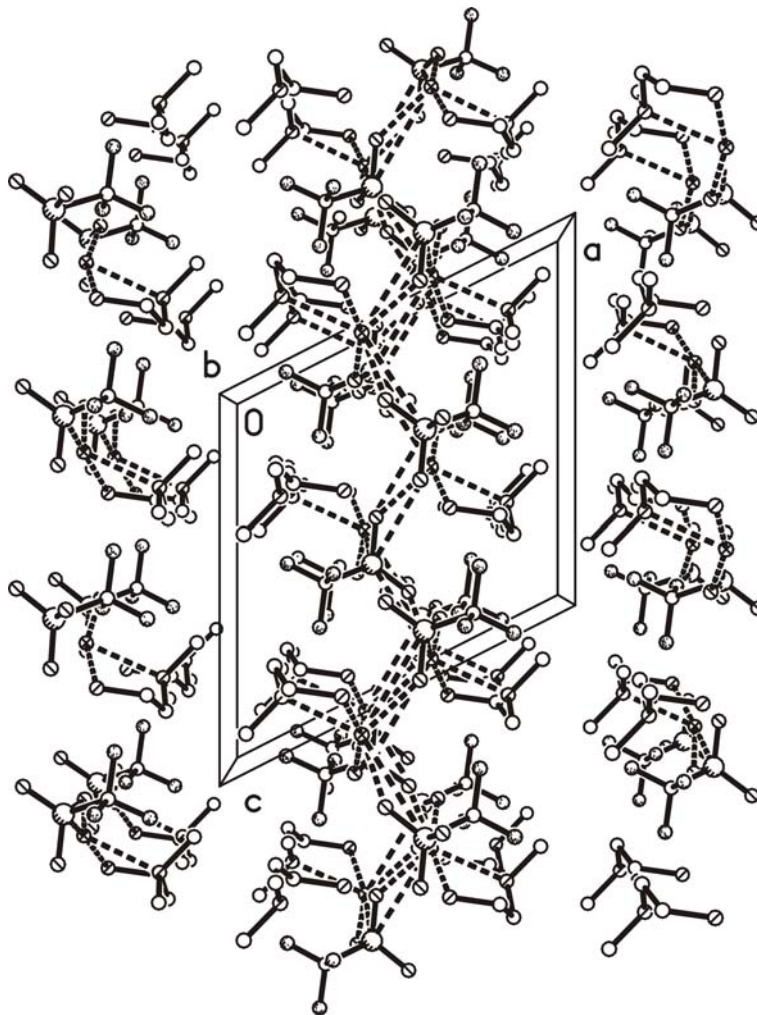


**Figure 4.5.** Packing diagram of the DMEDA:NaTf crystal projected down the crystallographic *b* axis. The crystal forms a polymeric two-dimensional structure in the *bc* crystallographic plane.

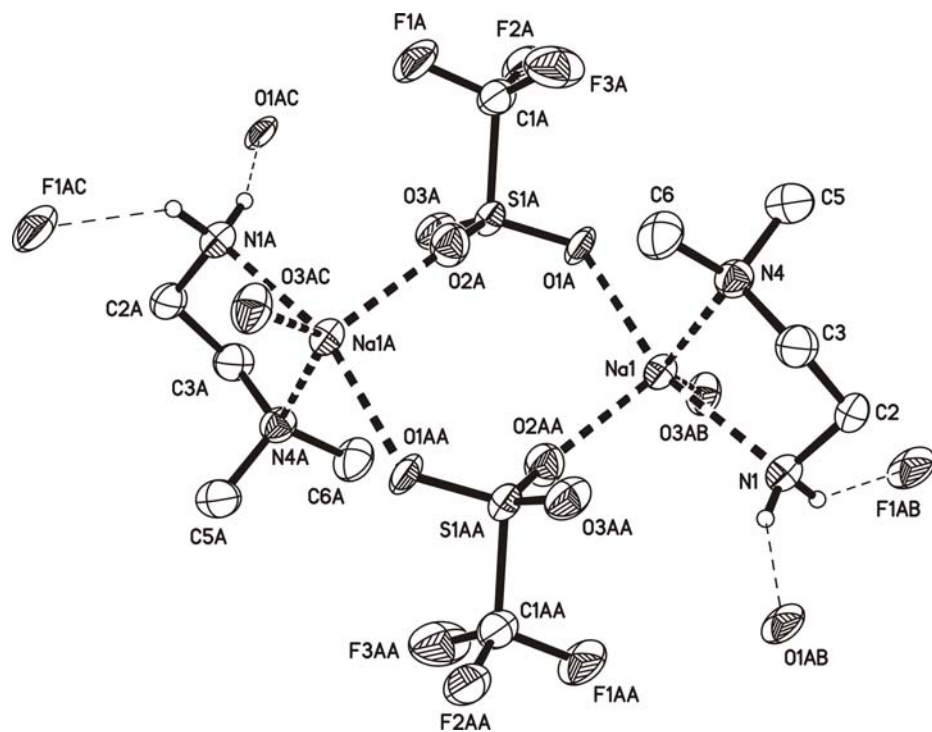


**Figure 4.6.** Crystal structure of DMEDA:NaTf showing the five-fold coordination of sodium and the hydrogen bonding environment of the primary amine groups. This picture highlights the formation of dimers.

*Comparison of the crystal structures.* In each DMEDA-salt complex, the hydrogen atoms of the NH<sub>2</sub> group are hydrogen bonded (Table 4.5). In the DMEDA:LiTf crystal, each of the two hydrogen atoms is hydrogen bonded to an oxygen atom from a different triflate group, whereas in the DMEDA:NaTf crystal one hydrogen bond takes place with a triflate oxygen, while the other hydrogen atom forms a hydrogen bond to a fluorine atom from a different triflate group. In both these structures, the relatively large N-H $\cdots$ O and N-H $\cdots$ F distances along with N-H-O and N-H-F angles that are significantly less than 180° suggest that DMEDA forms weak hydrogen bonds with LiTf and NaTf. Moreover, in both crystal structures, it is important to note that there are

no hydrogen bonding interactions between amine groups of DMEDA molecules. Structural details of the hydrogen bonds are summarized in Table 4.5.

**Table 4.5.** Hydrogen bond parameters for the DMEDA:LiTf crystal and DMEDA:NaTf crystal. All bond distances are in Angstroms (Å).

	N-H ... A	d (N-H)	d (H ... A)	D (N ... A)	< (NHA)
DMEDA:LiTf	N(1)-H(1D) ... O(1) #3	0.84	2.28	3.013(5)	147(2)
	N(1)-H(1D) ... O(1')#3	0.84	2.28	3.083(6)	162(2)
	N(1)-H(1E) ... O(1)#4	0.82	2.54	3.284(5)	150(2)
	N(1)-H(1E) ... O(1')#4	0.82	2.41	3.185(6)	157(2)
DMEDA:NaTf	N(1)-H(1A) ... O(1A)	0.89	2.43	3.242(6)	153(5)
	N(1)-H(1B) ... F(1A)	0.92	2.34	3.131(6)	144(4)

Symmetry transformation used to generate equivalent atoms:

#3  $x + 1, -y + 3/2, z + 1/2$     #4  $x + 1, y, z$

The overall conformation of the DMEDA oligomers can be described by the torsional angles of the N-C-C-N and C-N-C-C bond sequences, where gauche (abbreviated g) is  $60^\circ \pm 60^\circ$ ; trans (abbreviated t) is  $180^\circ \pm 60^\circ$ , and gauche minus (abbreviated  $\bar{g}$ ) is  $300^\circ \pm 60^\circ$ .<sup>3</sup> Particular attention is directed to the N-C-C-N angle as it is directly affected by the coordination of the cation to the nitrogen atoms. In DMEDA:LiTf crystal, the N-C-C-N dihedral angle of the DMEDA molecule is gauche ( $59.0^\circ$ ), which results in  $xg$  conformations where  $x = t$  or  $g$  and represents the C-N-C-C dihedral angle. In DMEDA:NaTf crystal, the N-C-C-N dihedral angle is gauche minus ( $-66.1^\circ$ ), which leads in  $x\bar{g}$  conformations ( $x = t$  or  $\bar{g}$ ) (Table 4.6). In the Table, the last two rows for each crystal entry result from the two methyl groups terminating the

nitrogen atoms. The DMEDA conformation in both crystals is similar to that previously observed in N,N'-dimethylethylenediamine:NaTf crystal ( $\bar{t}g$  and  $gt$ ).

**Table 4.6.** Torsional angles of DMEDA:LiTf and DMEDA:NaTf crystals and the corresponding conformations.

Bond sequence	Torsional angle (°)	Conformation
DMEDA:LiTf		
N1-C3-C4-N2	59.0(3)	g
C1-N2-C4-C3	-162.3 (2)	t
C2-N2-C4-C3	76.8(2)	g
DMEDA:NaTf		
N1-C2-C3-N4	-66.1(6)	$\bar{g}$
C5-N4-C3-C2	-75.2(5)	$\bar{g}$
C6-N4-C3-C2	163.5(4)	t

The cation – heteroatom bond distances are summarized in Table 4.7. In the DMEDA:LiTf crystal, the static disorder does not affect the lithium – oxygen coordination bond distances, as they are very similar for each position. The Li-N coordination bond distance is around 2.1 Å, while the Li-O bond length lies between 1.85 and 1.97 Å. In the sodium compound, the corresponding Na-N (~2.5 Å) and Na-O (~2.3 Å) bond lengths are much larger than in the lithium compound. The differences between the lithium and sodium ionic radii is 0.29 Å, which is smaller than the differences in the coordination bond distances to either nitrogen or oxygen atoms. This suggests that the lithium ion coordinates the nitrogen atom more strongly than does the sodium cation, which is consistent with the higher charge density of lithium. Furthermore, the N-Li<sup>+</sup>-N

(88.38°) angle is about 14.6° larger than the N-Na<sup>+</sup>-N angle (73.80°) (Table 4.7). Considering that the N-C-C-N torsional angles are similar in the two compounds (Table 4.6), the 14.6° difference in the N-X<sup>+</sup>-N angles (X<sup>+</sup>=Li<sup>+</sup> or Na<sup>+</sup>) is consistent with the differences in the cation – nitrogen coordination bond distances. Other nitrogen compounds such as N,N,N',N'-tetramethylethylenediamine<sup>1</sup> (TMEDA), and hexamethyltriethylenetetramine<sup>2</sup> (HMTTA) also form complexes with lithium triflate and sodium triflate. The coordination bond distances, and the N-X<sup>+</sup>-N angles (X<sup>+</sup>=Li<sup>+</sup>, Na<sup>+</sup>) in those complexes compare very well with those found in the DMEDA:LiTf and DMEDA:NaTf compounds.

**Table 4.7.** Selected bond length (Å) and angles (°) for the DMEDA:LiTf and DMEDA:NaTf crystals.

	Bond distance X-N		Bond distance X-O	Angle N-X-N
X = Li	2.100(4)	tertiary	1.932(7)	88.38(13)
	2.039(3)	primary	1.942(9)	
			1.968(7)	
			1.848(8)	
X = Na	2.507(5)	tertiary	2.293(4)	73.80(15)
	2.466(5)	primary	2.314(4)	
			2.370(4)	

The N,N-DMEDA molecule contains two methyl groups attached to one of the nitrogen atoms and two hydrogen atoms on the other nitrogen atom. The difference in the steric accessibility of the two nitrogen atoms of the DMEDA molecule seems to have a small effect on the coordination of the cation. The Li<sup>+</sup> - primary nitrogen bond length is 0.06 Å shorter than the Li<sup>+</sup> – tertiary nitrogen bond length in the DMEDA:LiTf crystal.

Similarly, the Na<sup>+</sup> – primary nitrogen bond length in the DMEDA:NaTf crystal is 0.04 Å shorter than the Na<sup>+</sup> – tertiary nitrogen bond distance.

**Thermal analysis.** Differential scanning calorimetry was used to study melting and recrystallization processes in the crystals. In the DSC thermogram of the DMEDA:NaTf crystal, a sharp endotherm occurs with an onset at 41°C, and the onset of recrystallization occurs at 21°C. In a subsequent thermal cycle, the onsets of melting and recrystallization temperatures decrease to 38 and 17°C, respectively, which suggests some thermal hysteresis. Upon further cycling, the melting peak becomes smaller and broader, probably caused by a loss of crystallinity of the sample.

The DSC thermograms of the DMEDA:LiTf crystal are not as straightforward. First, the DMEDA:LiTf crystal was cycled between 0 and 60°C. During the first heating period (25 to 60°C), a sharp endothermic peak occurs with an onset at 48°C due to the melting of the crystalline compound. In the cooling phase, two exothermic transitions are observed with onsets at 6 and ~ 19°C. In a second thermal cycle, two endothermic peaks are observed in the heating portion with onsets at 13 and 46°C; and upon cooling the onsets are observed at 5 and 18°C, respectively. When more thermal cycles are performed (between 0 and 60°C), the onsets of these thermal transitions keep decreasing slowly in value. This may indicate some degree of thermal hysteresis. When the DMEDA:LiTf crystal is cycled between 0 and 150°C, the first endotherm occurs with an onset at 48°C (first cycle between 25 and 150°C). In the following cooling and reheating periods, the onsets of the thermal transitions described above behave in a similar manner, but a third endotherm starts to appear at higher temperatures. This third transition peak

does not occur at the same temperature for successive measurements. In the second heating cycle, the endotherm is small and occurs with an onset around 57°C (onset of exotherm at 61°C in the following cooling period), and in the fourth cycle it is at 92°C (onset of exotherm at 110°C in the following cooling period). The appearance of the third endothermic peak might indicate the formation of a new crystalline phase at higher temperatures or the incongruent melting of the DMEDA:LiTf crystal.

#### **4.1.3. Dipropylamine:LiTf**

The DPA:LiTf crystals form a monoclinic unit cell in the P2(1)/c space group, with four (DPA:LiTf) asymmetric units in the cell. The packing forms a polymeric chain-like one-dimensional network in the *a* direction as illustrated in Figure 4.7. Each repeat unit of the network is composed of a (DPA:LiTf)<sub>2</sub> dimer that forms the chain via the coordination of lithium to triflate oxygen. In this network, each lithium ion is coordinated to one nitrogen atom from the dipropylamine molecule and three triflate oxygen atoms from three different triflate groups, as shown in Figure 4.8. Two of these triflate ions belong to the repeat unit of the chain and the third triflate ion belongs to an adjacent unit. Structural data of the crystal are summarized in Table 4.8. The DSC thermograms of the DPA:LiTf crystal showed three endothermic transitions (onset 87°C, midpoint 99°C; onset 105°C, midpoint 120°C, and onset 99°C, midpoint 127°C) that are not reproduced upon cooling and subsequent reheating of the sample. These data suggest that the compound melts incongruently.

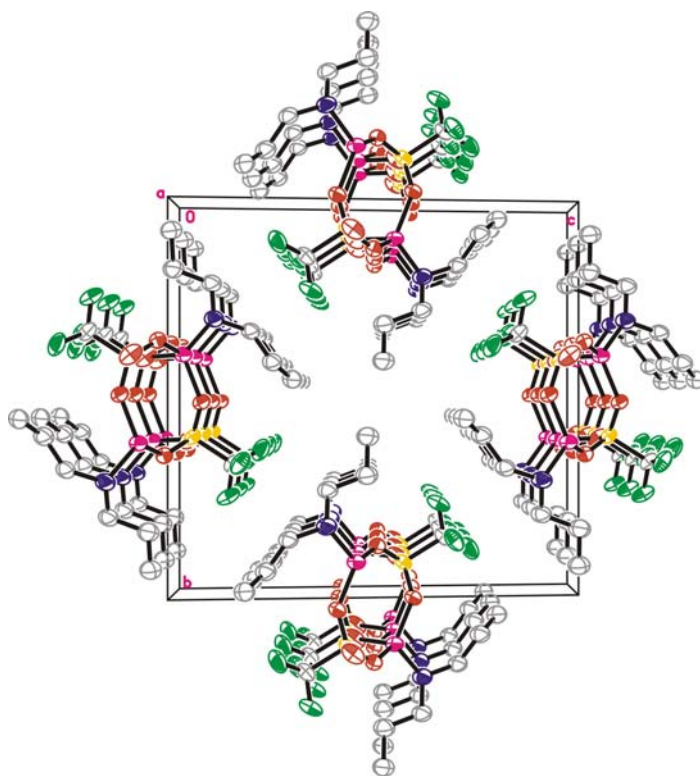


**Figure 4.7.** Packing diagram of the dipropylamine:LiTf crystal projected along the crystallographic *a* axis. The stacking of the dimers along the *a* axis forms a polymeric chain.

**Table 4.8.** Structural data of the DPA:LiTf crystal.

Crystal system	Monoclinic
Space group	P2(1)/c
Temperature	100(2) K
<i>a</i> (Å)	5.1842(4)
<i>b</i> (Å)	15.3790(13)
<i>c</i> (Å)	15.8877(13)
$\beta$	98.1100(10)
Volume (Å <sup>3</sup> )	1254.02(18)
<i>Z</i>	4
Density (Mg/m <sup>3</sup> )	1.362
R1	0.0490
Crystal size (mm <sup>3</sup> )	0.34 x 0.28 x 0.18

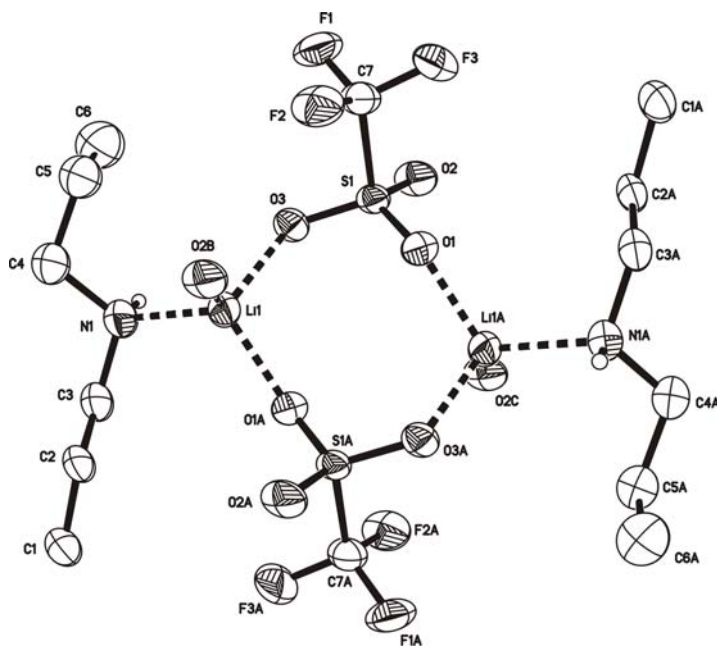


**Figure 4.8.** Crystal structure of dipropylamine:LiTf showing one dimer and the four-fold coordination of lithium. Only one position of the disordered dipropylamine molecule is shown for the purpose of clarity.

The crystal structure shows some static disorder with each dipropylamine molecule split into two distinct positions of 50% occupancy. In both positions, the lithium – oxygen and lithium – nitrogen coordination bond distances are very similar to the hexylamine:LiTf compound (Table 4.9). The hydrogen atoms of the N(1)H and N(1')H groups are pointing in opposite directions and therefore have very different environments. Only N(1')H group is shown in Figure 4.9 for purposes of clarity. In one of the two positions of the molecule, the hydrogen atom from the N(1')H group forms a hydrogen bond with a triflate oxygen from an adjacent plane. These hydrogen bonds are very weak, as the hydrogen – oxygen distance is 3.205(3) Å and the N(1')-H-O angle is 147.1°. In the other position of the dipropylamine molecule, no hydrogen bond is formed.

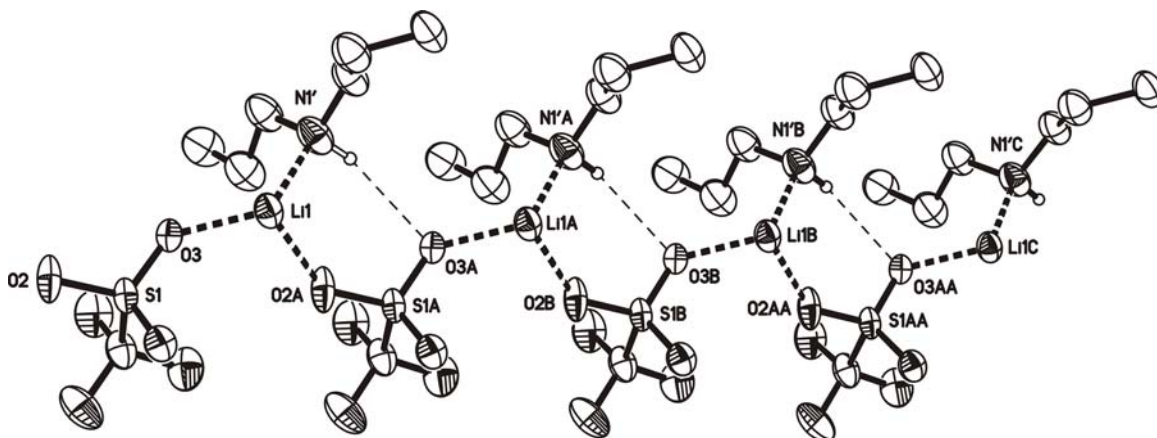


**Figure 4.9.** Crystal structure of dipropylamine:LiTf showing the N-H ... O hydrogen bonds. Only one dipropylamine is represented; in this view the other molecule would be superposed, with the N-H bond pointing 180° from the illustrated DPA molecule.

**Table 4.9.** Coordination bond distances for the lithium cation.

Bond	Bond length (Å)
O(1) – Li(1)	1.943(3)
O(2) – Li(1)2	1.934(4)
O(3) – Li(1)	1.935(4)
N(1) – Li(1)	2.144(4)
N(1') – Li(1)	1.998(4)

## 4.2. VIBRATIONAL SPECTROSCOPY

The primary amine group in hexylamine and DMEDA is a good spectroscopic probe to study cation - host and anion – host interactions because the NH stretching vibrations are particularly sensitive to these interactions. In particular, hydrogen bonding interactions between a primary amine hydrogen and a heteroatom, and the inductive effect of a cation upon coordination with a heteroatom alter the vibrations of the primary

amine group. These interactions change the intensities and shift the frequencies of the NH stretching vibrations, providing a useful tool to examine the underlying interactions.

In the hexylamine molecule, the primary amine group is covalently bound to a carbon atom that is part of a hexane chain; and in the DMEDA molecule, the primary amine group is covalently bound to a carbon atom that is part of an ethylene structure. To the extent that the NH stretching vibrations are not severely affected by the presence of the rest of the molecule (a very good approximation!),  $\nu_s(\text{NH}_2)$  and  $\nu_{as}(\text{NH}_2)$  can be considered as having a symmetric and asymmetric character, respectively.

#### **4.2.1. Hexylamine system**

##### **a) Pure hexylamine**

The NH stretching region of a primary amine consists of two bands: the asymmetric  $\text{NH}_2$  stretch,  $\nu_{as}(\text{NH}_2)$ , and the symmetric  $\text{NH}_2$  stretch,  $\nu_s(\text{NH}_2)$ . The intensity of these two bands in the IR and in the Raman spectrum is governed by the spectroscopic selection rules. In general, molecular vibrations that are symmetric, e.g.  $\nu_s(\text{NH}_2)$ , have strong Raman bands and weak infrared bands, whereas molecular vibrations that are antisymmetric, e.g.  $\nu_{as}(\text{NH}_2)$ , yield weak Raman bands and strong IR bands. In the case of a molecule with a center of symmetry, the symmetric vibrations are forbidden in the IR; conversely the antisymmetric vibrations are forbidden in the Raman.<sup>4</sup> Strictly speaking, the description of the two NH stretching modes of  $\text{NH}_2$  as symmetric and antisymmetric is true only for an isolated  $\text{NH}_2$  group or an environment in which the  $C_{2v}$  point group symmetry is preserved. In the condensed phase, intermolecular and

intramolecular interactions alter the nature and hence the effective symmetry of the vibration. These interactions usually lower the formal  $C_{2v}$  symmetry.

The IR spectrum of pure hexylamine (see Figure 4.10, lower portion) consists of two strong bands centered at  $3371\text{ cm}^{-1}$  and  $3293\text{ cm}^{-1}$ , corresponding to  $\nu_{as}(\text{NH}_2)$ , and  $\nu_s(\text{NH}_2)$ , respectively. The less intense shoulder centered roughly at  $3195\text{ cm}^{-1}$  is an overtone of the  $\text{NH}_2$  deformation band at  $1609\text{ cm}^{-1}$ .

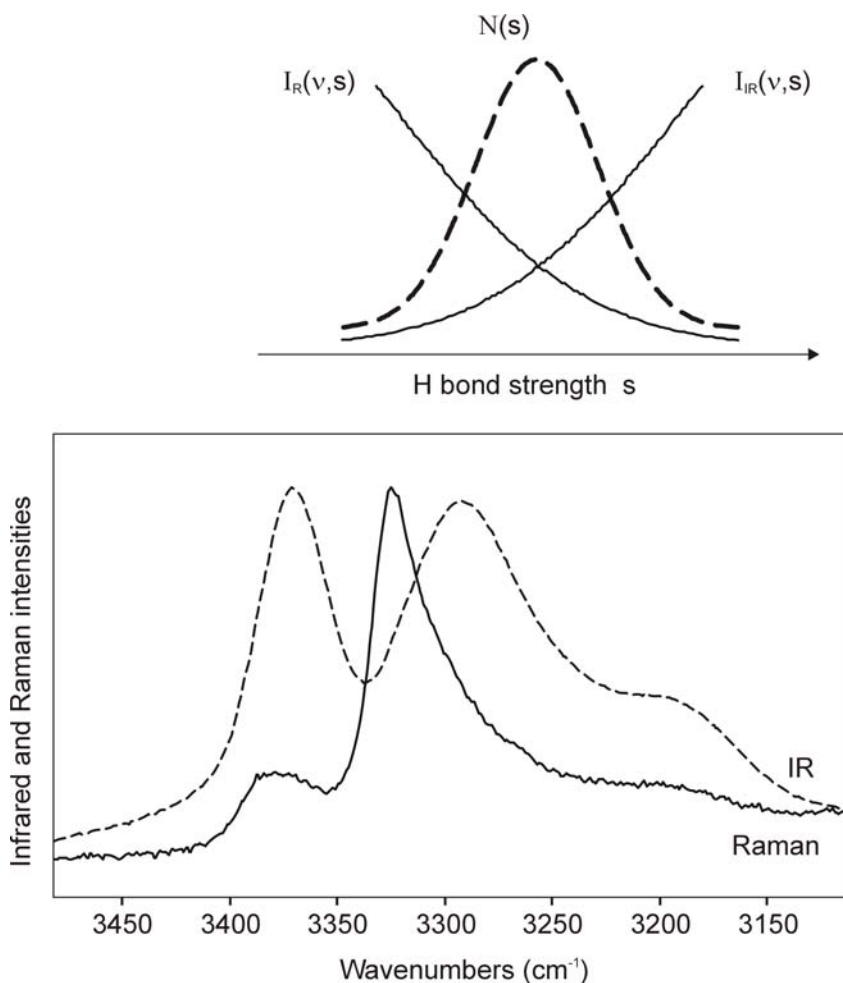


**Figure 4.10.** Bottom: IR spectrum (dashed line) and Raman spectrum (full line) of hexylamine in the N-H stretching region. Top: Representation of the population distribution of the N-H stretching vibrations in hexylamine as a function of hydrogen bond strength  $s$ . The corresponding band intensities in IR and Raman are also shown as a function of hydrogen bond strength.

The Raman spectrum of pure hexylamine in this region is dramatically different than the IR spectrum. The asymmetric stretch, centered around  $3376\text{ cm}^{-1}$ , has a very weak Raman intensity compared to the symmetric stretch, as expected. The maximum intensity of the symmetric stretch occurs at  $3324\text{ cm}^{-1}$ , but a long tail on the low frequency side strongly suggests the presence of hexylamine molecules with a distribution of hydrogen-bonded environments. Hydrogen bonding affects N-H stretching frequencies by removing electron density from the N-H bond, causing a shift to lower frequencies.<sup>5,6</sup>

The frequency and intensity data of Figure 4.10 may be explained in terms of a distribution of hydrogen bonding environments and the following two hypotheses:

- (1) The intensity and frequency of the  $\nu_s(\text{NH}_2)$  mode are quite sensitive to hydrogen bonding interactions because the perturbation of the  $\nu_s(\text{NH}_2)$  mode by interactions involving one of the amine hydrogen atoms is relatively strong. This arises (in part) because symmetric modes generally have larger Raman scattering cross-sections than antisymmetric (asymmetric) modes. Assuming that the heteroatom interacts with only one hydrogen atom of the  $\text{NH}_2$  group, this interaction necessarily imposes an asymmetric nature on a formerly symmetric mode, thus decreasing the scattering intensity. It is also known that in general the infrared intensity of a hydrogen stretching mode increases with increasing hydrogen bond strength, with a corresponding decrease of Raman scattering intensity. These trends are summarized on the figure by a plot of the Raman intensity  $I_R(\nu, s)$  and the infrared intensity  $I_{\text{IR}}(\nu, s)$  as a function of the hydrogen bond strength,  $s$ .

(2) The intensity of the  $\nu_{\text{as}}(\text{NH}_2)$  mode is less sensitive to hydrogen bonding than the  $\nu_{\text{s}}(\text{NH}_2)$  mode. If the heteroatom involved in hydrogen bonding interacts with only one hydrogen atom of the  $\text{NH}_2$  group, the perturbation of the  $\nu_{\text{as}}(\text{NH}_2)$  mode is relatively small because the mode already has a markedly antisymmetric or asymmetric nature.

Also shown in Figure 4.10 is a population distribution of hexylamine molecules, plotted as a function of hydrogen bond strength as indicated. The actual distribution is not known, and this form has been hypothesized for purposes of discussion. In the picture, the  $\nu_{\text{as}}(\text{NH}_2)$  vibrations of all  $\text{NH}_2$  groups occur over a small distribution of frequencies, since the frequency of this mode is relatively insensitive to hydrogen bonding. Consequently, the maxima of the IR band ( $3371 \text{ cm}^{-1}$ ) and the Raman band ( $3376 \text{ cm}^{-1}$ ) are almost coincident. Further, the Raman scattering intensity of this mode is significantly smaller than the intensity of the band at  $3324 \text{ cm}^{-1}$  that originates in the  $\nu_{\text{s}}(\text{NH}_2)$  vibration of  $\text{NH}_2$  groups in a weak hydrogen bonding environment. The Raman intensity of the symmetric mode decreases with decreasing frequency as the strength of the hydrogen bonding interactions increases and the mode becomes more antisymmetric in character (less Raman active). At the same time, the infrared intensity of the mode grows until its maximum at  $3293 \text{ cm}^{-1}$ , as seen in the Figure.

#### **b) Hexylamine in $\text{CCl}_4$**

When hexylamine is diluted in carbon tetrachloride, the interactions between the hexylamine molecules decrease to a significant degree.<sup>7,8</sup> In very dilute solutions, the vibrations of the  $\text{NH}_2$  group are expected to behave as “free” molecules.<sup>9,10</sup> Figure 4.11

shows a superposition of the IR and Raman spectra of pure hexylamine and various compositions of hexylamine dissolved in CCl<sub>4</sub>.

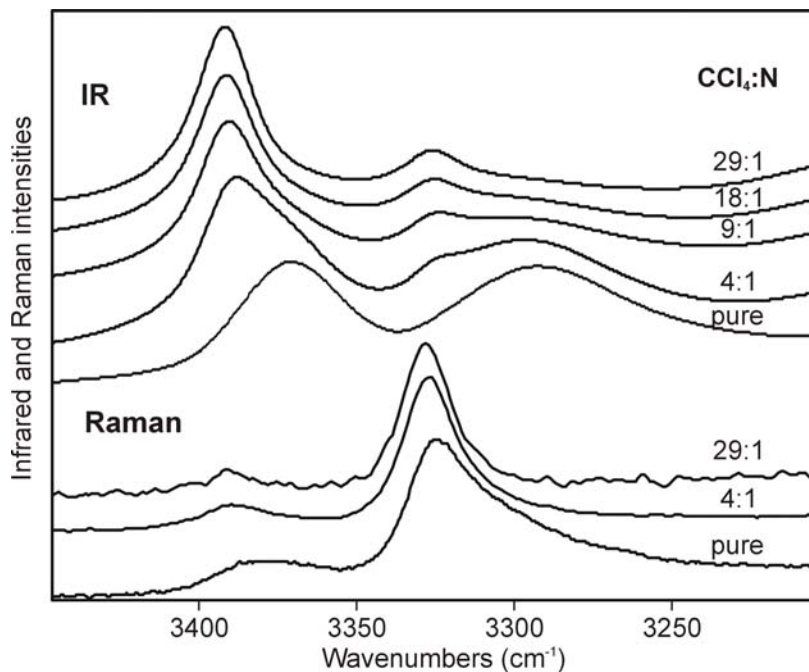


**Figure 4.11.** Infrared (top) and Raman (bottom) spectra of the N-H stretching region for pure HEXA and HEXA dissolved in carbon tetrachloride at different concentrations (reported as CCl<sub>4</sub>:N molar ratios).

In the Raman spectra, the  $\nu_{as}(\text{NH}_2)$  and  $\nu_s(\text{NH}_2)$  bands shift from 3376 and 3324  $\text{cm}^{-1}$  to about 3390 and 3328  $\text{cm}^{-1}$ , respectively, in the most dilute solution (29:1 CCl<sub>4</sub>:hexylamine molar ratio). Also, the intensity of the  $\nu_s(\text{NH}_2)$  band low frequency tail in pure hexylamine greatly decreases in the 4:1 solution. Upon further dilution (18:1 solution), the intensity of the tail slightly decreases so that the shape of the  $\nu_s(\text{NH}_2)$  band is symmetrical and centered at 3328  $\text{cm}^{-1}$ . There are no additional spectral changes at higher dilutions. The Raman frequency of the  $\nu_s(\text{NH}_2)$  band of pure hexylamine is only 4  $\text{cm}^{-1}$  lower than that in the dilute solutions. This is expected, since the Raman scattering

intensity is larger for symmetric modes. Therefore the Raman spectrum of pure hexylamine selectively samples molecules that are undergoing minimal or no hydrogen bonding interactions, and very little spectral change should occur upon dilution.

The concentration dependence of hexylamine in  $\text{CCl}_4$  is also shown in the infrared spectrum in Figure 4.11. In pure hexylamine, the broad  $\nu_s(\text{NH}_2)$  band occurs at  $3293\text{ cm}^{-1}$ ; upon dilution, a shoulder appears around  $3324\text{ cm}^{-1}$  on the high frequency side of the band. As the solution becomes more dilute, the shoulder grows in intensity and the original band progressively decreases. When the composition reaches 29:1, the original band at  $3293\text{ cm}^{-1}$  has mostly disappeared, and is replaced by a new band at  $3326\text{ cm}^{-1}$ .

In contrast to the symmetric stretch, the  $\nu_{as}(\text{NH}_2)$  band seems to shift progressively to higher frequencies. But in fact, its behavior is very similar to that of the symmetric stretch. At a 4:1 composition, the maximum intensity of the band is at  $3388\text{ cm}^{-1}$  with a shoulder on the low frequency side. Upon further dilution, the maximum intensity of the band slightly shifts to  $3392\text{ cm}^{-1}$  in the 29:1 sample and the shoulder disappears. A curve fitting analysis of the 9:1 composition spectrum shows that the asymmetric stretch is composed of two peaks at  $3391$  and  $3369\text{ cm}^{-1}$ , and the symmetric stretch contains two peaks at  $3325$  and  $3299\text{ cm}^{-1}$ . For both the asymmetric and the symmetric stretches, the high frequency band corresponds to a population of hexylamine molecules that are mostly “free”. The frequencies of these bands are similar in the IR and in the Raman spectra within  $\pm 2$  wavenumbers. The lower frequency bands observed in the IR correspond to hexylamine molecules that undergo relatively strong hydrogen bonding interactions.<sup>7</sup>

It is important to note the relative intensity changes of the two NH stretches in the IR spectra as hexylamine is diluted with CCl<sub>4</sub>. In dilute solutions, hydrogen bonding interactions are greatly reduced; as a result the two hydrogen atoms of the amine group have approximately equivalent potential energy environments, and the symmetric and antisymmetric nature of the vibrational modes is easily observed. In pure hexylamine, the IR intensities of  $\nu_{\text{as}}(\text{NH}_2)$  and  $\nu_{\text{s}}(\text{NH}_2)$  are roughly equivalent. In the most dilute solution, the intensity of  $\nu_{\text{as}}(\text{NH}_2)$  is markedly greater than that of  $\nu_{\text{s}}(\text{NH}_2)$ . By contrast, the Raman intensity of  $\nu_{\text{s}}(\text{NH}_2)$  is greater than  $\nu_{\text{as}}(\text{NH}_2)$  in all solutions and pure hexylamine, since Raman measurement selects those molecules with the least amount of hydrogen-bonding interactions as noted earlier.

### c) Hexylamine – salt complexes

**Hexylamine – LiTf.** The effect of adding salt to hexylamine is illustrated in Figure 4.12, which shows the IR and Raman spectra of hexylamine - LiTf in the N-H stretching region. Upon addition of LiTf to bring the solution to a 3:1 composition, both  $\nu_{\text{s}}(\text{NH}_2)$  and  $\nu_{\text{as}}(\text{NH}_2)$  bands become sharper in the infrared spectrum. The antisymmetric band shifts lower by 14 wavenumbers ( $3357\text{ cm}^{-1}$ ), whereas the symmetric band shifts higher by 6 wavenumbers ( $3299\text{ cm}^{-1}$ ). In the crystalline sample, the peaks are similarly shifted;  $\nu_{\text{as}}(\text{NH}_2)$  and  $\nu_{\text{s}}(\text{NH}_2)$  occur at  $3358\text{ cm}^{-1}$  and  $3300\text{ cm}^{-1}$ , respectively. Moreover, a large decrease in the infrared intensity of the symmetric stretch compared to the asymmetric stretch is observed in the crystalline sample. The band shapes of the two stretching modes are slightly distorted in the crystalline sample, with both bands showing a high frequency tail and a slight but distinct minimum on the low frequency side. This is

a particle size effect that originates in a reflective scattering contribution to the intensity loss. It is most pronounced when the particle size is on the order of the wavelength of the incident radiation, and both the real and imaginary parts of the refractive index contribute to the intensity of transmitted light.<sup>11</sup>

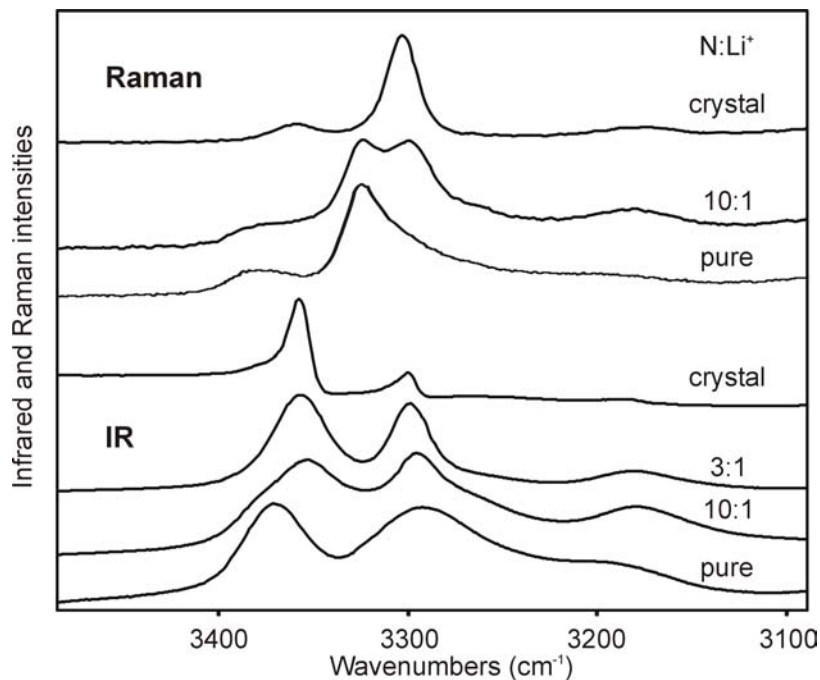


**Figure 4.12.** N-H stretching region of the IR and Raman spectra of HEXA:LiTf crystal, hexylamine – LiTf solutions with various N:Li<sup>+</sup> ratios, and hexylamine.

Equally dramatic spectral changes with increasing LiTf concentration are seen in the Raman spectra. With the addition of salt, a band at roughly 3300 cm<sup>-1</sup> grows out of the extensive low frequency wing of the 3324 cm<sup>-1</sup> hexylamine band. This is clearly visible in the spectrum of the 10:1 sample. At the same time, the intensity of the 3324 cm<sup>-1</sup> hexylamine band decreases until it vanishes in the spectrum of the crystal. The weaker Raman-active band at 3376 cm<sup>-1</sup> in pure hexylamine shifts to 3357 cm<sup>-1</sup> in the

crystal, with no significant change of intensity. In the crystalline compound, the N-H stretching frequencies of the IR and Raman bands are coincident within experimental error. The differences in the intensities of  $\nu_{\text{as}}(\text{NH}_2)$  and  $\nu_{\text{s}}(\text{NH}_2)$  in the compound can be explained in terms of the crystal structure. In the crystal (see Figure 4.2), each hydrogen atom of the  $\text{NH}_2$  groups is weakly hydrogen bonded to an oxygen atom of a triflate ion, with the hydrogen-bonding environment of each amine hydrogen atom roughly equivalent. Therefore, the  $\nu_{\text{as}}(\text{NH}_2)$  and  $\nu_{\text{s}}(\text{NH}_2)$  modes retain their (approximately) antisymmetric and symmetric nature, respectively, as reflected in the IR and Raman intensities of each mode.

In the LiTf solutions and the crystal, a lithium ion is coordinated to an  $\text{NH}_2$  group through the lone pair of the nitrogen atom, which changes the electronic distribution in the  $\text{NH}_2$  group. The accompanying decrease of the N-H stretching mode frequencies is known as the **inductive effect**.<sup>12,13</sup> The presence of relatively strong hydrogen bonding interactions in pure hexylamine makes it difficult to isolate the inductive effect when LiTf is added. However, it is still possible to draw some conclusions. In pure hexylamine, the  $\nu_{\text{s}}(\text{NH}_2)$  band at  $3324\text{ cm}^{-1}$  was shown to originate in the fraction of hexylamine molecules in which hydrogen bonding was present to a limited extent. The crystal structure (Figure 4.2) shows that each hydrogen atom of every  $\text{NH}_2$  group is weakly hydrogen bonded to an oxygen atom of a triflate ion. Therefore the shift of the  $3324\text{ cm}^{-1}$  band of pure hexylamine to  $3300\text{ cm}^{-1}$  in the infrared and Raman spectra the crystal is a reasonable measure of the inductive effect of a lithium ion on  $\nu_{\text{s}}(\text{NH}_2)$ , because of the minimal effect of hydrogen bonding interactions. Unfortunately, it is not possible to carry out a similar analysis of  $\nu_{\text{as}}(\text{NH}_2)$  without knowing how to compensate

for the effect of replacing relatively strong  $N\cdots H$  hydrogen bonds with significantly weaker  $O\cdots H$  hydrogen bonds. However, such a replacement should increase the  $\nu_{\text{as}}(\text{NH}_2)$  frequency. Instead, the frequency decreases from 3376 to 3357  $\text{cm}^{-1}$ . Therefore the inductive effect of lithium ion on the  $\nu_{\text{as}}(\text{NH}_2)$  mode is at least comparable to the effect on the  $\nu_{\text{s}}(\text{NH}_2)$  mode.

***Hexylamine - NaTf and hexylamine - TbaTf solutions.*** This hypothesis was further tested by spectroscopic measurements of two sets of solutions: NaTf in hexylamine and TbaTf in hexylamine. The pattern of IR and Raman frequency shifts of the symmetric stretch in the two solutions are summarized in Figure 4.13, along with the previously discussed data for the LiTf solution and pure hexylamine. All salt solutions are compared at a 3:1 molar composition. Tetrabutylammonium is a charge-protected cation; its bulky butyl groups sterically hinder strong interactions with the triflate ion or the nitrogen atom in hexylamine. Consequently, upon addition of tetrabutylammonium triflate salt, it is expected that no inductive effect will take place and the spectral changes will be due to changes in hydrogen bonding involving the primary amine group.

The data summarized in Figure 4.13 can be easily understood in terms of the picture introduced earlier. The infrared spectrum preferentially samples those hexylamine molecules whose interactions lead to an asymmetric potential energy environment for the two amine hydrogen atoms. This environment arises because in many of the hexylamine molecules the  $N\cdots H$  hydrogen bonds have been broken by nitrogen atom-cation interactions and replaced by  $O\cdots H$  hydrogen bonds. The frequency of the observed band is determined by two competing factors: a shift to higher

frequencies (breaking of hydrogen bonds), and a shift to lower frequencies (inductive effect). The ordering of  $\nu_s(\text{NH}_2)$  in the infrared spectra simply reflects the relative strength of the inductive effect for the three cations,  $\text{Li}^+ > \text{Na}^+ > \text{Tba}^+$ , which accompanies the simultaneous shift to higher frequency resulting from hydrogen-bond breaking. By contrast, the Raman spectrum preferentially samples those hexylamine molecules whose amine hydrogen atoms do not undergo hydrogen bonding interactions and therefore experience a relatively symmetric potential energy environment. Therefore the frequency shifts upon complexation with salt simply reflect the strength of the inductive effect, again in the order  $\text{Li}^+ > \text{Na}^+ > \text{Tba}^+$ .

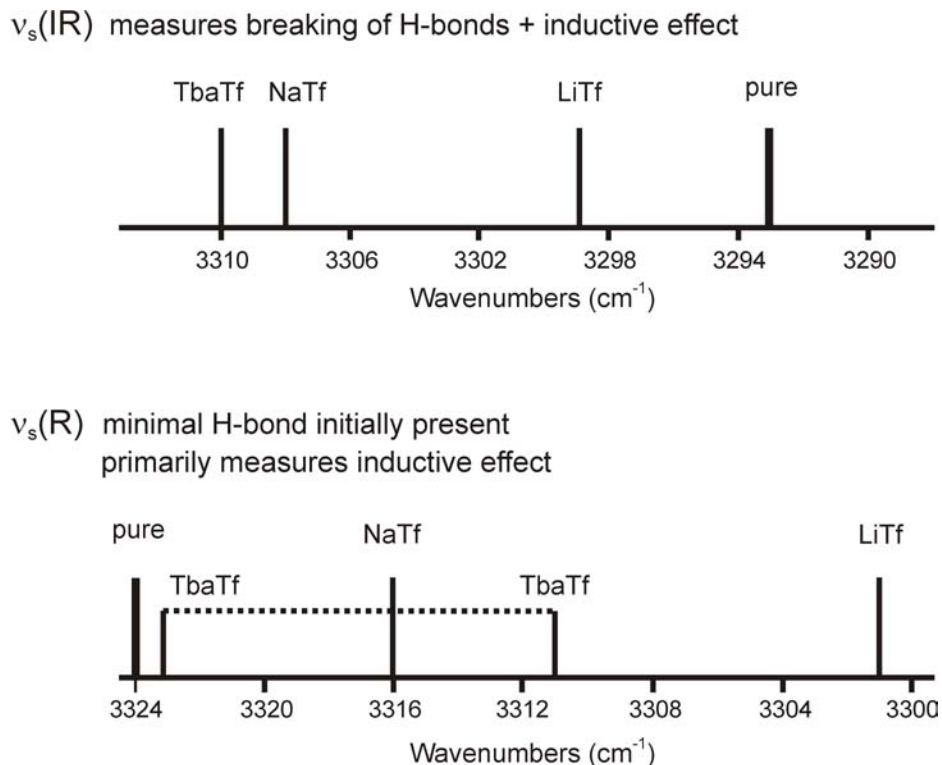


**Figure 4.13.** Summary of the  $\text{NH}_2$  symmetric stretch frequencies of hexylamine and the  $\text{N}:\text{Li}^+ = 3:1$  solutions of hexylamine – LiTf, hexylamine – NaTf, and hexylamine – TbaTf in the IR (top scale) and Raman (bottom scale).

A comparison of the infrared and Raman spectra of hexylamine with dissolved TbaTf (3:1 composition; see Figure 4.14) adds additional support to this general picture. The  $\nu_s(\text{NH}_2)$  band occurs at  $3310\text{ cm}^{-1}$  in the infrared spectrum, shifted from the pure hexylamine band at  $3293\text{ cm}^{-1}$  as explained above. In the Raman spectrum, there are two clearly discernible  $\nu_s(\text{NH}_2)$  features: a band at  $3323\text{ cm}^{-1}$  and a very marked shoulder at about  $3311\text{ cm}^{-1}$ . The band at  $3323\text{ cm}^{-1}$  is essentially due to unshifted hexylamine molecules because of the minimal interaction of the Tba cation with the nitrogen atom. However, in a significant fraction of the hexylamine molecules, the triflate ion oxygen atom forms a hydrogen bond with one of the amine hydrogen atoms, thus shifting the  $\nu_s(\text{NH}_2)$  band to  $3311\text{ cm}^{-1}$ .

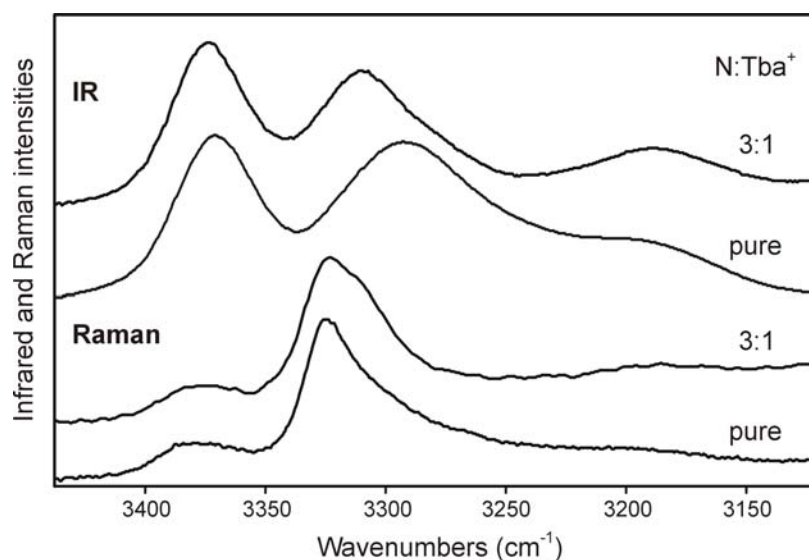


**Figure 4.14.** N-H stretching region of the IR and Raman spectra of hexylamine – TbaTf at a 3:1 molar composition and of pure hexylamine.

#### d) Hexylamine – LiTf in $\text{CCl}_4$

When a salt is dissolved in a primary amine, there are two effects that change the vibrational modes, particularly the N-H stretching vibrations: the breaking of the

hydrogen bonds and the cation inductive effect as the cation coordinates the nitrogen atom. Diluting hexylamine molecules in a  $\text{CCl}_4$  solution allows a study of the primary amine vibrational group when very limited intermolecular hydrogen bonding is present. Following the same line of reasoning, adding an electrolyte to a dilute solution of hexylamine in  $\text{CCl}_4$  allows one to study the effect of salt addition on the molecular host in the absence of significant intermolecular hydrogen bonding interactions.

Two solutions of different concentrations of hexylamine – LiTf electrolyte were dissolved in  $\text{CCl}_4$ . The results are very illuminating. Figure 4.15 shows the Raman spectra of HEXA – LiTf 5:1 (N:Li molar ratio) superposed with the Raman spectra of HEXA – LiTf 5:1 diluted in  $\text{CCl}_4$  at different concentrations (reported as  $\text{CCl}_4$ :N molar ratios).

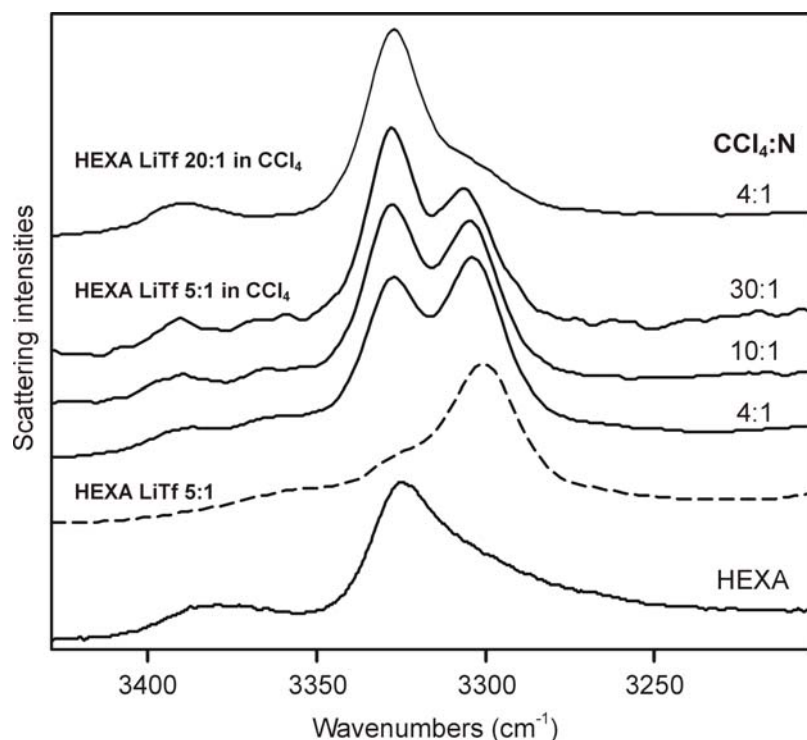


**Figure 4.15.** Raman spectra of HEXA – LiTf 5:1 (N:Li molar ratio) superposed with the Raman spectra of HEXA – LiTf 5:1 and HEXA – LiTf 20:1 diluted in  $\text{CCl}_4$  at different concentrations (reported as  $\text{CCl}_4$ :N molar ratios) in the N-H stretching region.

The asymmetric stretch has a very weak Raman scattering intensity; therefore only limited information can be obtained from this mode. The symmetric stretch of the HEXA – LiTf 5:1 solution occurs at  $3300\text{ cm}^{-1}$  with a shoulder around  $3325\text{ cm}^{-1}$ . The  $\nu_s(\text{NH}_2)$  region of all the HEXA – LiTf 5:1 complexes dissolved in  $\text{CCl}_4$  clearly contain two bands; in the most dilute solution ( $\text{CCl}_4:\text{N} = 30:1$ ) these occur at  $3328\text{ cm}^{-1}$  and  $3306\text{ cm}^{-1}$ . The scattering intensity of the former mode increases with increasing dilution and originates from hexylamine molecules not undergoing hydrogen bonding interactions or a cation – induced shift as noted in the previous discussion. The band at  $3306\text{ cm}^{-1}$  originates in hexylamine molecules undergoing a cation – induced shift (cation inductive effect) but no hydrogen bonding interactions. Since the nitrogen to lithium ratio is fixed at 5:1, the population of hexylamine molecules undergoing the lithium ion inductive effect is constant. Therefore the intensity increase of the higher frequency mode with dilution reflects the growing population of “free” hexylamine molecules that have significant Raman activity. *The strength of the cation-nitrogen coordinative interaction can be measured by the  $23\text{ cm}^{-1}$  shift to lower frequencies.*

In the Raman spectrum of HEXA – LiTf 20:1 in  $\text{CCl}_4$  at a 4:1  $\text{CCl}_4:\text{N}$  ratio (also shown in figure 4.15), the population of hexylamine molecules experiencing the inductive effect is very small because of the relatively few lithium cations present. The cation-shifted band is only seen as a shoulder on the low frequency side of the  $3328\text{ cm}^{-1}$  band.

The infrared spectra of a series of HEXA – LiTf 5:1 and HEXA – LiTf 20:1 compositions diluted in  $\text{CCl}_4$  at various concentrations (reported as  $\text{CCl}_4:\text{N}$  molar ratios) are shown in Figure 4.16. In both LiTf compositions, the  $\nu_{\text{as}}(\text{NH}_2)$  region has two bands

at 3391 and 3365  $\text{cm}^{-1}$  in the most dilute solutions, with the intensity of the higher frequency mode increasing with dilution relative to the lower frequency mode. In the  $\nu_s(\text{NH}_2)$  region of HEXA – LiTf 20:1, one main band occurs at 3300  $\text{cm}^{-1}$  and a weak band starts to grow upon dilution, reaching 3326  $\text{cm}^{-1}$  in the most dilute solution. In contrast, in HEXA – LiTf 5:1, only one band is observed at 3301  $\text{cm}^{-1}$ . The  $\text{NH}_2$  vibrations at 3391 and 3326  $\text{cm}^{-1}$  from the  $\nu_{\text{as}}(\text{NH}_2)$  and the  $\nu_s(\text{NH}_2)$  modes, respectively, have been attributed to the “free”  $\text{NH}_2$  groups. This assignment is supported by the IR and Raman spectra of the most dilute hexylamine –  $\text{CCl}_4$  solution because the frequencies of the two  $\text{NH}_2$  stretching modes correspond within  $\pm 2 \text{ cm}^{-1}$ , as shown in Figure 4.11. In both the asymmetric and symmetric stretching regions, the increase in intensity of the higher frequency mode with dilution reflects the increase in the population of “free” hexylamine molecules in the system with respect to the hydrogen bonded molecules. This increase was previously noted in the Raman and IR spectra of hexylamine diluted in  $\text{CCl}_4$ , and in the Raman spectra of HEXA – LiTf 5:1 in  $\text{CCl}_4$ . The lower frequency bands of  $\nu_{\text{as}}(\text{NH}_2)$  and  $\nu_s(\text{NH}_2)$  (3365 and 3301  $\text{cm}^{-1}$  in the most dilute solutions) are assigned to HEXA molecules coordinated by lithium with little intermolecular hydrogen bonding interactions between hexylamine molecules (less and less as the complex is more diluted). In the most dilute solutions, intermolecular hydrogen bonding interactions are essentially eliminated and the frequencies of these bands are due almost entirely to the cation inductive effect.

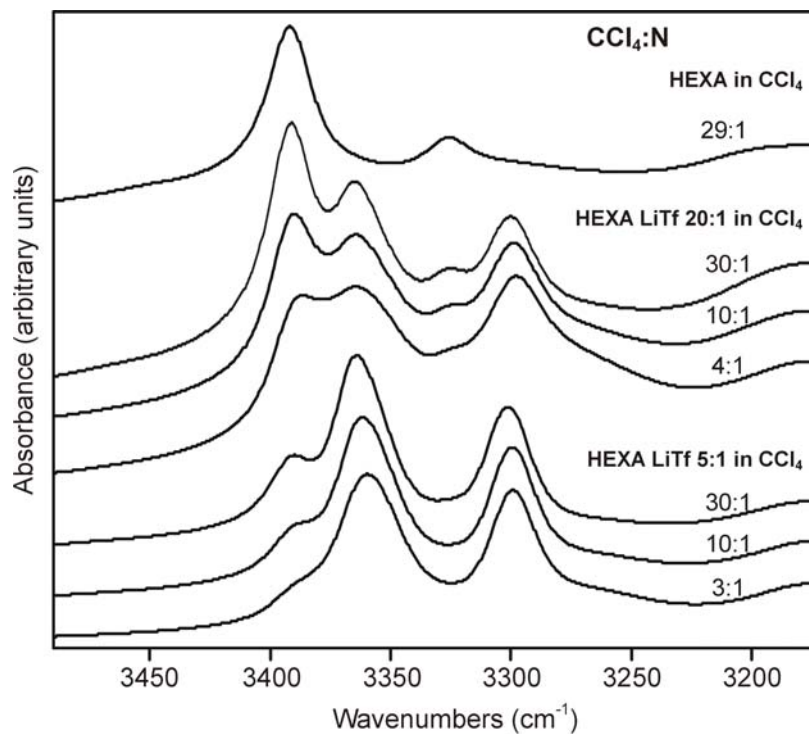


**Figure 4.16.** Infrared spectra of HEXA diluted in  $\text{CCl}_4$  at a 29:1 concentration superposed with HEXA – LiTf 20:1 and HEXA – LiTf 5:1 diluted in  $\text{CCl}_4$  at different concentrations (reported as  $\text{CCl}_4$ :N molar ratios) in the N-H stretching region.

For a given nitrogen to lithium ratio, the number of hexylamine molecules undergoing an inductive effect appears to be independent of the degree of dilution in  $\text{CCl}_4$ . When the amount of salt in the system increases (i.e. from a 20:1 to a 5:1 N:Li ratio), the population of molecules that are coordinated with lithium increases as reflected by the relative intensities of the two  $\nu_{\text{as}}(\text{NH}_2)$  modes in the two different dilution series. At a 5:1 N:Li ratio, the intensity of the  $3365\text{ cm}^{-1}$  band, which is due to lithium-coordinated hexylamine molecules, is very large compare to the “free”  $\text{NH}_2$  band at  $3391\text{ cm}^{-1}$ . In contrast, in the 20:1 N:Li solution, the bands at  $3391$  and  $3365\text{ cm}^{-1}$  have similar intensities, indicating a substantial amount of hexylamine molecules not affected by the

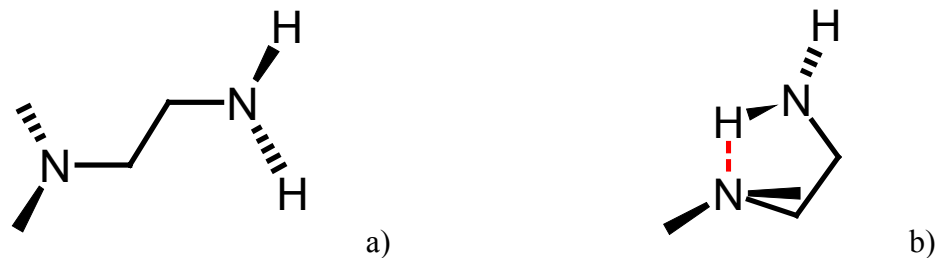
salt. This argument is also supported by the  $\nu_s(\text{NH}_2)$  region, where the presence of a “free” HEXA population is observed only in the HEXA – LiTf 20:1 dilution series.

The bands that are shifted to lower frequencies around 3365 and 3301  $\text{cm}^{-1}$  have been assigned to the population of amine groups that are coordinated with lithium. These frequencies differ from those of the IR of HEXA – LiTf (not diluted), where a mixture of hydrogen bonding interactions and the inductive effect alter the vibrational frequencies of the modes. On the other hand, the frequency of the  $\nu_s(\text{NH}_2)$  band at 3301  $\text{cm}^{-1}$  corresponds to that of the Raman spectrum of HEXA - LiTf (not diluted), where it was shown that the measurement samples the molecules that are the least hydrogen bonded and therefore more directly show the coordinative effect of lithium.

#### **4.2.2. N,N-DMEDA system**

##### **a) Evidence for intramolecular hydrogen bonding interactions**

The analysis of the vibrations of the primary amine group in DMEDA is very similar to that of hexylamine. However, due to the presence of a tertiary amine nitrogen separated from the primary amine group by an ethylene structure, one of the hydrogen atoms of the  $\text{NH}_2$  group has the possibility to form an intramolecular hydrogen bond, as shown in the sketches below. Unpublished gas phase quantum chemical calculations of pure DMEDA<sup>14</sup> show that the conformation adopted by the molecule leading to intramolecular hydrogen bonding is energetically stable.



**Sketch 4.1** DMEDA molecule in two different conformations. a) N-C-C-N dihedral angle in a trans conformation. b) N-C-C-N dihedral angle in a gauche conformation, where intramolecular hydrogen bonding is possible.

The formation of intramolecular hydrogen bonding interactions complicates the vibrational analysis of the primary amine group. In spite of this, the general picture developed in the hexylamine study is still valid.

Infrared spectra of the NH stretching region are plotted in Figure 4.17 for dilute solutions of hexylamine, benzylamine and DMEDA dissolved in carbon tetrachloride; each solution is prepared at a molar ratio of 30:1  $\text{CCl}_4:\text{NH}_2$ . In these dilute solutions, the intermolecular hydrogen bonding interactions are essentially eliminated. The  $\nu_s(\text{NH}_2)$  band occurs at 3326, 3327, and 3320  $\text{cm}^{-1}$  in solutions of hexylamine, benzylamine and DMEDA, respectively, while the  $\nu_{as}(\text{NH}_2)$  mode is observed at 3392, 3396, and 3394  $\text{cm}^{-1}$ , respectively. There is also a noticeable low frequency shoulder on the DMEDA  $\nu_{as}(\text{NH}_2)$  band. A comparison of the  $\nu_s(\text{NH}_2)$  bands shows that the vibrational potential energy environments of hexylamine and benzylamine are identical within experimental error. However, the lower frequency of the DMEDA  $\nu_s(\text{NH}_2)$  band (ca 6-7  $\text{cm}^{-1}$ ) suggests that some fraction of the molecules experiences a weak hydrogen bonding interaction that does not occur in hexylamine and benzylamine. This is attributed to intramolecular hydrogen bonding between a primary amine hydrogen atom and the

tertiary amine nitrogen atom. Support for this hypothesis is provided by the low frequency shoulder on the DMEDA  $\nu_{as}(\text{NH}_2)$  band. This feature also argues that some fraction of the DMEDA molecules is undergoing a hydrogen bonding interaction not experienced by either benzylamine or hexylamine.

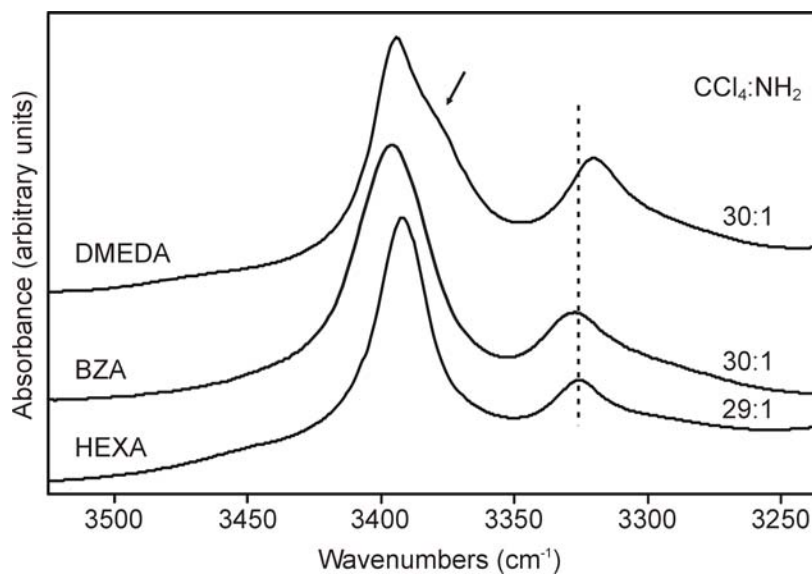


**Figure 4.17.** Infrared spectra of the N-H stretching region for solutions of hexylamine, benzylamine, and DMEDA dissolved in carbon tetrachloride at a molar ratio of 30:1 CCl<sub>4</sub>:NH<sub>2</sub>.

Intramolecular hydrogen bonding interactions are not as strong as intermolecular interactions because the N-C-C-N backbone of DMEDA is restricted to a particular conformation and therefore imposes a certain distance between the hydrogen atom of the primary amine group and the tertiary amine nitrogen. Such restriction does not exist while forming intermolecular hydrogen bonds and the hydrogen – tertiary amine nitrogen distance can be shorter, therefore forming stronger hydrogen bonds.

Furthermore, the intensity difference between the symmetric stretch compared to the asymmetric stretch is much smaller in DMEDA than in hexylamine, which implies

that the symmetric and asymmetric nature of the vibrations are not as defined in DMEDA compared with hexylamine. These observations reflect the larger distribution of hydrogen bonding environments in the DMEDA system, where intramolecular as well as intermolecular hydrogen bonds are present.

#### b) N,N-DMEDA and N,N-DMEDA in CCl<sub>4</sub>

Figure 4.18 shows the superposition of the IR and Raman spectra of pure DMEDA and DMEDA dissolved in carbon tetrachloride at various concentrations. The IR spectrum of pure DMEDA contains a strong  $\nu_{as}(\text{NH}_2)$  band centered at  $3366\text{ cm}^{-1}$  and a weaker, broader  $\nu_s(\text{NH}_2)$  band at  $3288\text{ cm}^{-1}$ . The less intense shoulder at roughly  $3192\text{ cm}^{-1}$  is an overtone of the  $\text{NH}_2$  deformation band at  $1596\text{ cm}^{-1}$  and is also seen in the IR spectra of the dilute DMEDA -  $\text{CCl}_4$  solutions.

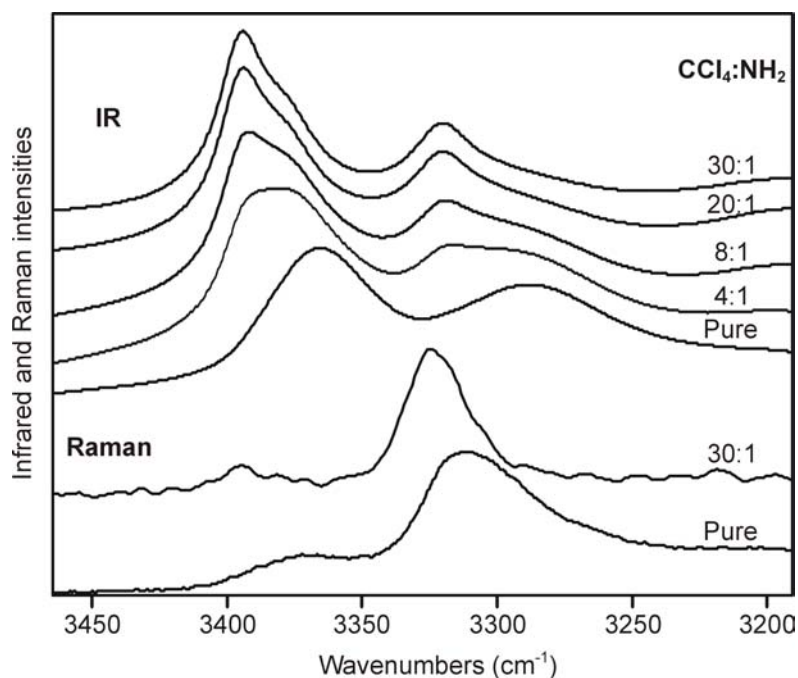


**Figure 4.18.** Infrared (top) and Raman (bottom) spectra of the N-H stretching region for pure DMEDA and DMEDA dissolved in carbon tetrachloride at different concentrations (reported as  $\text{CCl}_4:\text{NH}_2$  molar ratios).

Infrared and Raman spectra of DMEDA diluted in carbon tetrachloride resemble those of hexylamine. However, as discussed previously, noticeable differences point towards the different types of hydrogen bonding interactions occurring in DMEDA. When DMEDA is dissolved in CCl<sub>4</sub>, the  $\nu_{\text{as}}(\text{NH}_2)$  and  $\nu_{\text{s}}(\text{NH}_2)$  bands shift to higher frequencies as was seen in CCl<sub>4</sub> solutions of hexylamine. However in the DMEDA – CCl<sub>4</sub> solutions, both bands also exhibit low frequency shoulders. At a 30:1 CCl<sub>4</sub>:NH<sub>2</sub> molar ratio (or 15:1 CCl<sub>4</sub>:N molar ratio), band deconvolution shows that  $\nu_{\text{as}}(\text{NH}_2)$  has bands at 3395 cm<sup>-1</sup> and 3379 cm<sup>-1</sup>, while  $\nu_{\text{s}}(\text{NH}_2)$  has bands at 3320 cm<sup>-1</sup> and 3295 cm<sup>-1</sup>. The high frequency modes at 3395 and 3320 cm<sup>-1</sup> result from the “free” amine group, while the lower frequency modes with frequencies intermediate between “free” and *intermolecular* hydrogen bonded, probably result in the *intramolecular* hydrogen bonded molecules. The frequency data are summarized in Table 4.10. In these dilute solutions, the symmetric and antisymmetric character of the NH<sub>2</sub> vibrations are present to a significantly greater extent than in pure DMEDA, as evidenced by the relatively weak Raman scattering intensity, and the markedly stronger IR intensity of the  $\nu_{\text{as}}(\text{NH}_2)$  modes compare to the respective  $\nu_{\text{s}}(\text{NH}_2)$  modes.

**Table 4.10.** N-H stretching frequencies (cm<sup>-1</sup>) of pure N,N-DMEDA and dissolved in CCl<sub>4</sub> at a molar ratio of 30:1 CCl<sub>4</sub>:NH<sub>2</sub>.

		DMEDA	DMEDA in CCl <sub>4</sub>
IR	$\nu_{\text{as}}(\text{NH}_2)$	3366	3395, 3379
	$\nu_{\text{s}}(\text{NH}_2)$	3288	3320, 3295
Raman	$\nu_{\text{as}}(\text{NH}_2)$	3370	3392
	$\nu_{\text{s}}(\text{NH}_2)$	3311	3323

An interesting story emerges from the comparison of the two Raman spectra of Figure 4.18. In the dilute  $\text{CCl}_4$  solution, the maximum of  $\nu_s(\text{NH}_2)$  occurs at  $3323\text{ cm}^{-1}$  in the Raman spectrum which is intermediate between the IR frequency of  $\nu_s(\text{NH}_2)$  in dilute solutions of hexylamine, benzylamine, and DMEDA in  $\text{CCl}_4$  shown in Figure 4.17. In the dilute solutions of hexylamine and benzylamine, there are no intermolecular or intramolecular hydrogen bonding interactions. It appears that the Raman spectrum of DMEDA in the  $\nu_s(\text{NH}_2)$  region selectively samples those DMEDA molecules that also experience minimal intermolecular or intramolecular hydrogen bonding interactions. This selectivity results from the highly symmetric nature of those  $\text{NH}_2$  vibrations.

In the pure molecule, the band maximum of  $\nu_s(\text{NH}_2)$  at  $3311\text{ cm}^{-1}$  is lower than in hexylamine, reflecting a more strongly hydrogen bonded environment. A tail on the low frequency side of the band is attributed to a distribution of populations that are more strongly hydrogen bonded than the molecules contributing to the intensity in the band center. In the 30:1  $\text{CCl}_4$  solution, the band is about  $12\text{ cm}^{-1}$  higher than the corresponding band in the pure amine and the intensity of the low frequency wing decreases to leave a more symmetrical band. In hexylamine, in which intramolecular hydrogen bonding is impossible, the frequencies of the Raman bands of  $\nu_s(\text{NH}_2)$  in pure hexylamine and in a dilute  $\text{CCl}_4$  solution are quite close ( $3324$  and  $3328\text{ cm}^{-1}$ ). Therefore the larger frequency difference observed between pure and dilute  $\text{CCl}_4$  solutions of DMEDA is attributed to the fraction of molecules undergoing intramolecular hydrogen bonding interactions. These interactions may be present to a somewhat greater extent in the  $\text{CCl}_4$  solution than in pure DMEDA, because the intermolecular hydrogen bonding interactions present in

pure DMEDA would be expected to decrease the number of nitrogen sites available for intramolecular hydrogen bonding interactions.

In the IR and Raman spectra of the  $\text{CCl}_4$  solutions, the frequencies of  $\nu_s(\text{NH}_2)$  are almost coincident:  $3320\text{ cm}^{-1}$  in the IR and  $3323\text{ cm}^{-1}$  in the Raman. This is because the bands originate in the vibrations of the  $\text{NH}_2$  groups in which intermolecular hydrogen bonding does not occur. The same near coincidence is also observed for the  $\nu_{\text{as}}(\text{NH}_2)$  band:  $3395\text{ cm}^{-1}$  in IR and  $3392\text{ cm}^{-1}$  in Raman. In the IR spectrum of the dilute solution,  $\nu_{\text{as}}(\text{NH}_2)$  exhibits a shoulder on the low frequency side, and  $\nu_s(\text{NH}_2)$  has a long tail that extend beneath the pure DMEDA  $\nu_s(\text{NH}_2)$  IR band. Both features originate in the population distribution of hydrogen-bonded DMEDA molecules.

It is worthwhile to examine the spectra of pure DMEDA more carefully. As noted above, the IR spectrum contains a strong  $\nu_{\text{as}}(\text{NH}_2)$  band centered at  $3366\text{ cm}^{-1}$  and a weaker, broader  $\nu_s(\text{NH}_2)$  band at  $3288\text{ cm}^{-1}$ . The maximum Raman intensity of  $\nu_s(\text{NH}_2)$  occurs at  $3311\text{ cm}^{-1}$  and originates in the primary amine vibrations that are the most symmetric in nature. The intensity of this band then decreases slowly with decreasing frequency, indicating the presence of DMEDA molecules in an increasingly stronger hydrogen-bonded environment. The frequency differences between the IR and Raman band maxima are  $4\text{ cm}^{-1}$  for  $\nu_{\text{as}}(\text{NH}_2)$  and  $23\text{ cm}^{-1}$  for  $\nu_s(\text{NH}_2)$ . These differences confirm that the frequency of the  $\nu_s(\text{NH}_2)$  mode is more sensitive to hydrogen bonding interactions. The sensitivity arises because in the pure liquid, the Raman spectrum selectively picks out those molecules whose vibrations are the most symmetric, i.e. undergoing the least amount of hydrogen bonding interactions.

### c) N,N-DMEDA – salt complexes

*N-H stretching region of DMEDA-LiTf and DMEDA-NaTf solutions.* The effect of adding salt to DMEDA is illustrated in Figure 4.19, which shows the Raman spectra of DMEDA – LiTf in the NH stretching region. The broad, asymmetric  $\nu_s(\text{NH}_2)$  band at  $3311\text{ cm}^{-1}$  in pure DMEDA appears to shift to lower frequencies with increasing salt concentration, although this shift may result from an increase of scattering intensity on the low frequency side, perhaps accompanied by an intensity decrease of the original maximum in the band envelope. At a 10:1 composition, the band maximum is at  $3302\text{ cm}^{-1}$  in the LiTf solution. With further addition of salt,  $\nu_s(\text{NH}_2)$  then shifts to higher frequencies until at a 3:1 composition the band maximum is at  $3314\text{ cm}^{-1}$ . This trend continues on into the crystalline phase, where there is a single  $\nu_s(\text{NH}_2)$  band at  $3316\text{ cm}^{-1}$ . These frequency data are plotted in Figure 4.20, along with the corresponding data for the NaTf solutions (spectra not shown). In pure DMEDA, the Raman spectrum of  $\nu_s(\text{NH}_2)$  selectively samples those DMEDA molecules that undergo the weakest hydrogen bonding interactions. The frequency shift results from a combination of two opposing factors. The cation inductive effect shifts the bands to lower frequencies because the lone pair of the nitrogen atom is involved in the solvation of the cations, causing a weakening of the N-H bond by decreasing its electron density. However, the intermolecular or intramolecular hydrogen bonds in DMEDA are replaced by weaker hydrogen bonds to the triflate oxygen atoms, causing a shift to higher frequencies. Therefore, the resulting frequency of an N-H stretching band is dependent on the relative contribution of each factor. Noting that in the crystals there are only N–H $\cdots$ O hydrogen bond present, it is clear from comparing the frequencies in pure DMEDA with those in the DMEDA-LiTf

crystalline phase that the N–H···O hydrogen bond is weaker than the N–H···N hydrogen bond. For example,  $\nu_s(\text{NH}_2)$  in the Raman spectrum of the crystal is at 3316  $\text{cm}^{-1}$ , five wavenumbers higher than the value in pure DMEDA. This is in spite of the fact that the cation inductive effect in the crystal will shift the frequency to lower values.

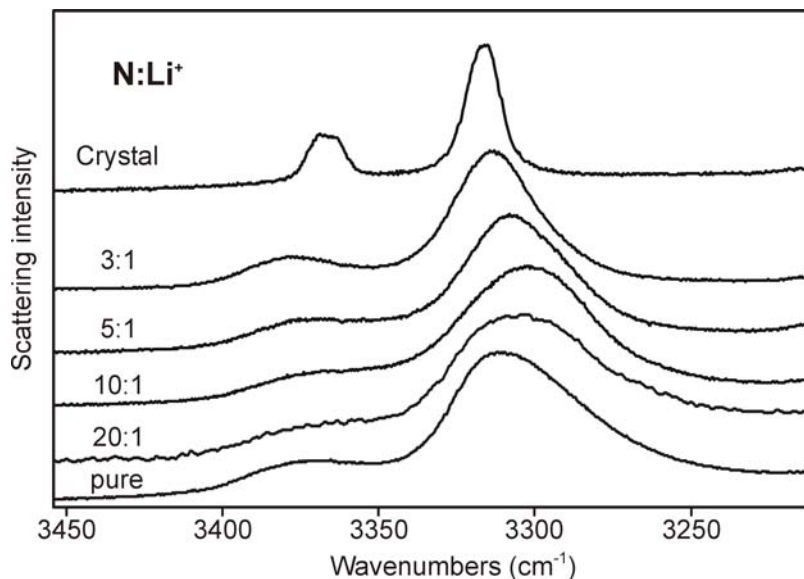


**Figure 4.19.** Raman spectra of DMEDA:LiTf crystal, DMEDA – LiTf solutions with various N:Li<sup>+</sup> ratios, and pure DMEDA in the N-H stretching region.

The initial shift to lower frequencies at low salt concentrations occurs because the cation coordinates those DMEDA molecules that are essentially “free” and therefore more accessible for coordinative interaction, and the cation inductive effect is dominant. Apparently in the more dilute solutions, the weaker N–H···O hydrogen bonds do not tend to form. However, as additional salt is added, the population of more strongly N–H···N hydrogen bonded DMEDA molecules is replaced by DMEDA molecules that are either more weakly hydrogen-bonded to triflate oxygen atoms or

perhaps not hydrogen bonded at all. This effect more than compensates for decrease due to the cation inductive effect, and the frequency of the NH stretching bands increases.

Qualitatively the same behavior occurs in the DMEDA-NaTf solutions as in the DMEDA-LiTf solutions (see Figure 4.20), i.e. the  $\nu_s(\text{NH}_2)$  frequency first decreases and then increases with increasing salt composition. Although the minimum occurs at the same 10:1 composition, the frequency shift from the pure liquid is not as large as in the LiTf solutions. Moreover, the frequency of  $\nu_s(\text{NH}_2)$  is 10 wavenumbers higher ( $3326 \text{ cm}^{-1}$ ) in the DMEDA-NaTf crystal than in the DMEDA-LiTf crystal ( $3316 \text{ cm}^{-1}$ ). This comparison argues that the cation inductive effect is weaker in the DMEDA-NaTf crystal than in the DMEDA-LiTf crystal.

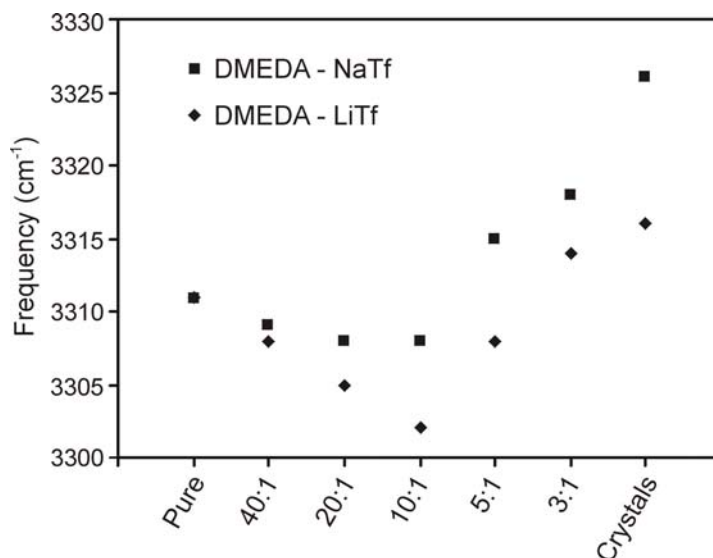


**Figure 4.20.** Summary of the  $\text{NH}_2$  symmetric stretch frequencies of DMEDA - LiTf and DMEDA - NaTf solutions at various N: $\text{M}^+$  ratios, and the respective crystals.

Figure 4.21 shows the IR spectra of DMEDA - LiTf solutions in the N-H stretching region. With increasing salt concentration, the frequency of  $\nu_{\text{as}}(\text{NH}_2)$  behaves

similarly to shifts observed in the Raman spectrum of  $\nu_s(\text{NH}_2)$  illustrated in Figure 4.19. The band at  $3366\text{ cm}^{-1}$  in pure DMEDA shifts to lower frequencies until a minimum of about  $3352\text{ cm}^{-1}$  is observed in the 10:1 composition. With further addition of salt, the band then shifts to higher frequencies. As in the case of the Raman spectra of  $\nu_s(\text{NH}_2)$ , the “shift” of  $\nu_{as}(\text{NH}_2)$  appears to be a poorly resolved band that grows on the low frequency side of  $\nu_{as}(\text{NH}_2)$ , until at the 10:1 composition, the band appears as a broad feature with poorly defined structure. In the 6:1 composition, the lower frequency feature is now a shoulder at roughly  $3351\text{ cm}^{-1}$  on the side of the dominant  $3367\text{ cm}^{-1}$  band. In the 3:1 sample, there is only a well-defined band at  $3376\text{ cm}^{-1}$ . The initial “shift” to lower frequencies at lower salt concentrations is again due to the cation inductive effect. At higher salt concentrations, the breaking of  $\text{N}-\text{H}\cdots\text{N}$  hydrogen bonds results in a shift to higher frequencies.

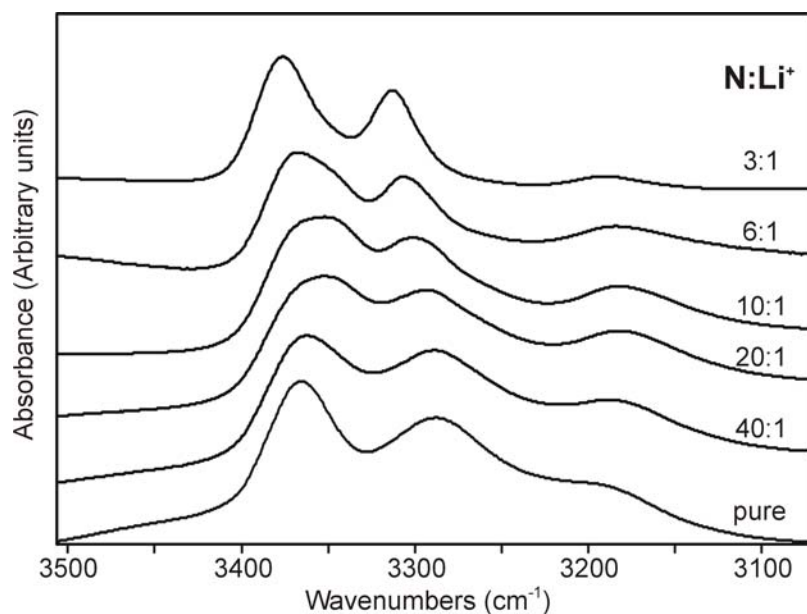


**Figure 4.21.** Infrared spectra of DMEDA – LiTf solutions with various N:Li<sup>+</sup> ratios, and pure DMEDA in the N-H stretching region.

In contrast to the  $\nu_{\text{as}}(\text{NH}_2)$  behavior in the IR spectrum,  $\nu_{\text{s}}(\text{NH}_2)$  at  $3288\text{ cm}^{-1}$  in pure DMEDA continuously shifts to higher frequencies with increasing LiTf concentration, finally reaching  $3313\text{ cm}^{-1}$  at the 3:1 composition. The failure to observe any initial decrease in frequency due to the cation inductive effect is attributed to the greater sensitivity of the  $\nu_{\text{s}}(\text{NH}_2)$  mode to hydrogen bonding. A study of tetrabutylammonium triflate dissolved in DMEDA supports this point. The bulky nature of the tetrabutylammonium cation prevents any coordination with the DMEDA host; consequently these measurements isolate the effect of hydrogen bond replacement. In a DMEDA - tetrabutylammonium triflate solution at a 3:1 composition, the  $\nu_{\text{as}}(\text{NH}_2)$  and  $\nu_{\text{s}}(\text{NH}_2)$  bands occur at  $3371$  and  $3307\text{ cm}^{-1}$ , respectively. Relative to pure DMEDA, these are shifts of  $+5$  and  $+19\text{ cm}^{-1}$ , which shows that  $\nu_{\text{s}}(\text{NH}_2)$  is considerably more sensitive to hydrogen bonding interactions. Consequently, in the DMEDA-LiTf solutions, the replacement of  $\text{N}-\text{H}\cdots\text{N}$  hydrogen bonds by weaker  $\text{N}-\text{H}\cdots\text{O}$  hydrogen bonds more than compensates for the cation inductive effect, and a continuous higher frequency shift of  $\nu_{\text{s}}(\text{NH}_2)$  with increasing salt concentration is observed.

Similar patterns of spectral behavior are found in the IR spectra of DMEDA – NaTf solutions, although the presence of the lower frequency feature on the side of  $\nu_{\text{as}}(\text{NH}_2)$  is barely visible. The shift of  $\nu_{\text{s}}(\text{NH}_2)$  from pure DMEDA to a 3:1 composition is  $+29\text{ cm}^{-1}$ , which is greater than the  $+25\text{ cm}^{-1}$  shift in the corresponding LiTf solution. An analogous pattern is found for  $\nu_{\text{as}}(\text{NH}_2)$ ; the shift is  $+15\text{ cm}^{-1}$  in the 3:1 composition of DMEDA:NaTf and only  $+10\text{ cm}^{-1}$  in the corresponding DMEDA:LiTf complex.

It is noteworthy that at the 3:1 composition, the  $\nu_{\text{s}}(\text{NH}_2)$  stretching frequencies of the IR and Raman bands are coincident (within experimental error) in both the LiTf and

NaTf solutions, with the frequencies of the NaTf solutions somewhat higher; the same is true of  $\nu_{\text{as}}(\text{NH}_2)$ . At this very high salt concentration, the hydrogen-bonding environment of the molecules is quite similar, as is their coordination with the cations. Therefore the Raman and IR selection rules cannot distinguish molecules within the general population and the bands are coincident.

***N-H stretching region of DMEDA-LiTf and DMEDA-NaTf crystals.*** In the crystalline phase, the  $\nu_{\text{as}}(\text{NH}_2)$  vibrations of DMEDA-LiTf and the  $\nu_{\text{s}}(\text{NH}_2)$  vibrations of DMEDA-NaTf are split into several components. The IR and Raman spectra of the two crystals are shown in Figure 4.22, and the data are summarized in Table 4.11.

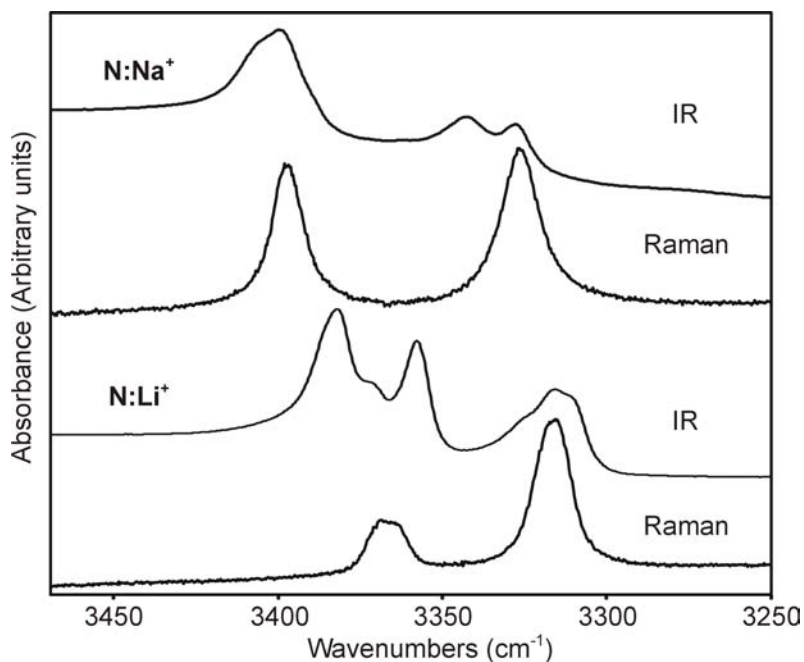


**Figure 4.22.** Raman and infrared spectra of DMEDA:NaTf crystal (top) and DMEDA:LiTf crystal (bottom) in the N-H stretching region.

**Table 4.11.** N-H stretching frequencies ( $\text{cm}^{-1}$ ) of DMEDA-LiTf and DMEDA-NaTf crystals.

		$\nu_{\text{as}}(\text{NH}_2)$	$\nu_{\text{s}}(\text{NH}_2)$
DMEDA-LiTf	Raman	3366	3316
		3382	
	IR	3371 (sh)	3316
		3358	
DMEDA-NaTf	Raman	3398	3326
	IR	3406 (sh)	3343
		3399	3327

This pattern results from the intermolecular coupling of vibrating  $\text{NH}_2$  groups in the primitive unit cell; the number of normal modes and their symmetry classification can be calculated using standard group theory methods.<sup>15</sup> Because both crystals belong to the same space group, they have the same unit cell group. Therefore a similar vibrational pattern is expected for both crystals. The vibrational modes originating in each kind of NH stretch and their classification according to the irreducible representations of the  $\text{C}_{2h}$  unit cell group (factor group) are:

$$\Gamma(\nu_{\text{s}}(\text{NH}_2)) = \Gamma(\nu_{\text{as}}(\text{NH}_2)) = A_{\text{g}} + B_{\text{g}} + A_{\text{u}} + B_{\text{u}} \quad (1)$$

Two infrared active modes and two Raman active modes are predicted for each of the  $\nu_{\text{s}}(\text{NH}_2)$  and  $\nu_{\text{as}}(\text{NH}_2)$  vibrations in the crystal. In the IR spectrum of the DMEDA:NaTf crystal,  $\nu_{\text{s}}(\text{NH}_2)$  has two distinct peaks at 3327 and 3343  $\text{cm}^{-1}$ , and  $\nu_{\text{as}}(\text{NH}_2)$  has one main band at 3399  $\text{cm}^{-1}$  with a shoulder around 3406  $\text{cm}^{-1}$ . In the DMEDA:LiTf crystal,  $\nu_{\text{s}}(\text{NH}_2)$  occurs at 3316  $\text{cm}^{-1}$  with two distinct shoulders on each side, while  $\nu_{\text{as}}(\text{NH}_2)$  clearly splits into two major components at 3358 and 3382  $\text{cm}^{-1}$  with

a shoulder at roughly  $3371\text{ cm}^{-1}$ . Because the sample is in the form of a microcrystalline powder when the spectra are measured, these minor “extra” features may originate in orientational effects. However, it is curious that these occur in the DMEDA:LiTf crystal, but not the DMEDA:NaTf crystal.

The importance of the cation inductive effect is apparent when comparing the spectra of the 3:1 solutions with those of the crystals. In the LiTf system, the  $\nu_s(\text{NH}_2)$  and  $\nu_{as}(\text{NH}_2)$  bands occur at about the same frequencies in both the 3:1 solution ( $\nu_s(\text{NH}_2) = 3314\text{ cm}^{-1}$ , Raman) and in the crystal ( $\nu_s(\text{NH}_2) = 3316\text{ cm}^{-1}$ , Raman), whereas in the DMEDA – NaTf system, the same comparison shows a striking shift to higher frequencies in the crystal ( $\Delta\nu_s(\text{NH}_2) = +8\text{ cm}^{-1}$ ). In the 3:1 solutions, there is still a significant amount of N–H $\cdots$ N hydrogen bonding interactions that are not broken until the crystals are formed. The crystal structures of both compounds clearly show that the N–H $\cdots$ N hydrogen bonds present in the solution phase have been replaced by weaker hydrogen bonds with the triflate oxygen atoms in the DMEDA:LiTf compound; in the DMEDA:NaTf compound, there is also a weak hydrogen bond with a fluorine atom (Table 4.5). Consequently, the difference between the two systems is most easily explained by the stronger inductive effect of the lithium ion. The inductive effect of sodium is not strong enough to compensate for breaking the hydrogen bonds that occur in the solution phase, consequently there is a marked shift to higher frequencies upon formation of the crystalline phase. On the other hand, in the DMEDA:LiTf crystal, the relatively stronger lithium ion inductive effect lowers the frequency, almost offsetting the shift to higher frequency that accompanies the replacement of relatively stronger hydrogen bonds in solution by weaker hydrogen bonds in the crystal.

The symmetry-based vibrational analysis (Eq. 1) predicts two Raman active modes for each of the two NH stretching modes. In the Raman spectrum of DMEDA:LiTf crystalline compound,  $\nu_s(\text{NH}_2)$  has a small sharp peak centered at  $3316\text{ cm}^{-1}$ , a frequency corresponding to one of the IR bands; whereas  $\nu_{as}(\text{NH}_2)$  occurs around  $3366\text{ cm}^{-1}$  with a much smaller scattering intensity and does not have a counterpart in the IR spectrum. The band shape of  $\nu_{as}(\text{NH}_2)$  suggests two underlying components, accounted for by the predicted factor group multiplet of Eq. 1. In the DMEDA:NaTf crystal, the NH stretching region of the Raman spectrum exhibits two relatively sharp peaks of similar intensity:  $\nu_s(\text{NH}_2)$  at  $3326\text{ cm}^{-1}$  and  $\nu_{as}(\text{NH}_2)$  at  $3398\text{ cm}^{-1}$ . These frequencies are coincident within experimental error with two of the IR bands.

The relative Raman intensities of  $\nu_{as}(\text{NH}_2)$  and  $\nu_s(\text{NH}_2)$  in the two compounds can be explained in terms of their crystal structures. In the DMEDA:LiTf crystal (Figure 4.4), each hydrogen atom of the  $\text{NH}_2$  groups is weakly hydrogen bonded to an oxygen atom of a triflate ion, with the hydrogen-bonding environment of each amine hydrogen atom roughly equivalent. Therefore, the  $\nu_{as}(\text{NH}_2)$  and  $\nu_s(\text{NH}_2)$  modes preserve their approximately antisymmetric and symmetric character, respectively, as reflected in the IR and Raman intensities of each mode. In contrast, in the DMEDA:NaTf crystal (Figure 4.6) the hydrogen atoms of the  $\text{NH}_2$  group form hydrogen bonds to an oxygen atom and to a fluorine atom. The significantly different potential energy environment of the two hydrogen atoms causes the  $\nu_{as}(\text{NH}_2)$  and  $\nu_s(\text{NH}_2)$  modes to lose their symmetric and antisymmetric character, as reflected in the intensities in the Raman spectrum. Interestingly, the relative IR intensities of the two modes appear to be insensitive to subtle differences in the potential energy environment of the two crystals.

***Conformation region of DMEDA-LiTf and DMEDA-NaTf.*** Figure 4.23 shows the IR spectra from 800 to 1000  $\text{cm}^{-1}$  of DMEDA, solutions of DMEDA-LiTf and DMEDA-NaTf at various compositions, and the corresponding DMEDA-salt crystals. Frequencies and intensities of bands in this spectral region are particularly sensitive to the coordinative interactions between the DMEDA nitrogen atoms and the cations. In DMEDA, the bands in this region are comprised mainly of a mixture of  $\text{CH}_2$  rocking, C-N stretching and  $\text{NH}_2$  wagging motions, plus a small contribution from C-C stretching.<sup>14,16</sup> With the addition of LiTf or NaTf, the  $\text{CH}_2$  rocking and  $\text{NH}_2$  wagging motions provide the primary contribution to the normal modes. These assignments are based on gas phase quantum chemical calculations of pure DMEDA, DMEDA-LiTf and DMEDA-NaTf systems.<sup>14</sup> In the IR spectrum, DMEDA has three bands of medium intensity at 851, 887 and 930  $\text{cm}^{-1}$ , with a weak band at 918  $\text{cm}^{-1}$ . As LiTf is initially added to DMEDA, a small, sharp band appears the high frequency side of the 851  $\text{cm}^{-1}$  band, at roughly 873  $\text{cm}^{-1}$ . Upon further addition of salt, the intensity of this band increases, but the frequency does not shift until crystal formation, where it occurs at 876  $\text{cm}^{-1}$ . With the addition of NaTf to DMEDA, similar behavior is observed. A new band appears at about 865  $\text{cm}^{-1}$ , on the high frequency side of the 851  $\text{cm}^{-1}$  DMEDA band. The new band increases in intensity with increasing salt concentration until the original 851  $\text{cm}^{-1}$  band is a weak, high frequency shoulder in the 6:1 composition. In the 3:1 composition, only one very broad band is observed. This band becomes much sharper in the crystal and shifts to 868  $\text{cm}^{-1}$ .

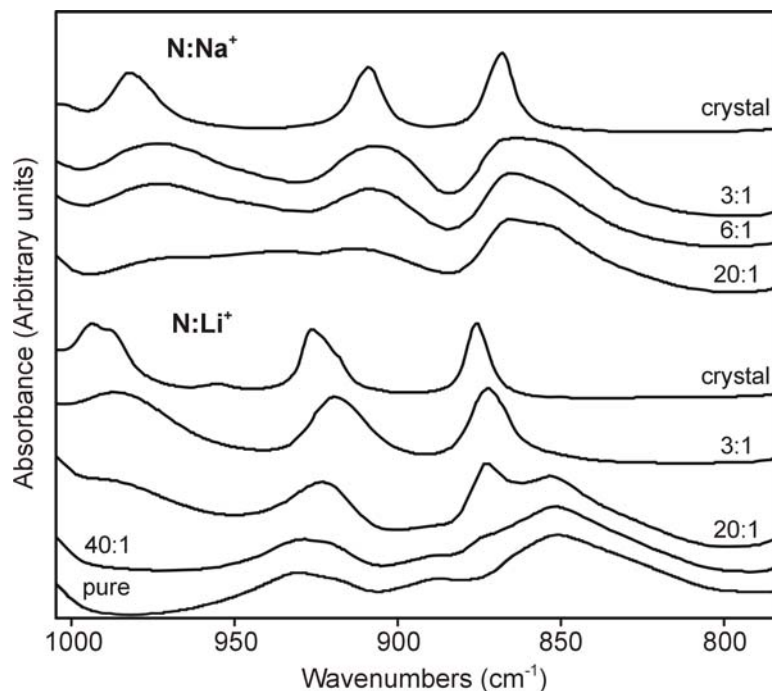


**Figure 4.23.** Infrared spectra of DMEDA – NaTf solutions (top) and DMEDA – LiTf solutions (bottom) with various N:M<sup>+</sup> ratios and the corresponding crystals in the conformation region.

Two other DMEDA bands in this region are markedly changed by the addition of salt. The band at 930 cm<sup>-1</sup> appears to initially broaden as LiTf is added, although this may be due to coalescence with the low frequency feature at 918 cm<sup>-1</sup> (clearly seen in the spectrum of pure DMEDA). The frequency of the band decreases with LiTf concentration to 919 cm<sup>-1</sup> in the 3:1 sample, and shifts to 926 cm<sup>-1</sup> in the crystalline phase, with two distinct shoulders on the low frequency side. At the same time, a weak, broad band appears at roughly 989 cm<sup>-1</sup> (20:1 composition), grows in intensity until it is a very distinct feature at 987 cm<sup>-1</sup> in the 3:1 sample. This band then appears as two bands at 994 and 988 cm<sup>-1</sup> in the crystal. The behavior with addition of NaTf appears to be somewhat different. The spectrum of the 20:1 sample suggests that the intensity of the DMEDA band at 930 cm<sup>-1</sup> decreases and its frequency increases, appearing as a weak

feature at  $935\text{ cm}^{-1}$ . At the same time, the intensity of the  $918\text{ cm}^{-1}$  band grows as the frequency decreases to  $913\text{ cm}^{-1}$ . In the 3:1 sample, this band is centered roughly at  $909\text{ cm}^{-1}$  and appears as a sharp band in the crystal at  $907\text{ cm}^{-1}$ . In addition, a weak, broad band at  $970\text{ cm}^{-1}$  is observed in the 20:1 spectrum and becomes a very broad feature centered roughly at  $973\text{ cm}^{-1}$  in the 3:1 composition. The band then shifts to  $982\text{ cm}^{-1}$  in the DMEDA-NaTf crystal.

The frequency shifts in this region are larger in the LiTf solutions than in the NaTf solutions, consistent with a stronger coordinative interaction of the lithium ion with DMEDA. Moreover, the bands that appear with addition of salt are much narrower in the LiTf solutions than in the NaTf solutions at all comparable compositions. The smaller bandwidths in the LiTf solutions reflect a narrower distribution of DMEDA-Li<sup>+</sup> coordinative interactions, which presumably originate in the stronger DMEDA-Li<sup>+</sup> interactions. The crystallographic data show that the N-C-C-N angles in the DMEDA:LiTf and DMEDA:NaTf crystals are  $59^\circ$  and  $-66^\circ$ , or  $\bar{g}$  and  $\bar{g}$ , respectively. Although these dihedral angles differ by only  $7^\circ$ , this value probably reflects the difference in the strength of cation-nitrogen atom coordination.

#### **d) N,N-DMEDA - LiTf in CCl<sub>4</sub>**

When salt is added to DMEDA in CCl<sub>4</sub> the changes observed in the Raman spectrum are not as dramatic as in the hexylamine in CCl<sub>4</sub> system and do not provide significant new information. In brief, DMEDA - LiTf 10:1 and DMEDA - LiTf 4:1 compositions were dissolved in various amounts of CCl<sub>4</sub> (spectra not shown). The  $\nu_s(\text{NH}_2)$  band shifts to  $3322\text{ cm}^{-1}$  in all the dilute solutions, and the low frequency wing

progressively decreases as the DMEDA – LiTf complex becomes more diluted in CCl<sub>4</sub>, but the wing never completely disappears. Unlike the hexylamine - LiTf system, no large shift to lower frequency is observed. This behavior is in accordance with the Raman spectra measured for the concentration dependence of DMEDA – LiTf with no addition of CCl<sub>4</sub>. A rough balance between the breaking of hydrogen bonds and the inductive effect of lithium prevented any large frequency shifts from occurring. The small changes in the Raman spectra of the dilute solutions do not permit a detailed analysis. The different spectral behavior in the hexylamine and DMEDA systems may be due to differences in the cation coordination strength, as well as differences in the types of hydrogen bonds present. In DMEDA, lithium coordinates two nitrogens from the same molecule, whereas in hexylamine, only one nitrogen atom is available. In both electrolytes, the coordination of lithium is satisfied via the triflate anion oxygen atoms.

In contrast to the Raman spectra, the IR spectra of DMEDA-LiTf 10:1 dissolved in CCl<sub>4</sub> shows marked changes upon dilution. The data are shown in Figure 4.24, along with the IR spectrum of DMEDA diluted in CCl<sub>4</sub> at a 30:1 molar ratio. Curve fitting of the three different CCl<sub>4</sub> dilutions of 10:1 DMEDA - LiTf shows that the original bands found in diluted DMEDA are still present when salt is added. A summary of the band deconvolution results is given in Tables 4.12 and 4.13 as an aid for the following discussion.

**Table 4.12.** IR frequencies for the  $\nu_{as}(\text{NH}_2)$  and the  $\nu_s(\text{NH}_2)$  modes of DMEDA diluted in CCl<sub>4</sub>. The 30:1 CCl<sub>4</sub>:NH<sub>2</sub> molar ratio is equivalent to a 15:1 CCl<sub>4</sub>:N molar ratio.

CCl <sub>4</sub> :NH <sub>2</sub>	$\nu_{as}(\text{NH}_2)$		$\nu_s(\text{NH}_2)$	
	“Free”	H-bonded	“Free”	H-bonded
30:1	3395	3379	3320	3295

**Table 4.13.** IR frequencies for the  $\nu_{as}(\text{NH}_2)$  and the  $\nu_s(\text{NH}_2)$  modes of DMEDA – LiTf 10:1 diluted in  $\text{CCl}_4$ . The ratios are  $\text{CCl}_4:\text{N}$  molar ratios.

$\text{CCl}_4:\text{N}$	$\nu_{as}(\text{NH}_2)$			$\nu_s(\text{NH}_2)$		
	“Free”	H-bonded	Complex	“Free”	H-bonded	Complex
30:1	3394	3380	3363	3319	3285	3306
10:1	3395	3381	3364	3319	3289	3306
4:1	Not converged			Not converged		

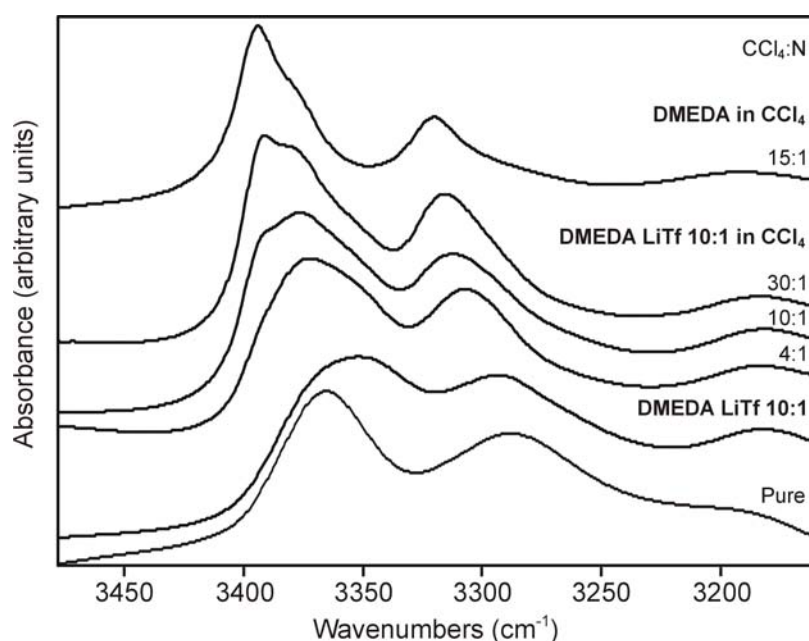


**Figure 4.24.** Infrared spectra of DMEDA – LiTf 10:1 (N:Li molar ratio) superposed with the infrared spectra of DMEDA diluted in  $\text{CCl}_4$  at a 15:1 concentration and DMEDA – LiTf 10:1 diluted in  $\text{CCl}_4$  at different concentrations (reported as  $\text{CCl}_4:\text{N}$  molar ratios) in the N-H stretching region.

The two bands present in the DMEDA -  $\text{CCl}_4$  solutions for each of the symmetric and asymmetric stretches are also present in the DMEDA - LiTf -  $\text{CCl}_4$  solutions, which indicates that the added salt does not affect the entire DMEDA population. As the concentration of DMEDA - LiTf complex increases, the intensities of the “free” and

hydrogen-bonded DMEDA bands decrease and the intensities of the bands that correspond to the DMEDA – LiTf complex increase. For the 30:1 and 10:1 dilutions in CCl<sub>4</sub>, the curve fitting analysis resulted in converged solutions from which several conclusions may be drawn. The DMEDA - LiTf complex in CCl<sub>4</sub> has a symmetric NH<sub>2</sub> stretching vibration around 3306 cm<sup>-1</sup> and an asymmetric stretching vibration around 3364 cm<sup>-1</sup>. As the concentration of the DMEDA – LiTf complex increases to a 4:1 composition (CCl<sub>4</sub>:N molar ratio), the appearance and frequencies of the  $\nu_s(\text{NH}_2)$  and  $\nu_{as}(\text{NH}_2)$  become more similar to that of the undiluted complex where a greater degree of inhomogeneity is reflected by the breadth of the bands. At this solution composition, the population of free primary amine groups is small and the sample is mainly composed of hydrogen bonded amines and amines coordinated with lithium ions. The curve fitting analysis did not converge.

The N-H stretching frequencies of the DMEDA - LiTf complex in CCl<sub>4</sub> (Table 4.13) are very close to those of hexylamine - LiTf in CCl<sub>4</sub>. The frequency of the  $\nu_{as}(\text{NH}_2)$  vibration occurs around 3364 cm<sup>-1</sup> for both complexes in CCl<sub>4</sub>. In contrast, the frequency of the  $\nu_s(\text{NH}_2)$  vibration is about 5 cm<sup>-1</sup> higher in the DMEDA complex (3306 cm<sup>-1</sup> vs. 3301 cm<sup>-1</sup> in HEXA – LiTf 5:1 in CCl<sub>4</sub> 30:1). This difference is due to the higher sensitivity of the symmetric NH<sub>2</sub> stretching mode to the hydrogen bonding environment of the amine group compared to the asymmetric stretching mode. This also explains the difference between the  $\nu_s(\text{NH}_2)$  frequency of the hydrogen bonded population in the DMEDA - LiTf in CCl<sub>4</sub> (3285 – 3289 cm<sup>-1</sup>) and DMEDA in CCl<sub>4</sub> (3295 cm<sup>-1</sup>).

### 4.2.3. Dipropylamine system

#### a) Dipropylamine and dipropylamine in CCl<sub>4</sub>

Figure 4.25 shows the IR and Raman spectra in the  $\nu(\text{NH})$  region for pure DPA, and DPA dissolved in CCl<sub>4</sub> at various molar ratios. The IR spectrum of DPA consists of one broad band centered around 3289 cm<sup>-1</sup>, whereas the Raman spectrum has two weak overlapping bands centered at 3327 and 3315 cm<sup>-1</sup>. These data are consistent with the spectra of hexylamine and DMEDA, where the IR spectrum samples molecules that are in a more hydrogen bonded environment as reflected by a lower NH stretching frequency, and the Raman spectrum samples molecules that are less hydrogen bonded. The presence of two different peaks in the Raman spectrum indicates two distinctly different types of weakly hydrogen bonded NH groups in pure dipropylamine.

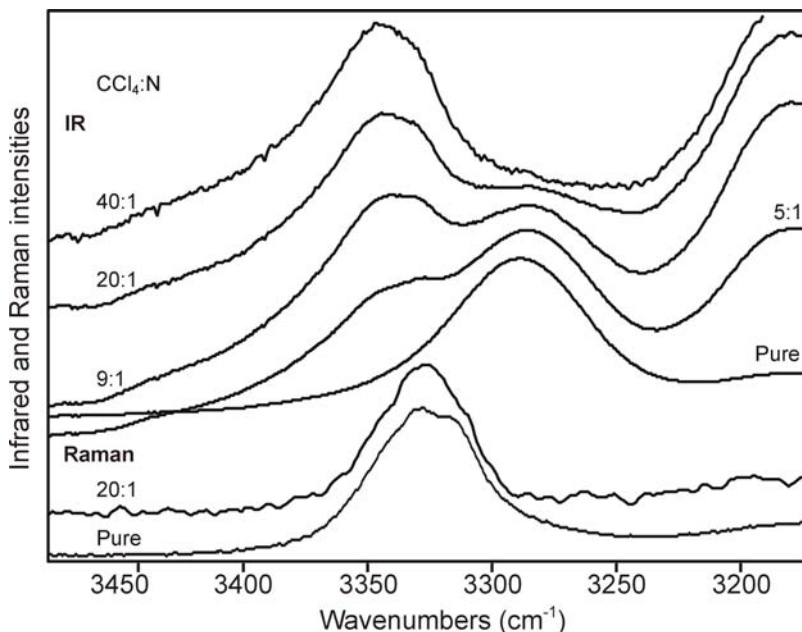


**Figure 4.25.** Infrared (top) and Raman (bottom) spectra of the N-H stretching region for pure DPA and DPA dissolved in carbon tetrachloride at different concentrations (reported as CCl<sub>4</sub>:N molar ratios).

As DPA is dissolved in  $\text{CCl}_4$ , two broad bands around  $3328$  and  $3346\text{ cm}^{-1}$  appear in the IR spectra. The growth of these bands with increasing dilution is accompanied by a decreasing intensity of the original  $3289\text{ cm}^{-1}$  band. At a 9:1  $\text{CCl}_4$ :NH molar ratio, the two new bands have about the same intensity, and at very high dilution, the band at  $3346\text{ cm}^{-1}$  has the highest intensity while the  $3328\text{ cm}^{-1}$  band appears as a shoulder. The original band at  $3289\text{ cm}^{-1}$  disappears between the 20:1 and 40:1 compositions. In the Raman spectra, the frequency of the band at  $3327\text{ cm}^{-1}$  does not shift when the concentration in dipropylamine decreases, but its intensity rapidly diminishes as seen by the decrease in the signal to noise ratio. The second band at  $3315\text{ cm}^{-1}$  slowly disappears upon dilution.

Wolff and Gamer<sup>17</sup> studied hydrogen bonding interactions in dimethylamine, a molecule very similar to dipropylamine.<sup>18</sup> When dimethylamine is dissolved in  $\text{CCl}_4$ , two bands are observed in the IR spectra. One band around  $3356\text{ cm}^{-1}$  increased with dilution and temperature and was attributed to the free NH groups. The other band, whose intensity decreased with dilution and temperature, was attributed to hydrogen bonded NH groups. They found two different populations of hydrogen bonded groups: one at  $3302\text{ cm}^{-1}$  when diluted in  $\text{CCl}_4$ , and the other one at  $3294\text{ cm}^{-1}$  in pure dimethylamine. Unfortunately, no Raman spectra were reported.

In the dipropylamine –  $\text{CCl}_4$  solution, the IR band at higher frequency ( $3346\text{ cm}^{-1}$ ) probably originates in the “free” NH groups, i.e. the groups not involved in hydrogen bonding. The band at  $3328\text{ cm}^{-1}$  appears to come from the vibrations of a hydrogen-bonded population of molecules that are diluted in  $\text{CCl}_4$ . The intensity of the  $3346\text{ cm}^{-1}$  band increases with  $\text{CCl}_4$  dilution until at the 40:1 dilution it is the dominant feature in

this region, with the  $3328\text{ cm}^{-1}$  band appearing as a clearly discernable low frequency shoulder. The close overlap of these two broad features makes a spectral deconvolution very problematic. However, the qualitative trend in the relative intensities suggests a set of coupled equilibrium between species with different degrees of hydrogen bonding. It is clear that with progressive dilution the IR intensities of the “free” DPA band at  $3346\text{ cm}^{-1}$  increases at the expense of the weakly hydrogen bonded DPA band at  $3328\text{ cm}^{-1}$ .

These results are similar to conclusions obtained from studies of hydrogen bonding interactions in solvated alcohols, which have been the subject of numerous investigations.<sup>5,6,19-21</sup> The general infrared characteristics of the OH stretching region are now well known. In methanol, for example, the molecules form a highly hydrogen bonded network. At various stages of dilution, many bands appear in the spectra and are assigned to the various species present: monomers (or free), dimers, and polymeric species. Analogously in dipropylamine and its dilute solutions, the various bands may be assigned to different types of associated molecules such as dimeric structures and higher order structures. These assignments are incomplete.

### **b) Dipropylamine - LiTf**

Figure 4.26 shows the IR and Raman spectra in the  $\nu(\text{NH})$  region for pure DPA, DPA:LiTf solutions, and the DPA:LiTf crystal. When LiTf is added to DPA, no major shift in the infrared band at  $3289\text{ cm}^{-1}$  is observed, but the band becomes sharper until it splits into two distinct peaks at  $3302\text{ cm}^{-1}$  and  $3288\text{ cm}^{-1}$  at the 5:1 composition. The splitting persists in the crystalline sample, with the two peaks observed at  $3303\text{ cm}^{-1}$  and  $3289\text{ cm}^{-1}$ . These two components can be explained with reference to the crystal

structure. The static disorder creates two different environments for the hydrogen atom of the NH group: one of the hydrogen atoms is weakly hydrogen bonded to a triflate oxygen, while the other hydrogen atom is free. Each band of the  $\nu(\text{NH})$  region corresponds to one of the two possible positions for the hydrogen atoms in the crystal. The band at  $3289\text{ cm}^{-1}$  is assigned to the hydrogen-bonded population, while the band at  $3303\text{ cm}^{-1}$  corresponds to the non-hydrogen-bonded population.

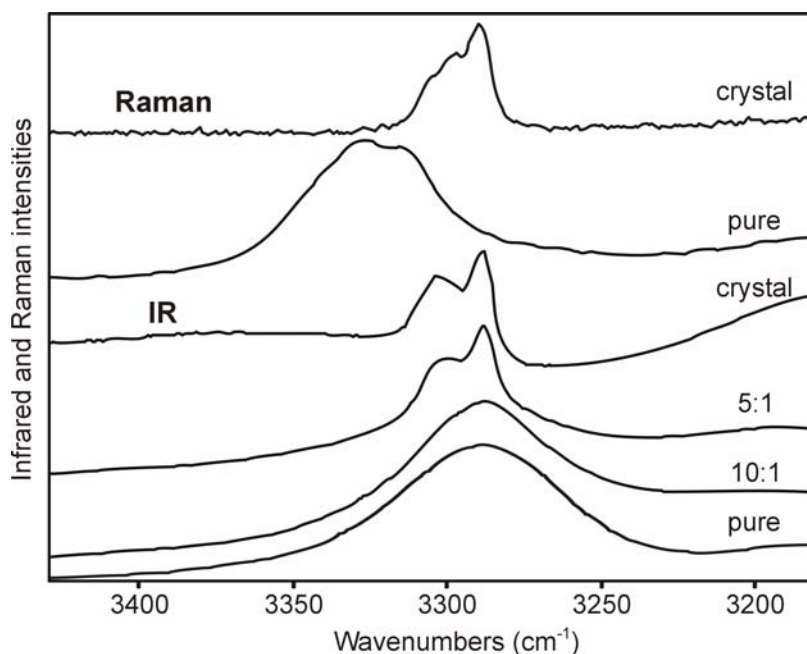


**Figure 4.26.** N-H stretching region of the IR and Raman spectra of DPA:LiTf crystal, dipropylamine:LiTf solutions with various N:Li<sup>+</sup> ratios, and dipropylamine. In this region, the 5:1 Raman spectrum (not shown) is identical to that of the pure solution, while the 3:1 Raman spectrum (not shown) is identical to that of the crystal.

In the Raman spectrum, the two bands shift to lower frequency and become two clearly-resolved bands in a composition range between 5:1 and 3:1. The spectrum of the crystal is very similar to that of the 3:1 sample, with one band at  $3289\text{ cm}^{-1}$  and a weaker

band at about  $3302\text{ cm}^{-1}$ . This shift to lower frequencies in the Raman spectra was also observed in the Raman spectra of the hexylamine – LiTf system. Unfortunately, TbaTf is insoluble in dipropylamine and no comparison of cation inductive effects could be made.

### c) Dipropylamine – LiTf in $\text{CCl}_4$

The effect of adding salt to dipropylamine in  $\text{CCl}_4$  is illustrated in Figure 4.27, which shows the IR spectra of DPA, DPA – LiTf 5:1, and DPA – LiTf 5:1 diluted in  $\text{CCl}_4$  at various concentrations.

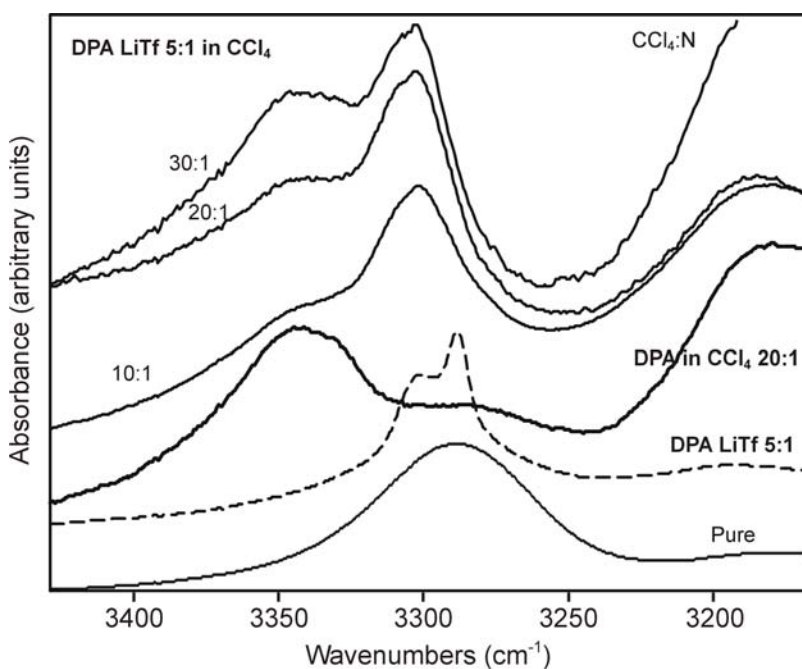


**Figure 4.27.** Infrared spectra of DPA – LiTf 5:1 (N:Li molar ratio) superposed with the infrared spectra of DPA diluted in  $\text{CCl}_4$  at a 20:1 concentration and DPA – LiTf 5:1 diluted in  $\text{CCl}_4$  at different concentrations (reported as  $\text{CCl}_4$ :N molar ratios) in the N-H stretching region.

At all salt concentrations, the IR spectra have a band at  $3302\text{ cm}^{-1}$  with a shoulder around  $3346\text{ cm}^{-1}$ . As discussed previously, the band around  $3346\text{ cm}^{-1}$  represents a population of DPA molecules undergoing limited or no hydrogen bonding interactions, and accordingly increases with dilution. As the solution becomes more concentrated in electrolyte, the band at  $3302\text{ cm}^{-1}$  increases in intensity relative to the  $3346\text{ cm}^{-1}$  band. This band is attributed to DPA molecules coordinated with the lithium cation.

As discussed previously, upon addition of LiTf to DPA (with no  $\text{CCl}_4$ ), the band at  $3289\text{ cm}^{-1}$  becomes sharper and splits into two components at  $3302$  and  $3288\text{ cm}^{-1}$  in the 5:1 composition; this splitting persists in the crystalline state (see Figure 4.26). These two components are attributed to the two different environments for the hydrogen atom of the NH group that are found in the crystal structure: the latter band corresponds to the hydrogen atom that is weakly hydrogen bonded to a triflate oxygen, while the other band corresponds to a “free” hydrogen atom. The correspondence between the band at  $3302\text{ cm}^{-1}$  in the crystal and in the dilute  $\text{CCl}_4$  solution shows that when DPA and LiTf in a 5:1 molar ratio are diluted in  $\text{CCl}_4$ , the local  $\text{NH}_2$  environment present in the crystal is preserved to some extent in the solution.

### 4.3. ANION – HOST INTERACTIONS:

#### HEXA – NaBPh<sub>4</sub> and N,N-DMEDA – NaBPh<sub>4</sub> systems

##### 4.3.1. Crystal structures and thermal analysis

*Crystalline phase of N,N-DMEDA:NaBPh<sub>4</sub>.* Crystal data for the title compound (slightly abbreviated as (DMEDA)<sub>3</sub>:NaBPh<sub>4</sub>) is presented in Table 4.14. The crystals form an orthorhombic unit cell in the Pbc<sub>a</sub> space group, with 8 (DMEDA)<sub>3</sub>:NaBPh<sub>4</sub> asymmetric units in the cell (Figure 4.28).

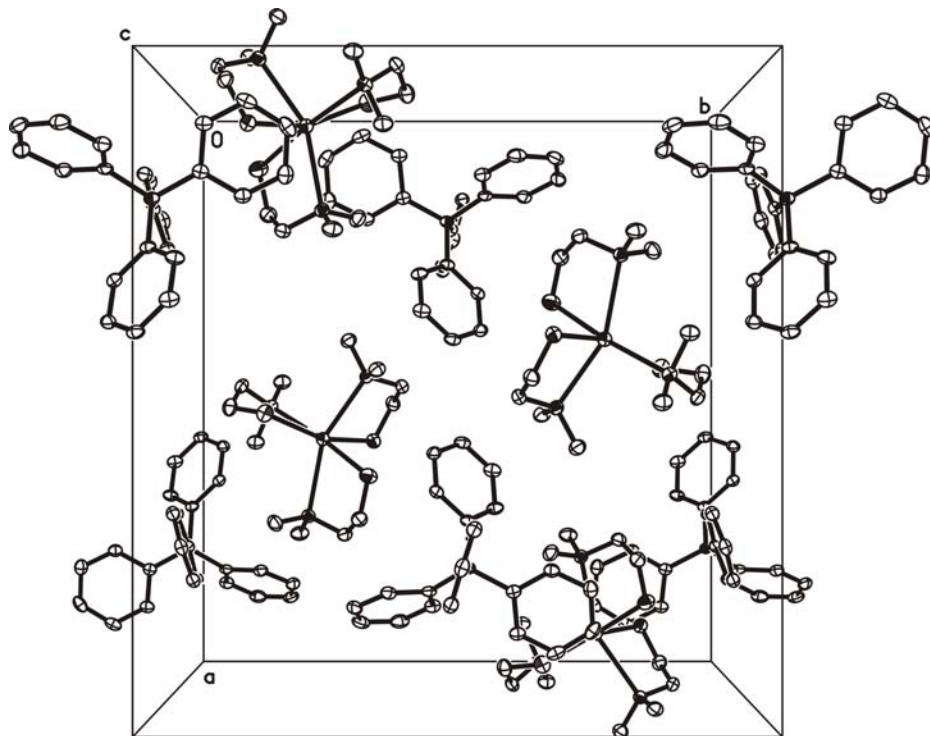


**Figure 4.28.** Packing diagram of the DMEDA:NaBPh<sub>4</sub> crystal projected down the crystallographic *c* axis.

As shown in Figure 4.29, each sodium ion is coordinated to six nitrogen atoms from three DMEDA molecules, corresponding to a nitrogen-to-sodium ratio of 6:1. The BPh<sub>4</sub> anion does not participate in the coordination with the sodium cation, as it is a

bulky, charge-protected cation. The coordination geometry can be described as a distorted octahedron.

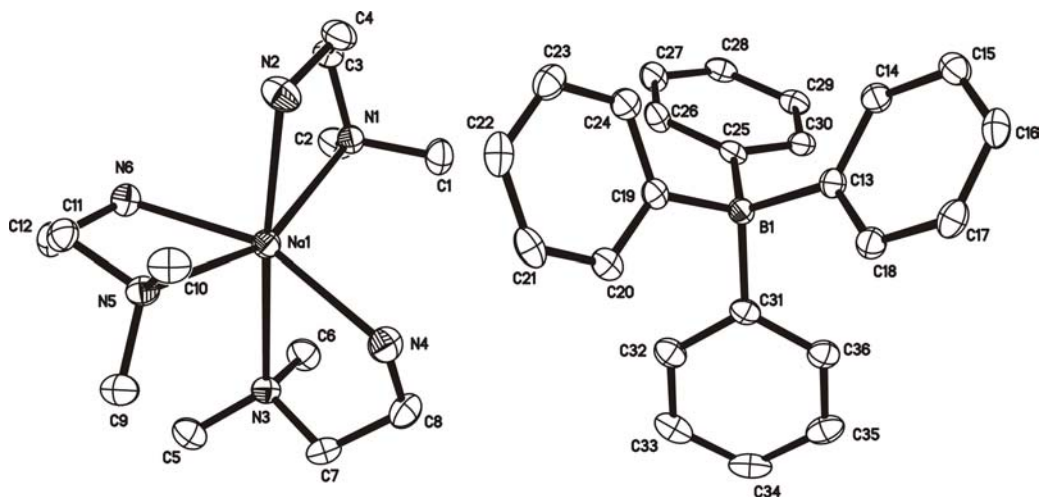


**Figure 4.29.** Crystal structure of DMEDA:NaBPh<sub>4</sub> showing the six-fold coordination of sodium.

**Table 4.14.** Structural data of the DMEDA:NaBPh<sub>4</sub> crystal.

Crystal system	Orthorhombic
Space group	Pbca
Temperature (K)	95(2)
a (Å)	19.6792(16)
b (Å)	18.4942(15)
c (Å)	19.6886(16)
$\alpha, \beta, \gamma$	90
Volume (Å <sup>3</sup> )	7165.7(10)
Z	8
Density (Mg/m <sup>3</sup> )	1.125
R1	0.0421
Crystal size (mm <sup>3</sup> )	0.42 x 0.24 x 0.18

The N,N-DMEDA molecule contains a tertiary amine group (two methyl groups attached to one of the nitrogen atoms) and a primary amine group (two hydrogen atoms on the other nitrogen atom). Both the primary and tertiary nitrogen atoms of the DMEDA molecule are involved in coordinating the sodium ion, although some differences between the tertiary and primary groups can be noted. The nitrogen – sodium bond distances lie between 2.45 and 2.51 Å for the primary amine nitrogen atoms, whereas this bond length is greater for the tertiary amine nitrogen atoms (2.61 – 2.67 Å), as expected. The tertiary part of the DMEDA molecule can be compared to N,N,N',N'-tetramethylethylenediamine<sup>1</sup> (TMEDA), which contains two tertiary amine groups. TMEDA forms a crystal with sodium triflate with nitrogen – sodium bond distances between 2.47 and 2.52 Å, a somewhat smaller average bond distance than the same average in DMEDA:NaBPh<sub>4</sub>. This difference can be explained by the crystal structures of the two compounds. In (DMEDA)<sub>3</sub>:NaBPh<sub>4</sub>, three DMEDA molecules are clustered around one sodium and more tightly “wrapped”, whereas TMEDA:NaTf forms a tetramer in which one sodium ion is coordinated to one TMEDA molecule and three triflate oxygen atoms originating from three different triflate groups.

As seen previously, N,N-DMEDA also forms a crystalline phase with sodium triflate. The nitrogen – sodium bond distances lie around 2.47 Å for the primary amine nitrogens and 2.51 Å for the tertiary nitrogen, which represents a 0.04 Å difference. The disparity between DMEDA:NaTf and (DMEDA)<sub>3</sub>:NaBPh<sub>4</sub> complexes can be explained by the packing requirement of the compounds; the DMEDA:NaTf complex forms a 2D network in which one sodium coordinates to one DMEDA molecule and three oxygens from different triflate anion. In the (DMEDA)<sub>3</sub>:NaBPh<sub>4</sub> complex, three DMEDA

molecules are clustered around one sodium cation, and the steric hindrance becomes an important factor.

There is a striking similarity between the structures of (DMEDA)<sub>3</sub>:NaBPh<sub>4</sub> and the 3:1 compound of monoglyme-LiSbF<sub>6</sub>, [CH<sub>3</sub>(OCH<sub>2</sub>CH<sub>2</sub>)OCH<sub>3</sub>]<sub>3</sub>:LiSbF<sub>6</sub>.<sup>22</sup> In both crystals, each cation is six-fold coordinated to the two heteroatoms from each of three molecules. Further, the anion does not coordinate the cation in either compound.

The conformation of DMEDA in the structure can be described by the C-N-C-C and the N-C-C-N dihedral angles (Table 4.15). The three DMEDA ligands that coordinate to the sodium cation all have the same  $t\bar{g}$  or  $\bar{t}g$  conformation. This is comparable to the DMEDA:NaTf crystal, where a mixture of  $t\bar{g}$  and  $\bar{g}\bar{g}$  conformations were found.

**Table 4.15.** Dihedral angles of DMEDA:NaBPh<sub>4</sub> crystal and the corresponding conformations.

Bond sequence	Dihedral angle (°)	Conformation
C1-N1-C3-C4	-61.41	$\bar{g}$
C2-N1-C3-C4	179.29	t
N1-C3-C4-N2	-60.86	$\bar{g}$
C4-N2-H(2D or 2E)	108.8	s
C6-N3-C7-C8	67.12	g
C5-N3-C7-C8	-173.79	$\bar{t}$
N3-C7-C8-N4	58.92	g
C8-N4-H(4C or 4D)	109.1	s
C9-N5-C11-C12	-74.93	$\bar{g}$
C10-N5-C11-C12	165.19	t
N5-C11-C12-N6	-65.35	$\bar{g}$
C12-N6-H(6D or 6E)	109.7	s

DSC was used to study the melting and recrystallization processes in the crystal. The measurements showed an onset of melting at 66°C with a midpoint at 71°C, and an onset of recrystallization at 62°C with a midpoint at 58°C. The crystal decomposes at 153°C.

**Crystalline phase of hexylamine:NaBPh<sub>4</sub>.** The compound hexylamine:NaBPh<sub>4</sub> crystallizes in a monoclinic unit cell in the Pn space group, with Z=4 [(C<sub>6</sub>H<sub>15</sub>N)<sub>2</sub>(NaBPh<sub>4</sub>)]<sub>2</sub> asymmetric units in the cell (Figure 4.30). One of the (C<sub>6</sub>H<sub>15</sub>N)<sub>2</sub>(NaBPh<sub>4</sub>) molecule of the asymmetric unit is disordered. Nevertheless, the overall geometry of the molecule and the coordination of sodium resemble that of the non-disordered molecule. For these reasons as well as for clarity purposes, the figures and the following discussion focus on the non-disordered molecule of the asymmetric unit. The structural data are summarized in Table 4.16.

**Table 4.16.** Structural data of the HEXA:NaBPh<sub>4</sub> crystal.

<b>Crystal system</b>	<b>Monoclinic</b>
Space group	Pn
Temperature (K)	100(2)
a (Å)	10.4167(19)
b (Å)	20.038(4)
c (Å)	15.864(3)
β	91.217(3)
Volume (Å <sup>3</sup> )	3310.6(11))
Z	4
Density (Mg/m <sup>3</sup> )	1.093
R1	0.086
Crystal size (mm <sup>3</sup> )	0.48 x 0.42 x 0.26

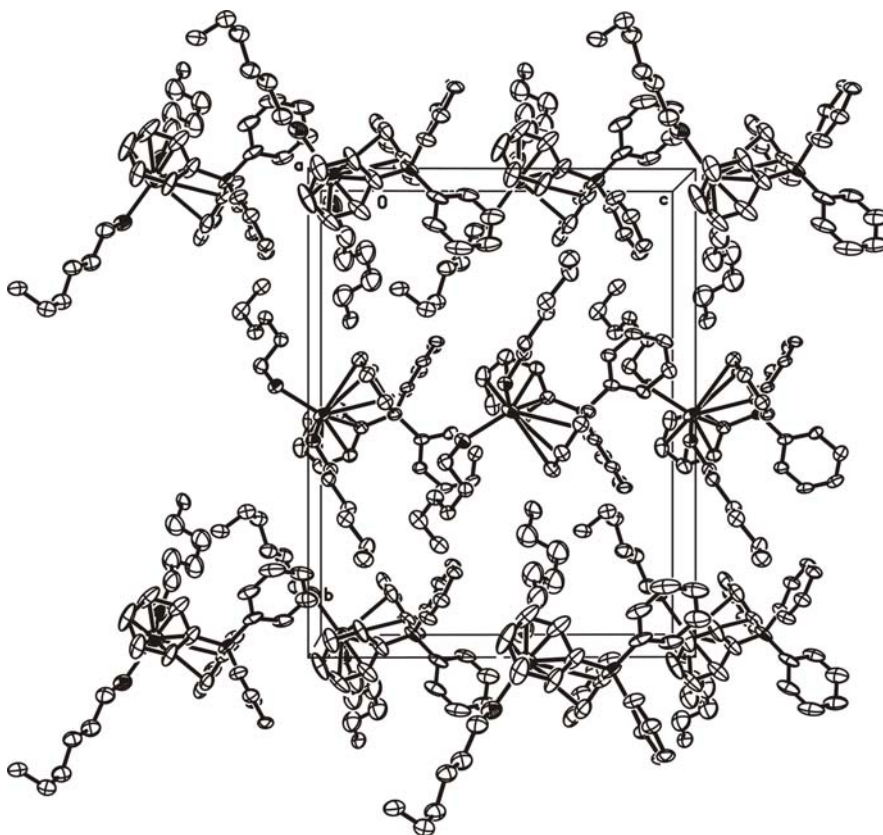


**Figure 4.30.** Packing diagram of the HEXA:NaBPh<sub>4</sub> crystal projected down the crystallographic *a* axis.

As shown in Figure 4.31, the sodium ion is located between two phenyl rings; it coordinates five carbon atoms of one ring, three carbon atoms of the other ring, and two nitrogen atoms of two hexylamine molecules. The nitrogen – sodium bond distances are 2.3595(15) and 2.3644(15) Å, and the carbon – sodium bond distances lie between 2.67 and 3.10 Å. The N-Na-N angle formed upon coordination of the hexylamine molecules with the sodium cation is radically different in each molecule of the asymmetric unit. In the non-disordered molecule, this angle is 87.74°; while in the disordered part, this angle is 112.97° and 122.86° for each component of the molecule respectively.

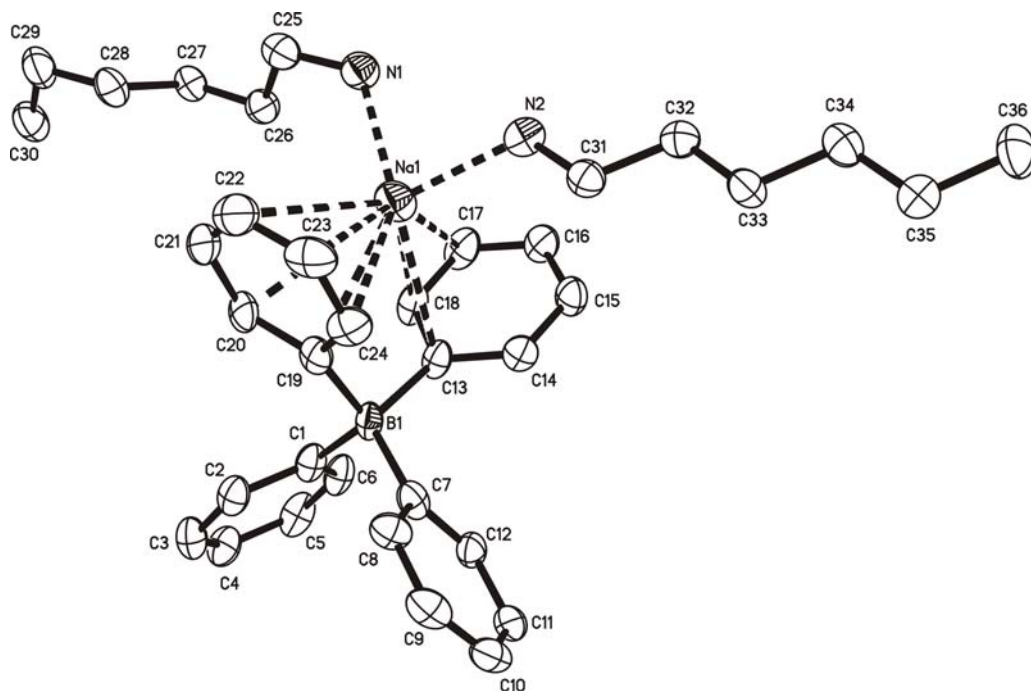


**Figure 4.31.** Crystal structure of HEXA:NaBPh<sub>4</sub> showing the coordination of sodium. Only the non-disordered (C<sub>6</sub>H<sub>15</sub>N)<sub>2</sub>(NaBPh<sub>4</sub>) molecule of the asymmetric unit is shown.

In this crystal, the anion plays an important role in the coordination of sodium, contrarily to the DMEDA:NaBPh<sub>4</sub> crystal where tetraphenylborate does not participate in the coordination. The sodium ion usually coordinates 5 or 6 heteroatoms; however hexylamine has only one primary amine group available for coordination and the steric hindrance might be too large for 5 or 6 hexylamine molecules to wrap around sodium. This is not a problem in the DMEDA crystal since two nitrogen atoms per molecule are available for coordination.

DSC measurements showed two endothermic transitions with onsets at 7°C (midpoint=14°C), and 50°C (midpoint=55°C); and two exothermic transitions with onset at 19°C (midpoint=17°C), and 3°C (midpoint=-1°C). The crystal decomposes at 134°C.

### 4.3.2. Vibrational spectroscopy

**DMEDA:NaBPh<sub>4</sub> system.** The vibrational spectroscopic features of the primary amine group in the DMEDA:NaBPh<sub>4</sub> complex are especially interesting. In particular, the NH stretching and NH bending regions of the spectrum exhibit uncommon behavior. Figure 4.32 shows the superposition of the IR and Raman spectra of DMEDA, DMEDA with NaBPh<sub>4</sub> at various concentrations, and the crystal. The addition of NaBPh<sub>4</sub> to DMEDA causes the NH stretching bands to sharpen and split into multiple bands. At a 5:1 composition, the asymmetric stretch splits into three bands and the symmetric stretch band sharpens. Additionally, two small distinct peaks appear at 3556 and 3618 cm<sup>-1</sup>. These two peaks become stronger and sharper as the salt concentration increases.

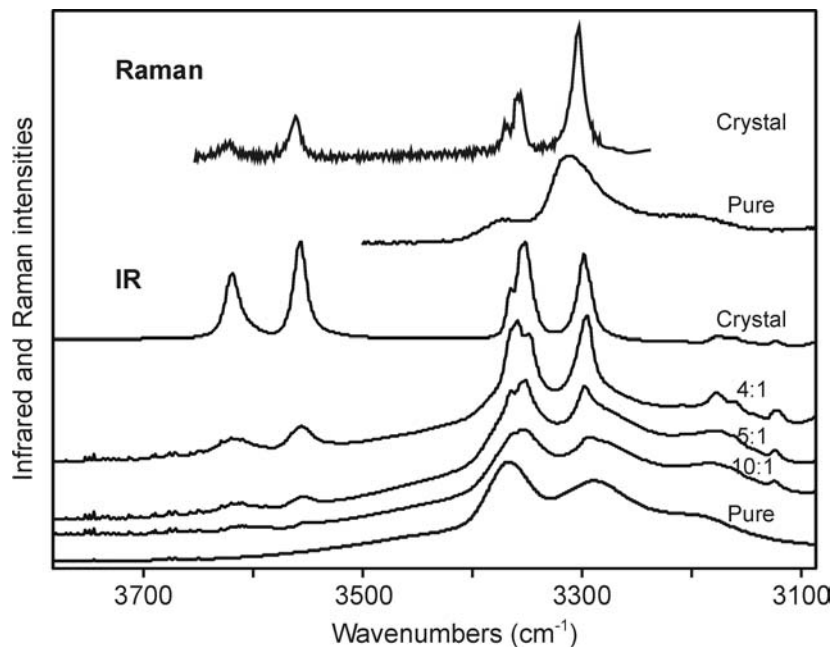


**Figure 4.32.** N-H stretching region of the IR and Raman spectra of DMEDA:NaBPh<sub>4</sub> crystal, DMEDA – NaBPh<sub>4</sub> solutions with various N:Na<sup>+</sup> ratios, and DMEDA.

In the crystal,  $\nu_{\text{as}}(\text{NH}_2)$  has three bands at 3350, 3354, and 3364  $\text{cm}^{-1}$  and  $\nu_{\text{s}}(\text{NH}_2)$  one band at 3297  $\text{cm}^{-1}$ . The intensity of the two high frequency peaks is about the same as the intensity of the symmetric and asymmetric stretches and their frequency remains the same as in the 5:1 sample. The Raman spectrum of the crystal in the NH stretching region has the same number of bands as occur in the IR spectrum; however, all Raman bands have frequencies higher by 4 to 5  $\text{cm}^{-1}$  compared to the IR spectrum.

In the crystal, the intramolecular vibrations of the individual DMEDA molecules are correlated through intermolecular forces, leading to the observed normal modes. A symmetry-based analysis of the resulting vibrational modes is afforded by the correlation method.<sup>15</sup> This method describes the motion of constituent groups (e.g. the  $\text{NH}_2$  stretching motion of the primary amine group) in terms of the irreducible representations of the factor group (unit cell group) of the crystal, which is  $D_{2h}$ . The crystalline compound DMEDA: $\text{NaBPh}_4$  has 8  $(\text{DMEDA})_3(\text{NaBPh}_4)$  asymmetric units in the cell. In this compound, each primary amine group occupies a general position of  $C_1$  site symmetry. Application of the correlation method leads to

$$\Gamma(\nu_{\text{s}}) = 3A_{\text{g}} + 3B_{1\text{g}} + 3B_{2\text{g}} + 3B_{3\text{g}} + 3A_{\text{u}} + 3B_{1\text{u}} + 3B_{2\text{u}} + 3B_{3\text{u}} \quad (1)$$

$$\Gamma(\nu_{\text{as}}) = 3A_{\text{g}} + 3B_{1\text{g}} + 3B_{2\text{g}} + 3B_{3\text{g}} + 3A_{\text{u}} + 3B_{1\text{u}} + 3B_{2\text{u}} + 3B_{3\text{u}} \quad (2)$$

In principal, a normal mode of  $A_{\text{g}}$  symmetry could contain contributions from three different linear combinations of  $\text{NH}_2$  symmetric stretching motion, three different linear combinations of antisymmetric  $\text{NH}_2$  stretching motion, plus contributions from all other linear combinations of DMEDA, tetraphenylborate ion and sodium ion motions that

transform according to  $A_g$ . However, the large frequency separation between the  $NH_2$  stretching motions and all other vibrational motions in the crystal lead to very little vibrational “mixing” with the lower frequency motions, i.e. the normal modes observed in Figures 4.32 consist almost exclusively of N-H stretching motion.

***HEXA:NaBPh<sub>4</sub> system.*** The IR and Raman of the NH stretching region of pure hexylamine, hexylamine with NaBPh<sub>4</sub> at various concentrations, and the crystal are shown in Figure 4.33. All the frequency shifts relative to pure hexylamine result primarily from two factors: changes in hydrogen bonding environment, and the inductive effect of the cation upon coordination to the nitrogen atom. Both affect the NH stretching frequencies by removing electron density from the N-H bond, causing a decrease to lower frequencies. In the Raman spectrum of pure hexylamine, the  $\nu_s(NH_2)$  band at  $3324\text{ cm}^{-1}$  represents the fraction of hexylamine molecules that are not hydrogen bonded to each other. This band is very weak in the Raman spectrum of the hexylamine:NaBPh<sub>4</sub> complex, which is probably due to significant amount of fluorescence emitted from the sample (crystals are brownish - pink). The band center frequency is at approximately  $3291\text{ cm}^{-1}$ . The 33 wavenumbers shift can only be attributed to the coordination of the sodium cation and the phenyl rings since no hydrogen bonding interaction occurs in the crystal.

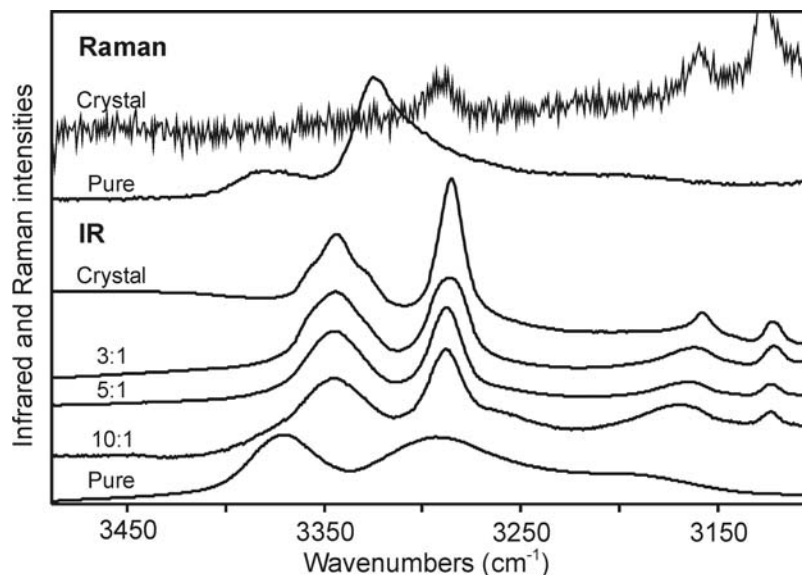


**Figure 4.33.** N-H stretching region of the IR and Raman spectra of HEXA:NaBPh<sub>4</sub> crystal, HEXA – NaBPh<sub>4</sub> solutions with various N:Na<sup>+</sup> ratios, and HEXA.

In the IR spectrum, the broad  $\nu_s(\text{NH}_2)$  band at  $3293\text{ cm}^{-1}$ , which corresponds to primary amine group with more of an antisymmetric character caused by intermolecular hydrogen bonding, shifts to  $3285\text{ cm}^{-1}$  in the crystal and becomes narrower. This shift results from the combination of two factors: first, an increase in the inductive effect, which causes a large shift to lower frequencies; and second, a decrease in the hydrogen bond interactions upon crystal formation, which causes a smaller shift to higher frequencies. The  $8\text{ cm}^{-1}$  shift indicates that overall, the inductive effect is stronger than the effect of breaking the hydrogen bonds initially present in hexylamine. The  $\nu_{as}(\text{NH}_2)$  band shifts to lower frequencies for the reasons mentioned above and splits into three bands at  $3329$ ,  $3343$ , and  $3357\text{ cm}^{-1}$ . The relative area of each band, found by curve fitting analysis, is 24%, 50%, and 26%, respectively. The splitting of  $\nu_{as}(\text{NH}_2)$  can be explained with reference to the crystal structure. The static disorder creates two different

environments for the primary amine group in one of the two molecules of the asymmetric unit. The non-disordered molecule represents 50% of the crystal and each component of the disordered molecule represent 25% of the crystal. It is possible that each band of the  $\nu_{\text{as}}(\text{NH}_2)$  region corresponds to the asymmetric vibration of a primary amine group with a different environment. The N-Na-N angle is the only parameter that is drastically different in each molecule of the asymmetric unit. The ratio of each of the three peaks might be related to the proportion of molecules with different angles.

#### 4.4. CONCLUSIONS

The infrared and Raman spectra in the NH stretching region of pure hexylamine were shown to selectively sample the population distribution of hydrogen-bonded molecules. The NH stretching band was observed in the Raman spectrum with an intensity maximum at a significantly higher frequency than in the infrared spectrum. This observation was explained by a model in which the Raman spectrum effectively sampled molecules with weak hydrogen-bonding interactions, while the infrared spectrum sampled molecules with relatively stronger hydrogen-bonding interactions. Moreover, comparison of the pure hexylamine bands with solutions of hexylamine dissolved in  $\text{CCl}_4$  reinforced our understanding of this system by eliminating to some degree hydrogen bonding interactions between the molecules.

In general, the overall picture developed in the hexylamine system also provides an explanation for the amine group stretching vibrations of DMEDA and DPA. Studies similar to that of the hexylamine system have been conducted for these two systems. In DMEDA, the presence of intermolecular as well as intramolecular hydrogen bonding

interactions complicates the analysis of the spectra. The dilution series in  $\text{CCl}_4$  significantly helped to sort out these interactions.

Studies of all the solution systems were considerably aided by the formation of crystalline compounds whose structures were solved by single crystal x-ray diffraction methods. In all the crystals, the cation coordination is determined unambiguously. In some of the crystals, the structural data indicate the presence of weak hydrogen bonds between the amine hydrogen atoms and the oxygen atoms of the triflate anion. In DMEDA:NaTf, a hydrogen bond forms with the fluorine atom of the triflate ion. However in any of the systems, there are no hydrogen bonds between the amine groups of adjacent molecules.

In all the model compounds, progressive changes in the IR and Raman spectra with the addition of salt were noted. A spectroscopic comparison of the solution data and corresponding spectra of the crystals, complemented by knowledge of the crystal structures, led to a deeper understanding of cation coordination with a primary amine group and a secondary amine group. Frequency shifts observed in the NH stretching region were attributed to a combination of two effects: *a change in the hydrogen bonding environment upon addition of salt as well as the inductive effect of the cation upon coordination to the nitrogen atom.* The symmetric NH stretch was shown to be more sensitive to both effects than the asymmetric stretch. This is due to the fact that the symmetry of the mode is disturbed more readily when a perturbation is applied to it. Moreover, the combination of Raman and IR experiments allowed a separation, to a certain extent, of the contribution from the two effects. This study was further aided by investigating HEXA – LiTf, DMEDA – LiTf, and DPA – LiTf electrolytes dissolved in

CCl<sub>4</sub>. This allowed to eliminate hydrogen bonding interactions between molecules, therefore focusing on the cation coordination effect on the amine vibrations.

#### 4.5. REFERENCES

- (1) Sanders, R. A.; Frech, R.; Khan, M. A. *J. Phys. Chem. B* **2003**, *107*, 8310.
- (2) York, S. S.; Rocher, N. M.; Frech, R.; Khan, M. **To be submitted**.
- (3) Tagokoro, H. *Structure of Crystalline Polymers*; John Wiley and Sons: New York, 1979.
- (4) Colthup, N. B.; Daly, L. H.; Wiberley, S. E. *Introduction to Infrared and Raman Spectroscopy*, Third ed.; Academic Press, Inc.: San Diego, 1990.
- (5) Jeffrey, G. A. *An Introduction to Hydrogen Bonding*; Oxford University Press: New York, 1997.
- (6) Pimental, G. C.; McClellan, A. L. *The Hydrogen Bond*; W.H. Freeman: San Francisco, 1960.
- (7) Wolff, H.; Schmidt, U. *Ber. Bunsenges. Phys. Chem.* **1964**, *68*, 579.
- (8) Mason, S. F. *J. Chem. Soc. (London)* **1958**, 3619.
- (9) Bellamy, L. J.; Williams, R. L. *Spectrochim. Acta* **1957**, *9*, 341.
- (10) Wolff, H. *J. Chem. Phys.* **1970**, *52*, 2800.
- (11) Born, M.; Wolf, E.; Bhatia, A. B. *Principles of Optics*, 7th ed.; Cambridge University Press: Cambridge, New York, 1999.
- (12) Gerrard, W.; Goldstein, M.; Mooney, E. F. *J. Inorg. Nucl. Chem.* **1969**, *31*, 107.
- (13) Harris, C. S.; Ratner, M. A.; Shriver, D. F. *Macromolecules* **1987**, *20*, 1778.
- (14) Boesh, S.; Wheeler, R. *Calculation of N,N-DMEDA, N,N-DMEDA - LiTf, and N,N-DMEDA - NaTf were performed using B3LYP, a hybrid Hartree-Fock density functional method, with a basis set of 6-31G(d), unreported results.*
- (15) Fateley, W. G.; Dollish, F. R.; McDevitt, N. T.; Bentley, F. F. *Infrared and Raman Selection Rules for Molecular and Lattice Vibrations: The Correlation Method*; John Wiley & Sons, Inc.: New York, 1972.
- (16) Sanders, R. A.; Frech, R.; Khan, M. A. *J. Phys. Chem. B* **2004**, *108*, 2186.
- (17) Wolff, H.; Gamer, G. *J. Phys. Chem.* **1972**, *76*, 871.

- (18) Buttler, M. J.; McKean, D. C. *Spectrochim. Acta* **1965**, *21*, 465.
- (19) Liddel, U.; Becker, E. D. *Spectrochim. Acta* **1957**, *10*, 70.
- (20) Symons, M. C. R.; Thomas, V. K. *J. Chem. Soc., Faraday Trans. 1* **1981**, *77*, 1883.
- (21) Kristiansson, O. *J. Mol. Struct.* **1999**, *477*, 105.
- (22) Seneviratne, V. A. Local structures in poly(ethylene oxide) - lithium(X) (X=hexafluoroantimonate, tetrafluoroborate, trifluoromethylsulfonate) and glyme-lithium(X) (X= hexafluoroantimonate, tetrafluoroborate) systems., University of Oklahoma, 2004.

## 5. BRANCHED POLY(ETHYLENIMINE)

The complexity of the BPEI system, and BPEI - salt complexes makes it difficult to develop even a qualitative, molecular-level understanding of the nature of the ionic conductivity. Cation-polymer and cation-anion interactions, as well as hydrogen-bonding interactions are expected to play a major role in the mechanism of ion transport. Unfortunately, all these factors are interdependent in the BPEI-salt systems. Studies of polymer electrolyte systems have been greatly enhanced by examining the structure and dynamics of these interactions in small model compounds whose structure mimic local structures found in the higher molecular weight systems. Hexylamine, N,N-dimethylethylenediamine, and dipropylamine were chosen as model compounds for the BPEI polymer. In these systems, vibrational spectroscopy is a powerful tool to analyze cation-host interactions as salt is added to the system, although the simultaneous presence of the cation inductive effect and alterations in the hydrogen bonding interactions greatly complicate the interpretation of the observed spectrum. These studies were greatly aided by the investigation of the three models in carbon tetrachloride ( $\text{CCl}_4$ ), as the intermolecular hydrogen bonding interactions are greatly decreased upon dilution.

To further the examination of BPEI – salt complexes, the effects of the cation and anion were separated to some degree. In a first part, BPEI was complexed with LiTf, NaTf, and TbaTf. These three salts were selected to separate the different effects caused by the coordination of the cation, assuming to some extent similar behavior from the common anion. In a second part, a comparative spectroscopic study of BPEI complexed with NaTf and with NaBPh<sub>4</sub> offers an excellent opportunity to understand the effect of

the anion upon salt addition. The sodium ion of both salts is expected to coordinatively interact with the nitrogen atom of BPEI, although to a different extent because of the presence of relatively strong cation-anion interactions in the NaTf complexes. However, the lack of heteroatoms in the tetraphenylborate anion precludes the formation of hydrogen bonds with the N-H groups upon complexation, in contrast to the N-H...O hydrogen bonds expected in the NaTf complexes.

## 5.1. COMPARISON OF BPEI AND THE MODEL COMPOUNDS

### 5.1.1. NH stretching region

The IR and Raman spectra of BPEI in the N-H stretching region are illustrated in Figure 5.1. In this region, the spectra of BPEI appear to be dominated by the primary amine groups, in part because the vibrational frequency of the secondary amino group in BPEI,  $\nu(\text{NH})$ , overlaps with  $\nu_s(\text{NH}_2)$  and cannot be distinguished.<sup>1</sup> The shoulder present in both IR and Raman spectra at roughly  $3185\text{ cm}^{-1}$  is an overtone of the  $\text{NH}_2$  deformation band at  $1594\text{ cm}^{-1}$ .

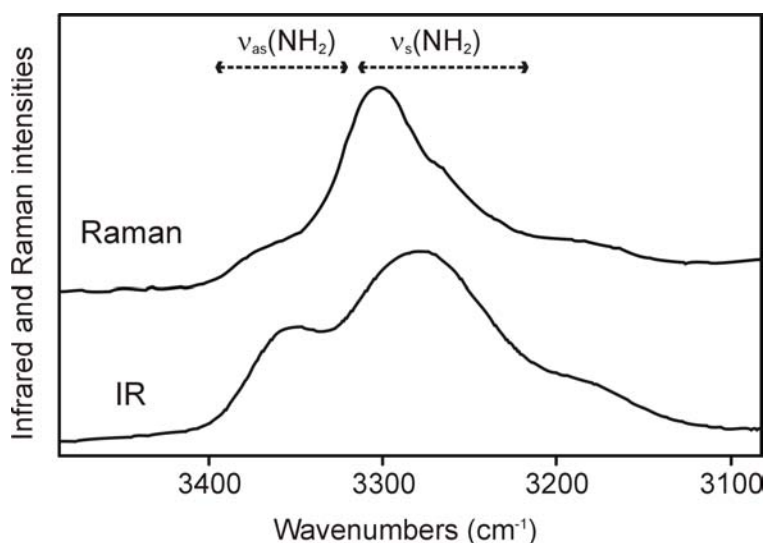


**Figure 5.1.** IR and Raman spectra of the N-H stretching vibrations of BPEI.

The strong  $\nu_s(\text{NH}_2)$  band of the BPEI primary amino group occurs at  $3302\text{ cm}^{-1}$  in the Raman spectrum, while the corresponding maximum intensity of  $\nu_s(\text{NH}_2)$  in the infrared spectrum is observed at  $3278\text{ cm}^{-1}$ . The strong  $\nu_s(\text{NH}_2)$  Raman band has a weak shoulder at roughly  $3266\text{ cm}^{-1}$ , suggesting that there are two groups of hydrogen bonded  $\text{NH}_2$  units, although they are barely distinguishable via Raman spectroscopy. The breadth of the bands in the BPEI spectrum is characteristic of the heterogeneous hydrogen-bonding environment in the amorphous host that leads to a distribution of intermolecular and intramolecular interactions. As in the case of hexylamine and DMEDA, the frequency of  $\nu_s(\text{NH}_2)$  in the Raman spectrum is higher than its frequency in the infrared spectrum, with a slightly asymmetric lower frequency wing that extends beneath the infrared active  $\nu_s(\text{NH}_2)$  feature. Consequently, the pure BPEI spectra can be analyzed using the same model previously applied to HEXA, DMEDA, and DPA and will not be repeated here. However, there is a significant difference between BPEI and the three model systems that is discussed in the following paragraphs.

The IR and Raman frequencies of BPEI, HEXA, and DMEDA in the N-H stretching region are graphically illustrated in Figure 5.2 as an aide for the following discussion. The N-H stretching bands in the Raman spectrum of BPEI occur at markedly lower frequencies than the corresponding bands of HEXA: i.e. the HEXA $\rightarrow$ BPEI shift of  $\nu_s(\text{NH}_2)$  is  $-22\text{ cm}^{-1}$  and the  $\nu_{as}(\text{NH}_2)$  band at  $3360\text{ cm}^{-1}$  corresponds to a HEXA $\rightarrow$ BPEI shift of  $-16\text{ cm}^{-1}$ . The significantly lower frequencies in BPEI compared with HEXA indicates that the  $\text{NH}_2$  groups in BPEI are more strongly hydrogen bonded than in HEXA. The same conclusion is reached comparing the IR spectra, where the primary

amino group in BPEI gives rise to  $\nu_s(\text{NH}_2)$  at  $3278\text{ cm}^{-1}$  and a weaker  $\nu_{as}(\text{NH}_2)$  band at  $3352\text{ cm}^{-1}$ . These frequencies are significantly lower than the analogous modes in hexylamine,  $3293\text{ cm}^{-1}$  and  $3371\text{ cm}^{-1}$ , respectively.

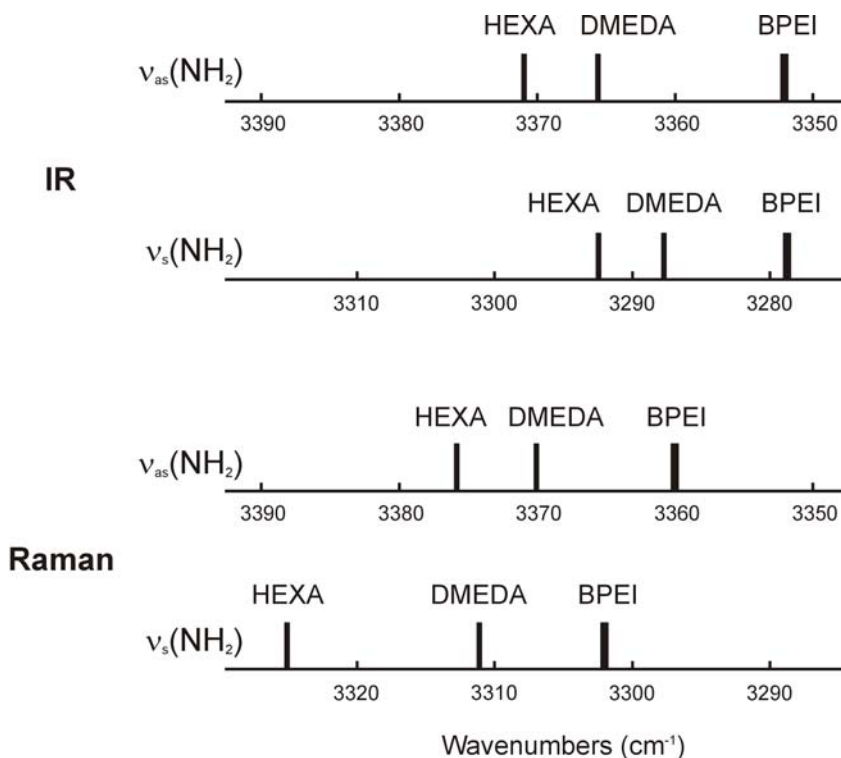


**Figure 5.2.** Summary of the  $\text{NH}_2$  symmetric and antisymmetric stretching frequencies of hexylamine, DMEDA, and BPEI in the IR (top scales) and in the Raman spectra (bottom scales).

The N-H stretching vibrations of DMEDA in the IR and Raman are also compared to those of BPEI. As illustrated in Figure 5.2, the difference in the N-H stretching frequencies between the DMEDA and BPEI systems is much smaller than between the HEXA and BPEI systems. The most noticeable difference when comparing hexylamine and DMEDA to BPEI occurs in the Raman spectrum. The DMEDA→BPEI shift of  $\nu_s(\text{NH}_2)$  is only  $-9\text{ cm}^{-1}$  compared to a  $-22\text{ cm}^{-1}$  shift between HEXA and BPEI.

In hexylamine, the  $\nu_s(\text{NH}_2)$  band at  $3324\text{ cm}^{-1}$  corresponds to the population of molecules that are the least hydrogen bonded. In DMEDA, and even more in BPEI, the presence of intramolecular hydrogen bonding interactions shifts the stretching modes to lower frequencies. DMEDA is a better model compound than hexylamine in order to study the intermolecular interactions occurring in the polymer. However, the complexity of the IR and Raman spectra is greatly augmented due to the presence of *intramolecular hydrogen bonding* interactions, and at first, less information can be obtained. The study of a simple primary amine is necessary to understand the first step, i.e. intermolecular interactions; the study of intramolecular interactions can only be developed in a subsequent step.

It was noted earlier that the NH stretching frequency  $\nu(\text{NH})$  of BPEI occurs in the same region as the symmetric stretching vibration of the  $\text{NH}_2$  group. However, a comparison of the secondary amine NH stretching intensity in the DPA spectrum with the intensity of the primary amine  $\nu_s(\text{NH}_2)$  mode in HEXA or in DMEDA (see section 4) shows that the Raman scattering intensity of  $\nu(\text{NH})$  is much less than  $\nu_s(\text{NH}_2)$ . Therefore, conclusions about hydrogen bonding effects on stretching frequencies in these systems based on a comparison of Raman data are more reliable than comparison of infrared data. In spite of this caveat, it is reassuring to see the same trends in the infrared and Raman spectra.

The effect of adding lithium triflate to BPEI is compared to the results obtained from HEXA – LiTf and DMEDA – LiTf solutions. In BPEI, the  $\nu_s(\text{NH}_2)$  and  $\nu_{\text{as}}(\text{NH}_2)$  bands shift to higher frequencies in both the Raman spectrum ( $3307$  and  $3368\text{ cm}^{-1}$ , respectively) and the infrared spectrum ( $3305$  and  $3370\text{ cm}^{-1}$ , respectively). These data

agree within experimental error with the IR data reported by Paul et al.<sup>2</sup> for BPEI:LiTf at a 4:1 composition. After the addition of salt to bring the composition to 3:1, the band intensity maxima are coincident (within experimental error) in the infrared and Raman spectra, as previously observed in all the hexylamine, DMEDA, and DPA solutions. The net effect of adding LiTf to BPEI, hexylamine, and DMEDA to bring the compositions to 3:1 are summarized in Table 5.1. In the table, the shift  $\Delta v_s(\text{NH}_2)$  is defined as  $v_s(\text{NH}_2; 3:1 \text{ complex}) - v_s(\text{NH}_2; \text{pure})$ , with a similar definition for  $\Delta v_{as}(\text{NH}_2)$ .

**Table 5.1.** Comparison of frequency shift data ( $\text{cm}^{-1}$ ) for HEXA, DMEDA, and BPEI complexed with LiTf at a 3:1 composition.

	$\Delta v_s(\text{NH}_2)$		$\Delta v_{as}(\text{NH}_2)$	
	Raman	IR	Raman	IR
HEXA	-23	5	-21	-14
DMEDA	3	25	7	10
BPEI	5	27	8	18

In the Raman spectra, the  $+5 \text{ cm}^{-1}$  shift of  $v_s(\text{NH}_2)$  upon addition of LiTf to BPEI should be contrasted to the  $-23 \text{ cm}^{-1}$  shift in HEXA - LiTf. The  $v_s(\text{NH}_2)$  Raman band in pure BPEI and HEXA results from  $\text{NH}_2$  groups undergoing the least amount of hydrogen bonding, with the Raman band maximum in HEXA originating in  $\text{NH}_2$  groups experiencing little or no hydrogen bonding. Therefore, in HEXA the  $-23 \text{ cm}^{-1}$  Raman shift of  $v_s(\text{NH}_2)$  can be attributed almost entirely to the cation inductive effect, although there is a small positive shift contribution from the formation of weak  $\text{N-H}\cdots\text{O}$  hydrogen bonds with the triflate oxygen atoms. This replacement was pointed out by Paul et al.<sup>2</sup> in BPEI - LiTf. However, in BPEI, the corresponding shift of  $+5 \text{ cm}^{-1}$  is presumably due to

partial disruption of hydrogen bonds that are considerably stronger than those in HEXA. As noted before, the coordination of the cation with the nitrogen atom breaks hydrogen bonds, thus increasing the frequency, while the accompanying inductive effect decreases the frequency. In  $\text{NH}_2$  groups undergoing significant hydrogen bonding, a weak interaction of the cation with the nitrogen atom would be sufficient to produce a measurable disruption of hydrogen bonding, however a stronger, coordinative interaction may be required to produce a substantial cation inductive effect. A comparison of the BPEI and HEXA  $\nu_{\text{as}}(\text{NH}_2)$  spectral shifts is informative. In both the Raman and IR spectra, the BPEI band increases with salt addition, while in HEXA the band decreases. Since the “free”  $\nu_{\text{as}}(\text{NH}_2)$  frequency is about  $3392 \text{ cm}^{-1}$  in HEXA (from the dilute  $\text{CCl}_4$  solution measurement), the large negative shift indicates that the breaking of hydrogen bonds (necessarily a positive shift) is accompanied by a larger negative shift due to the inductive effect. In contrast, the Raman and IR shifts in BPEI  $\nu_{\text{as}}(\text{NH}_2)$  are both positive, suggesting that the strength of the cation interaction with the nitrogen atoms is significantly weaker in BPEI than in HEXA.

As shown in the table, the shifts of  $\nu_{\text{as}}(\text{NH}_2)$  and  $\nu_{\text{s}}(\text{NH}_2)$  that occur upon addition of salt to DMEDA compare very closely with those of BPEI in both the IR and Raman spectra. In DMEDA, the presence of intramolecular interactions as well as intermolecular interactions gives a better picture of the analogous interactions occurring in the polymer. From this data, it is clear that intramolecular interactions play a major role in the way the salt interacts with the polymer. As discussed above, the strength of the lithium – nitrogen interaction is notably stronger in HEXA than in DMEDA, and BPEI. In DMEDA – LiTf, lithium coordinates both nitrogen atoms of one molecule, as

shown by the crystal structure (section 4.1.2). In HEXA – LiTf, there is only one nitrogen atom per molecule, and the coordination of lithium is satisfied by the triflate ions. In the BPEI salt complex, the lithium ion probably coordinates either one or two nitrogen atoms, either from the same molecule, or very possibly from another polymeric chain.

The N-H stretching frequencies of BPEI, DMEDA, and HEXA complexed with LiTf at 3:1 concentration are compared in the Figure 5.3 below.

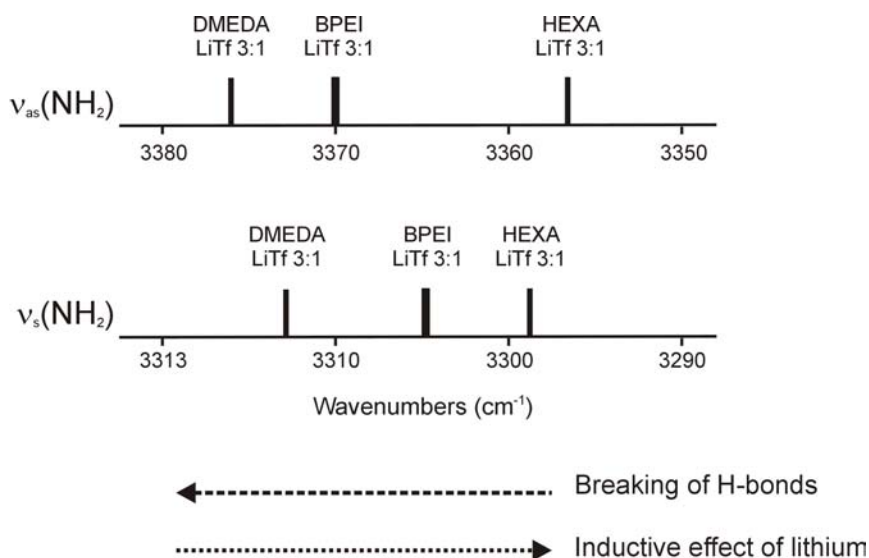


**Figure 5.3.** Schematic representation of the  $\nu_{as}(\text{NH}_2)$  and  $\nu_s(\text{NH}_2)$  frequency shifts in BPEI, DMEDA, and HEXA complexed with LiTf at 3:1 molar ratios. The data presented correspond to the IR frequencies, but also correspond to bands in the Raman spectra within  $\pm 2 \text{ cm}^{-1}$ .

The IR and Raman frequencies of  $\nu_{as}(\text{NH}_2)$  and  $\nu_s(\text{NH}_2)$  for the three complexes overlap each other within  $\pm 2 \text{ cm}^{-1}$  as discussed before. For the pure molecules, the  $\nu_{as}(\text{NH}_2)$  and  $\nu_s(\text{NH}_2)$  frequencies occur in the order: HEXA > DMEDA > BPEI in both IR and Raman, and reflect the strength of the hydrogen bonding interactions (Figure 5.2).

As LiTf is added, the order is consistent in the IR and Raman, but now in the sequence: DMEDA – LiTf 3:1 > BPEI – LiTf 3:1 > HEXA – LiTf 3:1. The frequencies of the observed bands are determined by two competing factors: breaking the hydrogen bonding interactions shifts the band frequencies upward, while the cation inductive effect pulls the frequencies downward. In HEXA – LiTf, the strong inductive effect and the limited hydrogen bonding interactions now broken by the addition of salt, cause the frequencies to be low. In BPEI – LiTf, strong hydrogen bonds and a weaker inductive effect keep the frequencies higher than in the hexylamine system, but lower than in the DMEDA system. In the latter, the addition of salt greatly disturbs the hydrogen bonds, shifting the bands to higher frequencies.

### 5.1.2. NH bending region

The frequency of the NH<sub>2</sub> internal bending mode,  $\delta(\text{NH}_2)$ , is also sensitive to hydrogen bonding interactions, although the NH<sub>2</sub> and NH bending modes have not been as well-studied as the stretching modes. Studies of the in-plane bending mode are complicated due to the mixing of the mode with other vibrational motions, e.g. CH<sub>2</sub> scissors and wagging motions. This means that there may be more than one band involving the bending motion, therefore the spectral changes accompanying perturbation of the motion are difficult to interpret. The O – H and N – H bending modes occur in the 1000 – 1700 cm<sup>-1</sup> spectral region. It has been determined that the band shifts to *higher frequencies with the formation of hydrogen bonds*<sup>3,4</sup>, in contrast to the decrease observed in the N – H stretching frequencies; moreover, the shifts are much smaller in amplitude compare to the stretching modes. However, the direction of the frequency shifts

accompanying the coordination of the cation for a bending vibration is not known. In general, the effects of hydrogen bonding interactions on the deformation motions are extremely complex in the sense that they are closely dependant on steric effects, rotational isomerism, and interactions with the C – H deformation motions.<sup>3</sup> A summary of the  $\delta(\text{NH}_2)$  frequency shifts in BPEI, DMEDA, and HEXA, as well as in their complexes with LiTf and NaTf at a 3:1 N:M<sup>+</sup> molar ratio is represented in Figure 5.4 below. In the IR spectrum of hexylamine, the  $\delta(\text{NH})$  mode is a very broad and asymmetric band centered around 1610 cm<sup>-1</sup> (spectrum shown in Figure 5.5), which is higher than the corresponding bands of DMEDA and BPEI. In the last two molecules, the bands are also very broad, and the frequencies of the modes are very close, with the DMEDA frequency slightly higher than the BPEI frequency. In these two systems, the presence of *intramolecular* hydrogen bonds, which does not occur in HEXA, has a significant effect on the frequencies as seen in the Figure. When the polymer – salt and DMEDA – salt complexes are formed with LiTf and NaTf, the  $\delta(\text{NH})$  frequencies shift upward, with a larger shift in the LiTf complexes. The situation is reversed in HEXA, where a downward shift is observed, with a smaller shift in the LiTf complex compared to the NaTf complex. In all the systems, the addition of salt causes the peaks to sharpen; this is indicative of the formation of a more uniform or ordered environment than in the pure liquids.

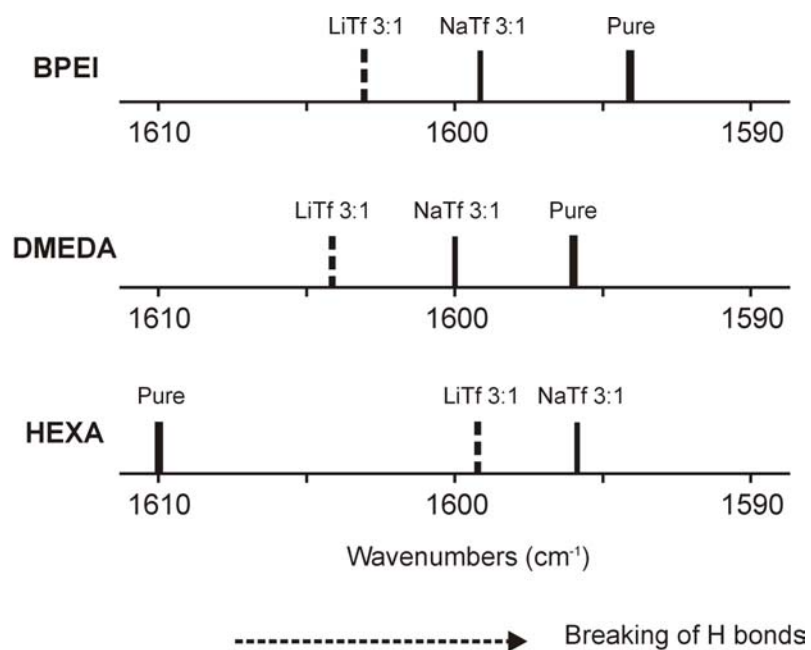


**Figure 5.4.** Schematic representation of the  $\delta(\text{NH}_2)$  frequency shifts in BPEI, DMEDA, and HEXA, and in their complexes with LiTf and NaTf at a 3:1 N:M<sup>+</sup> molar ratio in the IR spectra.

The frequency decrease of pure hexylamine with addition of LiTf and NaTf may be due to the breaking of the hydrogen bonding interactions (lowering the frequencies) and a contribution from the cation inductive effect (no reference). The positive shifts in BPEI and DMEDA is somewhat surprising because the breaking of the hydrogen bonds accompanied by a weak cation inductive effect might expect to lower the frequencies. The difficulty is that this vibration often contains contributions from other intramolecular motions. Changing the hydrogen bonding environment may alter the nature of the mode in terms of the admixture of intramolecular motions. Therefore, shifts in  $\delta(\text{NH}_2)$  are not as reliable as shifts in the N – H stretching frequency for drawing conclusions about hydrogen bonding interactions. Further complicating the picture is the lack of knowledge about the direction and magnitude of the  $\delta(\text{NH}_2)$  frequency shift due to the coordination of the cation. For a bending motion, the coordinative geometry, i.e. bond angle and bond

length, of the cation seems to play a major role in the perturbation of the vibration, in contrast to the stretching vibration where the charge density is the main factor.

Hexylamine and DMEDA were dissolved in  $\text{CCl}_4$  at various composition ratios. The IR spectra of the  $\text{NH}_2$  bending region are shown in Figure 5.5. The presence of a  $\text{CCl}_4$  band at  $1550\text{ cm}^{-1}$ , with a shoulder around  $1580\text{ cm}^{-1}$  impairs any quantitative analysis of the  $\delta(\text{NH}_2)$  mode. Nevertheless, a comparison of the two model compounds diluted in  $\text{CCl}_4$  in this region of the spectrum provides additional information.

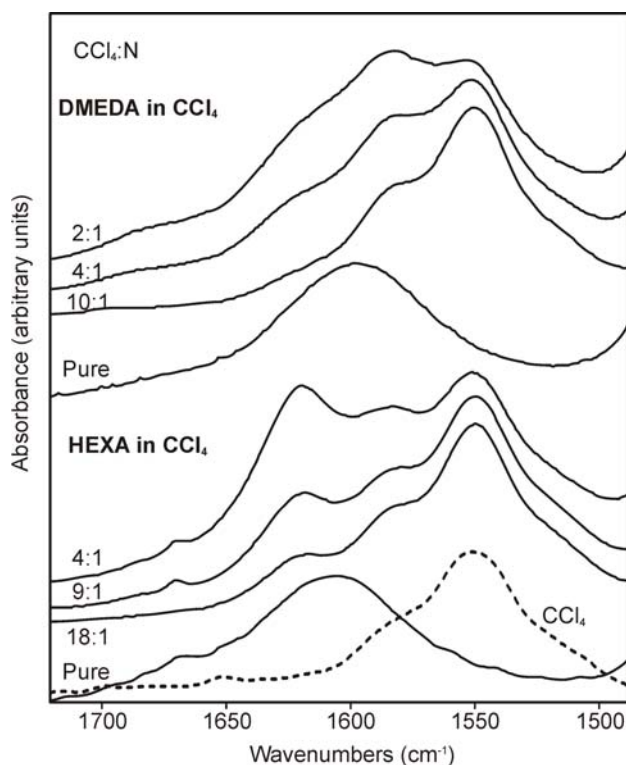


**Figure 5.5.** N-H bending region of the IR spectra of HEXA, DMEDA, and their solutions in  $\text{CCl}_4$  at varying  $\text{CCl}_4$ :nitrogen molar ratios.

In hexylamine, the  $\delta(\text{NH}_2)$  band occurs at  $1610\text{ cm}^{-1}$ . When it is dissolved in  $\text{CCl}_4$ , a shoulder starts to grow on the high frequency side of the  $\text{CCl}_4$  bands. This band increases in intensity compared to the other bands as the concentration in hexylamine

increases. At a 4:1 CCl<sub>4</sub>:N ratio, the maximum intensity is at 1620 cm<sup>-1</sup> and the peak is as intense as the CCl<sub>4</sub> peak around 1550 cm<sup>-1</sup>. So upon breaking intermolecular hydrogen bonding interactions, the δ(NH<sub>2</sub>) mode shifts to higher frequencies (+ 10 cm<sup>-1</sup>), which is the opposite direction predicted in the literature.<sup>3,4</sup> The dilution series in CCl<sub>4</sub> is also shown in Figure 5.5 for the DMEDA molecule. At very high dilution ratios, only a small shoulder around 1620 cm<sup>-1</sup> can be observed on the high frequency side of the CCl<sub>4</sub> band. When the concentration reaches a 2:1 CCl<sub>4</sub>:N ratio (or 4:1 CCl<sub>4</sub>:NH<sub>2</sub> ratio), the shoulder is still present, but a band at 1583 cm<sup>-1</sup>, superposed with a CCl<sub>4</sub> band grows in intensity. So, in DMEDA, it seems that there are two different populations occurring upon dilution; one population of DMEDA vibrates around 1620 cm<sup>-1</sup>, and has the same vibrational potential energy environment as the hexylamine molecules in CCl<sub>4</sub>, while the other population is shifted to lower frequency compare to pure DMEDA and vibrates around 1583 cm<sup>-1</sup>. The big surprise comes from the shift to higher frequency upon dilution in the hexylamine system. As a solution gets more dilute, the hydrogen bonding interactions between amine molecules decreases, and therefore the bending mode should shift downward. When amine molecules are dissolved in CCl<sub>4</sub>, there are small interactions between the hydrogen atom of the amine group and the chlorine atom.<sup>5-9</sup> Even though these interactions are very weak compare to amine – amine interactions, it is possible that they affect the bending motion of the NH<sub>2</sub> groups.

## 5.2. CATION – HOST INTERACTIONS:

### BPEI – LiTf, BPEI – NaTf, and BPEI – TbaTf systems

#### 5.2.1. Spectroscopic analysis

##### a) NH stretching region

As LiTf and NaTf are dissolved in BPEI, both the  $\nu_{as}$  and the  $\nu_s$  bands shift to higher frequencies than in the pure polymer, and the bandwidths decrease as shown in Figure 5.6. The frequency data are summarized in Table 5.2. As seen in the hexylamine system, substitution of  $\text{Li}^+$  by  $\text{Na}^+$  causes shifts to even higher frequencies, in agreement with a stronger inductive effect of  $\text{Li}^+$  than  $\text{Na}^+$  because of the higher charge density of the  $\text{Li}^+$  cation.

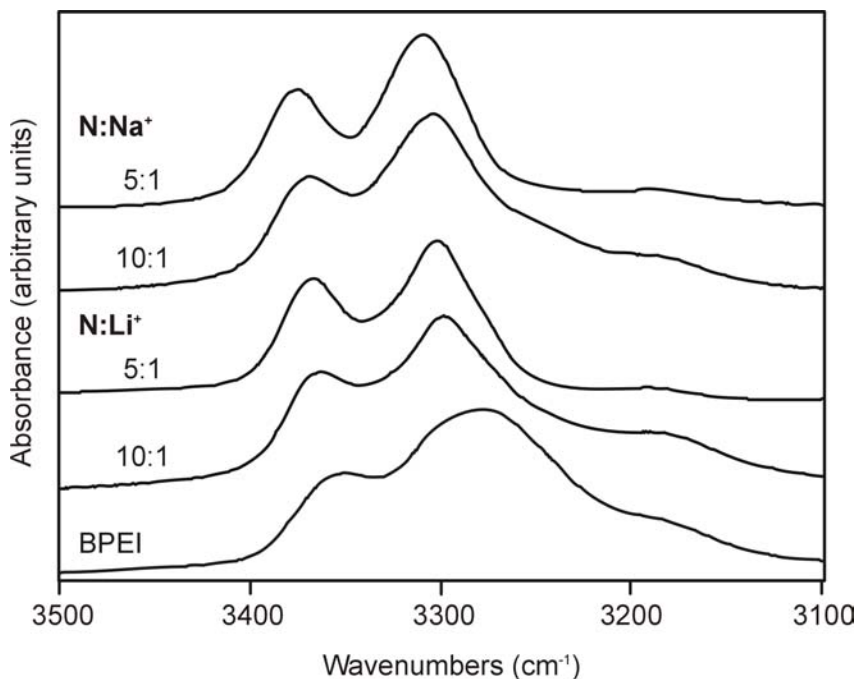


**Figure 5.6.** N-H stretching region of the IR spectra of BPEI and its complexes with NaTf, and LiTf at varying nitrogen:cation ratios.

**Table 5.2.** N-H stretching and N-H bending frequencies of BPEI and its complexes with NaTf and LiTf at varying nitrogen:cation ratios.

	$\nu_{as}(\text{NH}_2)$ $\text{cm}^{-1}$	$\nu_s(\text{NH}_2)$ $\text{cm}^{-1}$
BPEI	3352	3279
NaTf 10:1	3369	3304
NaTf 5:1	3376	3309
LiTf 10:1	3363	3298
LiTf 5:1	3367	3302

To further understand the cation – polymer and anion - polymer interactions in the BPEI matrix, complexes with tetrabutylammonium triflate salt were studied. Tetrabutylammonium is a charge-protected cation because of its bulky butyl groups. Consequently, it cannot undergo a direct coordinative interaction with the nitrogen atoms of BPEI. Therefore, TbaTf – BPEI complexes were studied to understand the interactions of the triflate ions with the polymer. The addition of TbaTf causes no shifts of the  $\nu_{as}(\text{NH}_2)$  and  $\nu_s(\text{NH}_2)$  polymer bands. In addition, the frequencies of all the triflate bands of the polymer – salt mixture are identical to those in the pure TbaTf salt, which leads to the conclusion that TbaTf does not dissolve in the BPEI polymer matrix. The triflate anions have the capability to form hydrogen bonds with the hydrogen atoms of the amine groups as seen in both BPEI:NaTf and BPEI:LiTf complexes. However, when TbaTf is added to BPEI, the triflate anion does not disrupt the N –H ... N hydrogen bonds in BPEI. This experiment shows that the interactions between the cation and the polymer host are very important for the solvation of the salt. The triflate ions alone cannot break

the polymer hydrogen bonds; the presence of a small cation such as  $\text{Na}^+$  or  $\text{Li}^+$  solvated by the nitrogen atoms is required for the triflate ions to interact with the polymer.

### **b) Polymer – salt interactions**

A number of spectral changes in the BPEI system occur with the addition of LiTf and NaTf. Upon complex formation, the C – N stretch region of the polymer is greatly affected. The two bands at  $1052\text{ cm}^{-1}$  and  $1128\text{ cm}^{-1}$  have been assigned to the asymmetric C – C – N stretch of the primary amines and the asymmetric C – N – C stretch of the secondary amines respectively.<sup>10,11</sup> The  $1052\text{ cm}^{-1}$  peak has a shoulder on the high frequency side ( $\sim 1073\text{ cm}^{-1}$ ) and the  $1128\text{ cm}^{-1}$  peak has a shoulder on the low frequency side ( $\sim 1107\text{ cm}^{-1}$ ). The vibrational frequencies of these two polymer bands are located between the  $\text{SO}_3$  symmetric stretch ( $1032\text{ cm}^{-1}$ ) and the  $\text{CF}_3$  asymmetric stretch ( $1155\text{ cm}^{-1}$ ) in these polymer – MTf complexes. Therefore as the salt concentration increases, the intensity of the triflate bands greatly increases compared to the intensity of the polymer bands, which prevents a detailed analysis of the polymer – salt interactions. However, some important observations can be made. Upon addition of salt, the shoulder at  $\sim 1107\text{ cm}^{-1}$  grows in intensity and shifts to  $1099\text{ cm}^{-1}$  and  $1108\text{ cm}^{-1}$  in the 3:1 BPEI:LiTf and BPEI:NaTf complexes, respectively. The polymer band at  $\sim 1073\text{ cm}^{-1}$  shifts to  $\sim 1067\text{ cm}^{-1}$  and  $1076\text{ cm}^{-1}$  in the 5:1 complexes, respectively. This band is overlapped by the  $\text{SO}_3$  symmetric stretch of the triflate ion in the 3:1 BPEI:LiTf complex. The C–N stretching vibrations appear to be more affected by the presence of the lithium than the sodium ion, in agreement with a higher charge density of  $\text{Li}^+$ . Also, in the LiTf complexes the polymer bands seem to shift to lower frequencies, whereas in the NaTf

complexes one of the bands does not significantly shift and the other one shifts to higher frequencies.

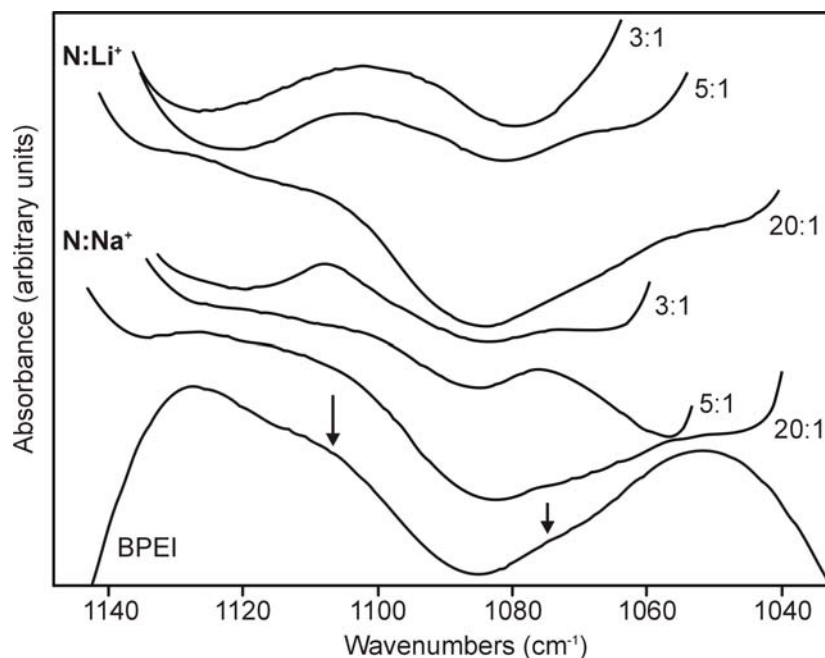


**Figure 5.7.** IR spectra of the asymmetric C-N stretching vibrations of BPEI and its complexes with LiTf and NaTf ( $N:M^+ = 20:1, 5:1$ ).

There are also changes in the BPEI spectra in the 700 to 1000  $\text{cm}^{-1}$  region upon the addition of NaTf and LiTf salts (Figure 5.8). The breadth and the very poorly resolved band structure in BPEI suggest that these peaks actually consist of several broad and overlapping bands. The modes in this region are comprised mainly of a mixture of N – H bending,  $\text{CH}_2$  rocking,  $\text{CH}_2$  wagging,  $\text{CH}_2$  twisting and N – H wagging motions. The  $\delta_s(\text{CF}_3)$  mode of the triflate anion occurs in this region as well. In both polymer – salt systems, the polymer bands at 775  $\text{cm}^{-1}$ , 855  $\text{cm}^{-1}$  and 899  $\text{cm}^{-1}$  shift to higher frequencies upon addition of salt. The 775  $\text{cm}^{-1}$  band seems to be shifted further in the BPEI:LiTf complexes than in the BPEI:NaTf complexes, probably because of the higher charge density of  $\text{Li}^+$  compare to  $\text{Na}^+$ . The spectrum of the 20:1 BPEI:NaTf sample

resembles that of pure BPEI with all the bands slightly more intense. In the 5:1 sample, the bands shift to higher frequencies and increase in intensity. However, in the BPEI:LiTf samples, the spectrum of the 20:1 composition resembles more the spectrum of the 5:1 composition than that of the pure polymer. At a 20:1 composition, the polymer bands are not much stronger in intensity, but a more defined band structure starts to appear. This trend continues as the LiTf concentration increases.

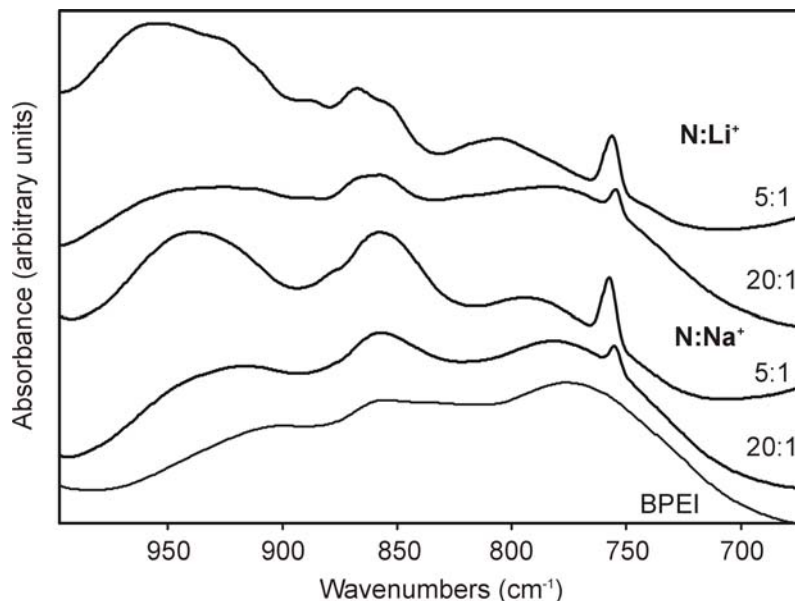


**Figure 5.8.** IR spectra of BPEI and its NaTf and LiTf complexes ( $N:M^+ = 20:1, 5:1$ ) in the conformation region of the polymer.

### c) Ionic association

The  $CF_3$  symmetric deformation band,  $\delta_s(CF_3)$ , and the  $SO_3$  symmetric stretching band,  $\nu_s(SO_3)$ , contain information about the cation – anion interactions of the triflate ion. However, in both BPEI:LiTf and BPEI:NaTf complexes, these triflate bands overlap with BPEI bands, which complicates the deconvolution of these peaks. The  $\delta_s(CF_3)$  and the  $\nu_s(SO_3)$  spectral regions contain distinct bands assigned to several ionically associated species: “free” ions, contact ion pair  $[MTf]$ , and triple cation  $[M_2Tf]^+$ . The band

assignments of these species have been developed in the ethylene oxide systems, although these assignments have been shown to be valid in ethylenimine systems.<sup>14,15</sup> The data are summarized in Tables 5.3 and 5.4 (spectra not shown).

In the BPEI:LiTf complex, the 20:1 and 10:1 compositions have one broad band at  $755\text{ cm}^{-1}$  in the  $\delta_s(\text{CF}_3)$  region. This frequency is slightly higher than a “free” triflate ion frequency in PEO:MTf systems ( $752 - 753\text{ cm}^{-1}$ ). The difference between the PEI and PEO systems has been attributed to weak hydrogen bonding interaction between the hydrogen of the amine groups and the triflate oxygen in the PEI systems. The replacement of N-H  $\cdots$  N hydrogen bonds by weaker N-H  $\cdots$  O hydrogen bonds with the triflate oxygen was previously pointed out by Paul et al.<sup>2</sup> For the same compositions, the  $\nu_s(\text{SO}_3)$  region shows one band at  $1031\text{ cm}^{-1}$ , which is slightly lower than a “free” triflate ion frequency in PEO:MTf systems ( $1032 - 1033\text{ cm}^{-1}$ ), and corresponds to a “free” ion frequency that is also disturbed by weak hydrogen bonding interactions between the amine hydrogen atom and the triflate anion. At a 5:1 composition, the presence of ion pairing is indicated by the  $757\text{ cm}^{-1}$  band in the  $\delta_s(\text{CF}_3)$  region and by the  $1037\text{ cm}^{-1}$  band in the  $\nu_s(\text{SO}_3)$  region. At higher salt concentrations, the bands at  $763\text{ cm}^{-1}$  and  $1044\text{ cm}^{-1}$  suggest the presence of highly associated ionic species. The  $759\text{ cm}^{-1}$  band in the  $\delta_s(\text{CF}_3)$  region probably corresponds to a contact ion pair with weak hydrogen bonding interactions.

The analysis of the ionic association in the BPEI:NaTf complex is very similar to the BPEI:LiTf complex. The 20:1 and 10:1 compositions have one broad band at  $755\text{ cm}^{-1}$  in the  $\delta_s(\text{CF}_3)$  region, and two bands at  $1031\text{ cm}^{-1}$  and  $1033\text{ cm}^{-1}$  for the 20:1 composition and  $1031\text{ cm}^{-1}$  and  $1034\text{ cm}^{-1}$  for the 10:1 composition in the  $\nu_s(\text{SO}_3)$  region.

The two bands seen in the  $\nu_s(\text{SO}_3)$  region correspond to “free” ions (1033 and 1034  $\text{cm}^{-1}$ ) and possibly “free” ions with a weak hydrogen bonding interaction (1031  $\text{cm}^{-1}$ ). Upon further addition of salt, the ionic species present become more associated, and the presence of ion pairs is supported by the 757  $\text{cm}^{-1}$  and the 1037  $\text{cm}^{-1}$  bands in the 5:1 composition. In the 3:1 complex, the majority of the present species is highly associated as indicated by the 761  $\text{cm}^{-1}$  and the 1041  $\text{cm}^{-1}$  bands.

**Table 5.3.** Band center frequency ( $\text{cm}^{-1}$ ) in the  $\delta_s(\text{CF}_3)$  region for BPEI:LiTf and BPEI:NaTf complexes at varying N:M<sup>+</sup> molar ratios.

Composition	BPEI:NaTf		BPEI:LiTf	
20:1		755		755
10:1		755		755
5:1		757	757	755
3:1	761		763 759	754

**Table 5.4.** Band center frequency ( $\text{cm}^{-1}$ ) in the  $\nu_s(\text{SO}_3)$  region for BPEI:LiTf and BPEI:NaTf complexes at varying N:M<sup>+</sup> molar ratios.

Composition	BPEI:NaTf			BPEI:LiTf		
20:1		1033	1031			1031
10:1		1034	1031			1031
5:1		1037	1032	1037		1031
3:1	1041	1037	1032	1044	1037	1031

Both BPEI:LiTf and BPEI:NaTf complexes show similar trends in the ionic association; as the salt concentration increases, the formation of the aggregate species increases while the proportion of ion pair and “free” ion decreases. However, the main difference between these two complexes is more evident at high salt concentrations. The

BPEI:NaTf complex tends to form more triple cation species than the BPEI:LiTf complex (~100% 761  $\text{cm}^{-1}$  and ~80% 1041  $\text{cm}^{-1}$  for BPEI:NaTf and ~60% 763  $\text{cm}^{-1}$  and ~70% 1044  $\text{cm}^{-1}$  for BPEI:LiTf). However, the vibrational frequencies of the aggregate species are higher in the LiTf complex (1044 and 763  $\text{cm}^{-1}$ ) than in the NaTf complex (1041 and 761  $\text{cm}^{-1}$ ).

The  $\text{SO}_3$  asymmetric stretch,  $\nu_{\text{as}}(\text{SO}_3)$ , is affected differently by the coordination of the lithium cation versus the sodium cation (Figure 5.9 below).

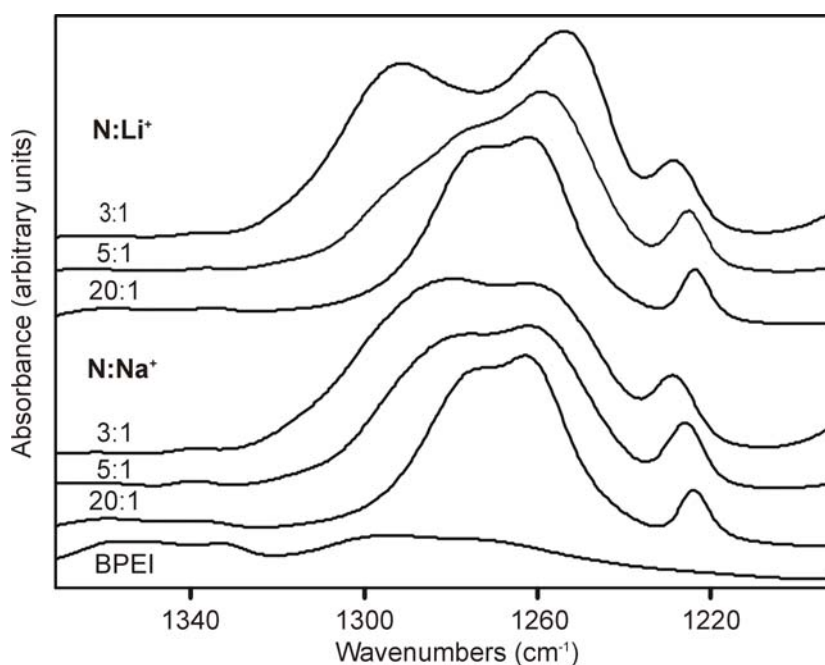


**Figure 5.9.** IR spectra of the  $\nu_{\text{as}}(\text{SO}_3)$  region of BPEI with 20:1, 5:1, and 3:1  $\text{N}:\text{M}^+$  molar ratios of NaTf and LiTf

The two  $\nu_{\text{as}}(\text{SO}_3)$  bands at 1274  $\text{cm}^{-1}$  and 1262  $\text{cm}^{-1}$  are identical in both complexes at a 20:1 composition. The differences remain small up to 10:1 composition. At high salt concentrations (compositions  $\leq 5:1$ ), the separation of the two bands becomes very different. In the 3:1 BPEI:LiTf complex these two bands (1291 and 1254  $\text{cm}^{-1}$ ) are separated by 37  $\text{cm}^{-1}$ , whereas in the 3:1 BPEI:NaTf complex the frequency separation is

only  $17\text{ cm}^{-1}$  ( $1280$  and  $1263\text{ cm}^{-1}$ ). The greater frequency separation in the BPEI:LiTf system indicates a stronger coordination of the triflate anion to lithium than to sodium cations.

The thermal analysis of these complexes shows that the 3:1 BPEI:NaTf complex has a  $T_g$  at  $1^\circ\text{C}$ , whereas the BPEI:LiTf complex has a  $T_g$  at  $33^\circ\text{C}$ . All the IR spectra were taken at room temperature ( $\sim 24^\circ\text{C}$ ), consequently these experiments were done above the  $T_g$  of the BPEI:NaTf complex, but below the  $T_g$  of the BPEI:LiTf complex. Therefore, at room temperature, the BPEI:LiTf 3:1 complex is in a glassy state, which implies less flexibility but not necessarily more order, whereas the BPEI:NaTf 3:1 complex is in an amorphous state.

### **5.2.2. Thermal analysis**

The glass transition temperatures ( $T_g$ ) of BPEI and BPEI with various compositions of NaTf and LiTf are summarized in Table 5.5. BPEI is a fully amorphous polymer at room temperature and has a glass transition temperature of  $-55^\circ\text{C}$ . Upon addition of NaTf or LiTf, the  $T_g$  increases as the systems become more locally ordered due to the coordination of the alkali-metal ions to the nitrogen atoms, which inhibits polymer segmental motion. In the BPEI:LiTf system, the  $T_g$  increases continuously to reach  $33^\circ\text{C}$  for a 3:1 composition. In contrast, in the BPEI:NaTf system, the  $T_g$  increases to a maximum of  $5^\circ\text{C}$  for a 5:1 composition and then plateaus at higher salt concentrations. These observations are consistent with the growth of vibrational band structure upon addition of salt, as seen in Figure 5.8. The study of crystalline structures of small molecules such as the glymes and their nitrogen homologues with LiTf and NaTf

salts has shown that sodium usually has a coordination number of 5 or 6 whereas lithium as a coordination number of 4 or 5. This difference can explain the plateau of the  $T_g$  values that occurs in the BPEI:NaTf complexes starting at a 5:1 composition. Above this composition, there are no more nitrogen atoms available to satisfy the coordination of sodium, which leads to a salting out of the sample. This behavior does not occur with the lithium salt because even at high salt concentrations the coordination of the lithium ion is satisfied.

**Table 5.5.** Glass transition temperatures  $T_g$  ( $^{\circ}\text{C}$ ) of BPEI, BPEI:NaTf, and BPEI:LiTf with varying nitrogen:cation ratios.

Composition N:M <sup>+</sup>	BPEI:NaTf	BPEI:LiTf
Pure BPEI	-55	-55
20:1	-46	-40
10:1	-21	-15
8:1	-10	-6
6:1	1	21
5:1	5	26
4:1	1	–
3:1	1	33

### 5.2.3. Ionic conductivity

Temperature dependent conductivity measurements were taken from room temperature to  $80^{\circ}\text{C}$  in increments of  $10^{\circ}\text{C}$ . A second set of measurements was performed after allowing the samples to cool overnight. No hysteresis was observed in the conductivity behavior. The samples were tested for water using IR spectroscopy. The

samples contaminated with water during the measurement process exhibit higher conductivity values by a factor of 10. These measurements were discarded.

The resulting conductivity values for BPEI:LiTf and BPEI:NaTf complexes are plotted in Figure 5.10. As can be seen in the plots, the 20:1 composition for both polymer-salt complexes shows the highest conductivity. This is in agreement with the low salt concentration / low  $T_g$  balance required for the best conductors. The conductivity of the 10:1 BPEI:LiTf complex is lower than the conductivity values of the 10:1 BPEI:NaTf complex. At this high salt concentration, it is possible that the charge density of the cation becomes an important factor. The lithium cation is strongly coordinated to the nitrogen of the polymer and its mobility is reduced.

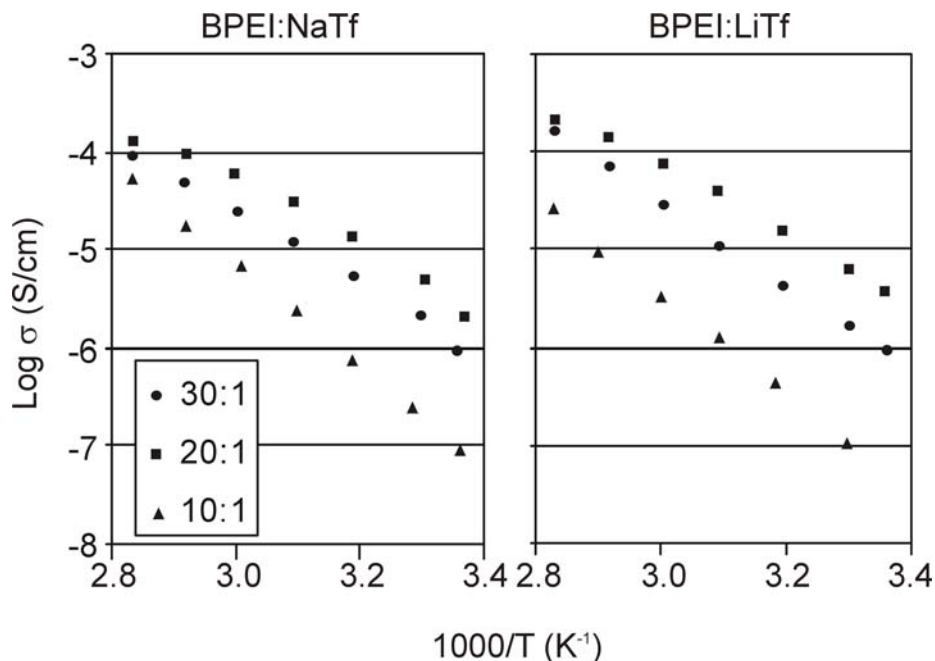


**Figure 5.10.** Temperature dependant conductivity data of BPEI at various compositions of NaTf and LiTf (30:1, 20:1, 10:1).

The comparison of the spectroscopic, conductivity and calorimetric data of the BPEI:NaTf and BPEI:LiTf complexes shows only small differences between the two

complexes, which most likely can be attributed to the higher charge density of the lithium cation. The conductivity data for both complexes are very similar to those previously published by Harris et al.<sup>10</sup> and Paul et al.<sup>2</sup>, and confirms that the highest conductivity value is obtained for a nitrogen to cation ratio of 20:1 and is on the order of  $10^{-6}$  S  $\text{cm}^{-1}$  at 25°C.

### 5.3. ANION – HOST INTERACTIONS:

#### BPEI – NaBPh<sub>4</sub> and BPEI – NaTf systems

##### 5.3.1. Spectroscopic analysis

###### a) NH stretch and NH bend

The NH stretching vibrations of the BPEI amine groups are shown in Figure 5.11 for BPEI and complexes of BPEI with NaTf and with NaBPh<sub>4</sub>.

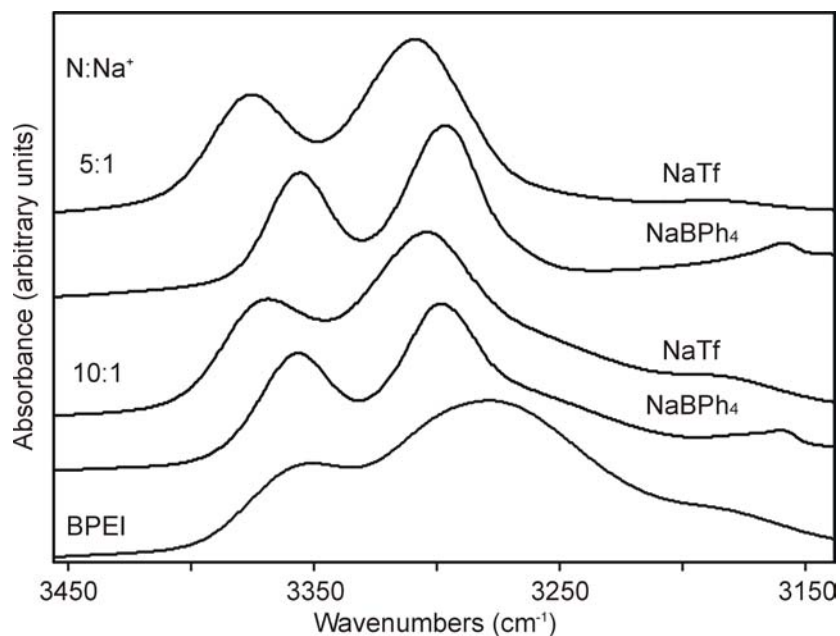


**Figure 5.11.** IR spectra of the N-H stretching vibrations of BPEI and its NaTf and NaBPh<sub>4</sub> complexes (N:Na<sup>+</sup> = 10:1, 5:1).

When NaTf or NaBPh<sub>4</sub> is dissolved in BPEI, both the  $\nu_{as}$  and the  $\nu_s$  bands shift to higher frequencies and the bandwidths decrease as shown in Figure 5.11. These frequency data are also summarized in Table 5.6. In general, a decrease in bandwidth signifies a decrease in heterogeneous broadening, i.e. a more homogeneous distribution of potential energy environments of the vibrating species. In the case of hydrogen-bonded species, a decrease of N-H stretching mode bandwidths also indicates a decrease in the strength of hydrogen-bonding interactions. It is probable that both of these effects occur upon complexation of BPEI with a salt. More detailed information can be gained from a closer examination of the frequency shifts.

**Table 5.6.** N-H stretching frequencies (cm<sup>-1</sup>) of BPEI and its complexes with NaTf and NaBPh<sub>4</sub>.

Composition	$\nu_{as}(\text{NH}_2)$		$\nu_s(\text{NH}_2)$	
	NaTf	NaBPh <sub>4</sub>	NaTf	NaBPh <sub>4</sub>
Pure	3352	3352	3279	3279
10:1	3369	3356	3304	3298
5:1	3376	3356	3309	3297

Paul et al.<sup>2</sup> have pointed out that with the addition of lithium triflate, there is a progressive replacement of hydrogen-bonded N–H···N groups by the entity Li<sup>+</sup>···N–H···O<sub>3</sub>S–CF<sub>3</sub>. As seen before in hexylamine and DMEDA, there are two effects in the salt complexes that shift the frequencies relative to the pure BPEI system. The replacement of the N–H···N hydrogen bonds by weaker N–H···O hydrogen bonds to the triflate oxygen atoms shifts the N-H stretching modes to higher frequencies. In addition, NH<sub>2</sub> frequency

shifts occur through the inductive effect, which results from the solvation of a cation by the lone pair of a nitrogen atom. This interaction weakens the N–H bond by decreasing its electron density and thereby decreases the mode frequency. However, the inductive effect also decreases the strength of the hydrogen bonds, which would tend to increase the NH<sub>2</sub> stretching frequencies. The simultaneous occurrence of these effects makes it difficult to understand their relative importance in determining the NH<sub>2</sub> frequency shifts observed in the NaTf complexes.

The tetraphenylborate anion does not contain heteroatoms that participate in hydrogen-bonding interactions. Therefore, a comparative study of the frequency shifts in BPEI-NaBPh<sub>4</sub> complexes with analogous shifts in BPEI-NaTf complexes provides an excellent opportunity to separate the relative contributions of the various effects present. The frequency data in Figure 5.11 and Table 5.6 are graphically illustrated in Figure 5.12 as an aid to the following discussion.

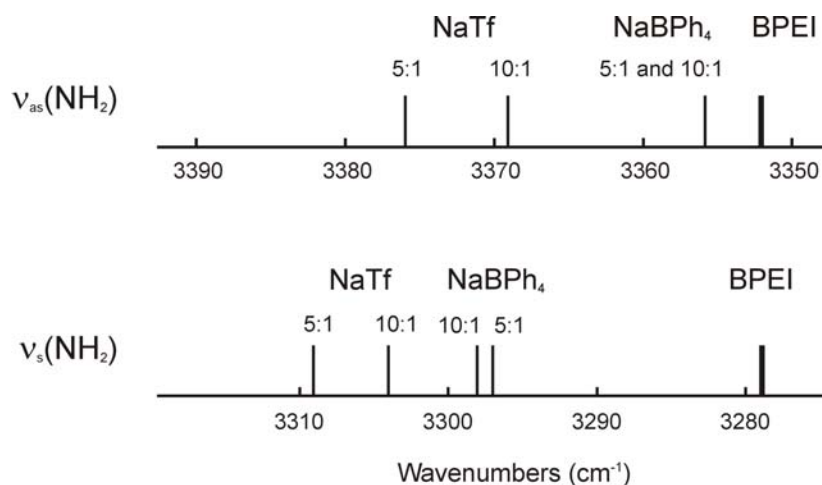


**Figure 5.12.** Schematic representation of the ν<sub>s</sub>(NH<sub>2</sub>) and the ν<sub>as</sub>(NH<sub>2</sub>) frequency shifts in BPEI:NaTf and BPEI:NaBPh<sub>4</sub> complexes (N:Na<sup>+</sup> = 10:1, 5:1) using the BPEI modes as a reference.

In general, the frequency shifts observed in the NaTf complexes are higher than in the NaBPh<sub>4</sub> complexes, in spite of the fact that there are weak hydrogen-bonding interactions of the NH<sub>2</sub> group with the triflate oxygen atoms, which would tend to slightly lower those frequencies. Therefore the inductive effect appears to be larger in BPEI-NaBPh<sub>4</sub> than in BPEI-NaTf, suggesting that the Na<sup>+</sup>-N interaction is slightly stronger in the former system. This difference may be due to significant cation-anion interactions in the NaTf complex that hinder the coordinative interaction of the sodium ions with the nitrogen of the NH<sub>2</sub> group, whereas tetraphenylborate is a charge-protected anion that is unable to significantly interact with the sodium cation.

The presence of strong cation-anion interactions in BPEI-NaTf is confirmed by an examination of triflate ion intramolecular modes whose frequencies are sensitive to cation-anion interactions. These data are summarized in Table 5.7 (spectra not shown).

**Table 5.7.** Band center frequencies (cm<sup>-1</sup>) in the  $\delta_s(\text{CF}_3)$  and  $\nu_s(\text{SO}_3)$  regions and splitting of  $\nu_{\text{as}}(\text{SO}_3)$  for BPEI:NaTf.

Composition	$\delta_s(\text{CF}_3)$		$\nu_s(\text{SO}_3)$			Assignment
20:1		755		1033	1031	“free” ions
10:1		755		1034	1031	
5:1	757		1037			ion pairs

The addition of salt increases the degree of ionic association as seen by the increase of the  $\delta_s(\text{CF}_3)$  and  $\nu_s(\text{SO}_3)$  frequencies. Another measure of ionic association is the splitting of the SO<sub>3</sub> antisymmetric stretching mode,  $\Delta\nu_{\text{as}}(\text{SO}_3)$ , which originates in the breaking of the two-fold degeneracy of the  $\nu_{\text{as}}(\text{SO}_3)$  mode through the sodium ion-

triflate ion interactions. The value of  $\Delta\nu_{\text{as}}(\text{SO}_3)$  increases from  $11\text{ cm}^{-1}$  in the 20:1 composition to  $15\text{ cm}^{-1}$  in the 5:1 composition. This increase in  $\Delta\nu_{\text{as}}(\text{SO}_3)$  reflects the growing importance of ion pair interactions with increasing salt concentration, and the accompanying decrease in the strength of the sodium ion-nitrogen atom interactions.

### b) Polymer – salt interactions

The addition of  $\text{NaBPh}_4$  or  $\text{NaTf}$  results in striking changes in the BPEI spectra in the  $700$  to  $1000\text{ cm}^{-1}$  region as illustrated in Figure 5.13.

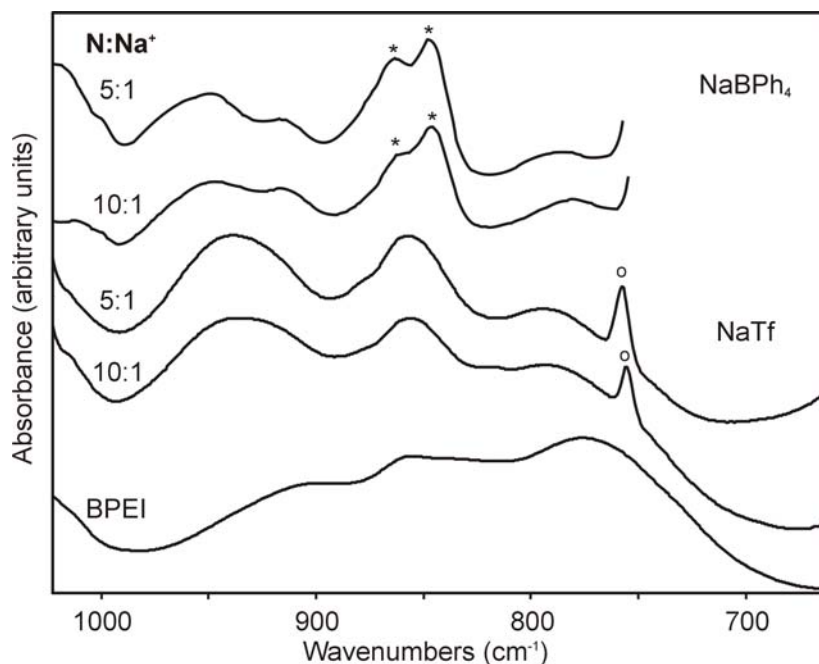


**Figure 5.13.** IR spectra of BPEI and its  $\text{NaTf}$  and  $\text{NaBPh}_4$  complexes ( $\text{N}:\text{Na}^+ = 10:1, 5:1$ ) from  $670$  to  $1020\text{ cm}^{-1}$ . Asterisks indicate tetraphenylborate bands and circles indicate triflate bands.

This figure shows a comparison of the IR spectra of pure BPEI,  $\text{BPEI}:\text{NaBPh}_4$  and  $\text{BPEI}:\text{NaTf}$ , both at 10:1 and 5:1 compositions. BPEI modes in this region are comprised mainly of a mixture of N–H bending,  $\text{CH}_2$  rocking,  $\text{CH}_2$  wagging,  $\text{CH}_2$

twisting and N–H wagging motions. The  $\delta_s(\text{CF}_3)$  mode of the triflate anion also occurs in this region at 755 and 757  $\text{cm}^{-1}$  for the BPEI:NaTf 10:1 and 5:1 compositions, respectively. In both BPEI:NaBPh<sub>4</sub> and BPEI:NaTf complexes, the polymer band at 775  $\text{cm}^{-1}$  shifts to a higher frequency with increasing salt concentration. The polymer band at 855  $\text{cm}^{-1}$  cannot be observed in the BPEI:NaBPh<sub>4</sub> complexes due to multiple tetraphenylborate bands. Upon addition of the sodium salts, the polymer band at 901  $\text{cm}^{-1}$  shifts to 932  $\text{cm}^{-1}$  in BPEI:NaTf 5:1 and to 947  $\text{cm}^{-1}$  with a second band at 916  $\text{cm}^{-1}$  in BPEI:NaBPh<sub>4</sub> 5:1. The larger frequency shift in the sodium tetraphenylborate complex is consistent with the stronger sodium ion-BPEI nitrogen atom interaction suggested earlier.

Spectral changes accompanying the addition of NaTf have been previously reported in the BPEI primary amine asymmetric C–C–N stretching mode,  $\nu_{\text{as}}(\text{CCN})$ , and the secondary amine asymmetric C–N–C stretching mode,  $\nu_{\text{as}}(\text{CNC})$ . A comparison of BPEI:NaBPh<sub>4</sub> and BPEI:NaTf in this region (Figure 5.14) provides additional information despite the presence of a number of tetraphenylborate and triflate bands.

The figure shows the IR spectra of the 5:1 and 20:1 compositions of BPEI:NaBPh<sub>4</sub> and BPEI:NaTf complexes in this region. The weak polymer band corresponding to the  $\nu_{\text{as}}(\text{CCN})$  mode of the primary amine at roughly 1073  $\text{cm}^{-1}$  (seen as an asymmetric wing on the high frequency side of the 1050  $\text{cm}^{-1}$  band and marked by an arrow) shifts to 1085  $\text{cm}^{-1}$  in 5:1 BPEI:NaBPh<sub>4</sub> (also marked by an arrow) and 1076  $\text{cm}^{-1}$  in 5:1 BPEI:NaTf. However, the  $\nu_{\text{as}}(\text{CNC})$  vibrations of the secondary amine at 1128  $\text{cm}^{-1}$  and 1107  $\text{cm}^{-1}$  shift to 1123  $\text{cm}^{-1}$  and 1101  $\text{cm}^{-1}$  in the 5:1 BPEI:NaBPh<sub>4</sub> complex but do not seem to shift in the BPEI:NaTf complex.

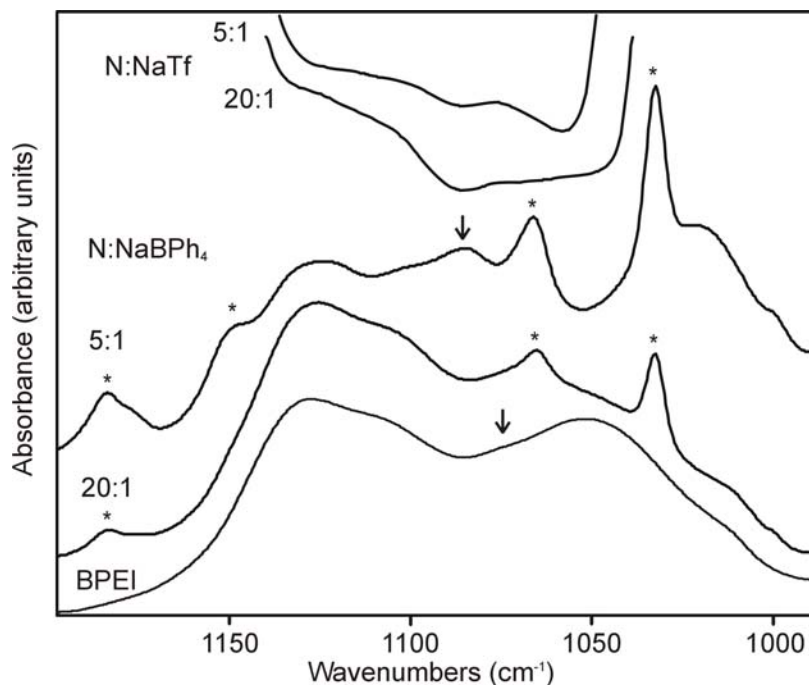


**Figure 5.14.** IR spectra of the asymmetric C-N stretching vibrations of BPEI and its complexes with NaTf and NaBPh<sub>4</sub> (N:Na<sup>+</sup> = 20:1, 5:1). Asterisks indicate tetraphenylborate bands.

In summary, the polymer bands in this spectral region seem to be more affected in the BPEI:NaBPh<sub>4</sub> complexes than in the BPEI:NaTf complexes. Additionally, in both salt complexes, the  $\nu_{\text{as}}(\text{CCN})$  band of the primary amines shifts further than the  $\nu_{\text{as}}(\text{CNC})$  band of the secondary amines of BPEI. This observation suggests that the primary amines are more involved in the solvation of the salt than the secondary amines. This result is consistent with an early study of the binding of metal ions by BPEI, which showed that the primary amine groups are more involved than the secondary amine groups in the formation of BPEI-metal ion complexes.

### 5.3.2. Thermal analysis

The glass transition temperatures ( $T_g$ ) of BPEI and BPEI with various compositions of NaTf and NaBPh<sub>4</sub> are summarized in Table 5.8. As noted earlier, BPEI is a fully amorphous polymer at room temperature and has a glass transition temperature of -55°C. Upon addition of NaTf or NaBPh<sub>4</sub>, the  $T_g$  increases as the coordination of the alkali-metal ions to the nitrogen atoms increasingly inhibits polymer segmental motion. However, the  $T_g$  values for the BPEI:NaTf system are significantly lower than the  $T_g$  values for the BPEI:NaBPh<sub>4</sub> system at all salt compositions. Again, this trend is consistent with stronger sodium ion-BPEI nitrogen interactions in the BPEI:NaBPh<sub>4</sub> complexes.

**Table 5.8.** Glass transition temperatures  $T_g$  (°C) of BPEI, BPEI:NaTf and BPEI:NaBPh<sub>4</sub> complexes at various nitrogen:cation ratios.

Composition N:Na	BPEI:NaTf	BPEI:NaBPh <sub>4</sub>
Pure BPEI	-55	-55
30:1	-49	-38
20:1	-46	-26
10:1	-21	13
5:1	5	57

The dramatic increase of the glass transition temperatures in the BPEI:NaBPh<sub>4</sub> system with increasing salt concentration was further investigated with vibrational spectroscopic techniques. Infrared measurements in the mid-IR and far-IR regions, as well as Raman scattering experiments, were performed on the BPEI:NaBPh<sub>4</sub> 5:1 sample, as it has the highest glass transition temperature. In the mid-IR and far-IR, the

measurements were performed from 20°C to 100°C in 10°C increments; in the Raman experiments, data were collected from 0°C to 100°C, in 10°C increments, in a region from 1000 cm<sup>-1</sup> to 50 cm<sup>-1</sup>. However, none of the spectra revealed any changes in the polymer backbone vibrations and the NH stretching vibrations upon crossing the glass transition temperature. Segmental motion of a polymer starts to occur in the vicinity of the glass transition temperature and increases with increasing temperature. In BPEI, segmental motion consists of torsional bending motions around the C – C and C – N bonds, presumably in both the backbone and side-chains. Below the glass transition temperature, the polymer chains exist in a variety of energetically favorable conformations, but they are “frozen” in place in the sense that there is no thermally driven change of local conformation. A spectroscopic measurement sees the distribution of “frozen” conformations. Above T<sub>g</sub>, the polymer segments have sufficient thermal energy to visit a variety of energetically favorable conformations. In a typical polymer electrolyte, segmental motion occurs at about 1GHz at room temperature, which is approximately 10<sup>3</sup> – 10<sup>5</sup> slower than the vibrations that are measured using infrared and Raman spectroscopy.<sup>12,13</sup> Therefore a vibrational measurement provides a static snapshot of the distribution now available to the polymer segments. The failure to observe any spectral changes as the sample passes through T<sub>g</sub> argues that the “frozen” population distribution below T<sub>g</sub> is essentially the ensemble average of the populations in dynamic equilibrium above T<sub>g</sub>.

### 5.3.3. Ionic conductivity

Conductivities of BPEI:NaTf and BPEI:NaBPh<sub>4</sub> were measured from room temperature to 80°C in increments of 10°C. A second set of measurements was performed after allowing the samples to cool over night. No hysteresis was observed in the conductivity behavior. The samples were examined for water using IR spectroscopy. Those samples that were found to be contaminated with water during the measurement process exhibited higher conductivity values, and these measurements were discarded. The resulting conductivity values for BPEI:NaTf and BPEI:NaBPh<sub>4</sub> complexes are plotted in Figure 5.15.

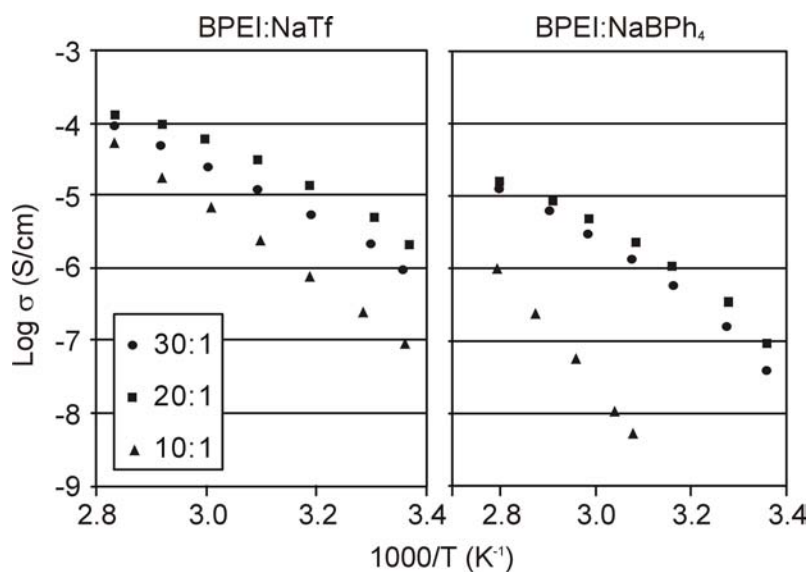


**Figure 5.15.** Temperature-dependant conductivity data of BPEI at various compositions of NaTf and NaBPh<sub>4</sub> (30:1, 20:1, 10:1).

The 20:1 composition for both polymer-salt complexes shows the highest conductivity, which results from the expected conductivity maximum in a plot of conductivity as a function of salt concentration. It is noteworthy that the conductivities of the BPEI:NaTf complexes are significantly higher than the conductivities of the

BPEI:NaBPh<sub>4</sub> complexes at all comparable compositions and temperatures, consistent with the observation that at comparable salt concentrations the glass transition temperature of BPEI:NaTf is markedly lower than that of BPEI:NaBPh<sub>4</sub>.

#### 5.4. CONCLUSIONS

The study of high molecular weight polymers can be greatly aided by comparative studies of small molecules that structurally and functionally mimic parts of the polymer chain. This is a particularly effective strategy to study ionic coordination in polymers when both the small molecules and the polymer have functional groups that coordinate ions in a similar manner. HEXA, DMEDA, and DPA were used to model the primary and secondary amine groups of branched poly(ethylenimine). HEXA and DMEDA were particularly useful to study hydrogen bonding interactions and the cation inductive effect accompanying the dissolution of LiTf. Extensive comparisons established that the hydrogen bonding interactions in BPEI were significantly stronger than in HEXA, and the spectroscopic behavior of the NH<sub>2</sub> group in BPEI is very similar to that of DMEDA. The presence of intramolecular hydrogen bonding interactions in the BPEI and DMEDA systems greatly complicates the analysis of the spectra. However, the occurrence of similar interactions in DMEDA and BPEI makes the DMEDA molecule a better model compound for the polymer. The strength of the cation interaction with the amine groups was smaller in BPEI and DMEDA compare to HEXA, possibly reflecting the tendency towards stronger hydrogen bond formation in former systems.

The situation is more complicated for the NH<sub>2</sub> bending mode. The comparison of the  $\delta(\text{NH}_2)$  frequencies in BPEI, DMEDA, and HEXA, as well as the shifts occurring

with addition of LiTf are difficult to explain. The mixing of this mode with other intramolecular motions, and the present inability to understand how the coordination of the cation affects this vibration renders the analysis of this mode very complex.

The comparison of the spectroscopic, conductivity, and calorimetric data of the BPEI:NaTf and BPEI:LiTf complexes shows only small differences between the two complexes, which most likely can be attributed to the higher charge density of the lithium cation. The conductivity data for both complexes are very similar to those previously published by Harris et al.<sup>10</sup> and Paul et al.<sup>2</sup>, and confirms that the highest conductivity value is obtained for a nitrogen to cation ratio of 20:1 and is on the order of  $10^{-6}$  S cm<sup>-1</sup> at 25°C.

The comparison of the spectroscopic, conductivity, and calorimetric data of the BPEI:NaTf and BPEI:NaBPh<sub>4</sub> complexes indicates an important difference in the nature of the cation-polymer interactions in the two complexes. The consistently higher values of the glass transition temperatures in the BPEI:NaBPh<sub>4</sub> complexes along with the greater frequency shifts of the BPEI backbone modes clearly indicates that the sodium ions interact more strongly with the amine nitrogen atoms in the BPEI:NaBPh<sub>4</sub> complexes.

The conductivity data for the NaTf complexes are consistently higher than those of the NaBPh<sub>4</sub> complexes, in spite of the fact that the BPh<sub>4</sub><sup>-</sup> anion does not undergo significant cation-anion interactions as occurs in the NaTf system. It is important to note that in almost all polymer-salt systems studied to date, the transference number of the anion is markedly larger than that of the cation, i.e. these systems are primarily anionic

conductors. Therefore, the relatively lower conductivity in BPEI:NaBPh<sub>4</sub> may result from a lower mobility of the bulky BPh<sub>4</sub><sup>-</sup> ion as compared with the Tf ion.

The spectroscopic comparison of BPEI:NaBPh<sub>4</sub> with BPEI:NaTf in the NH stretching region provides an opportunity to examine the relative importance of hydrogen bonding and the inductive effect. The following discussion is schematically illustrated in Figure 5.16.

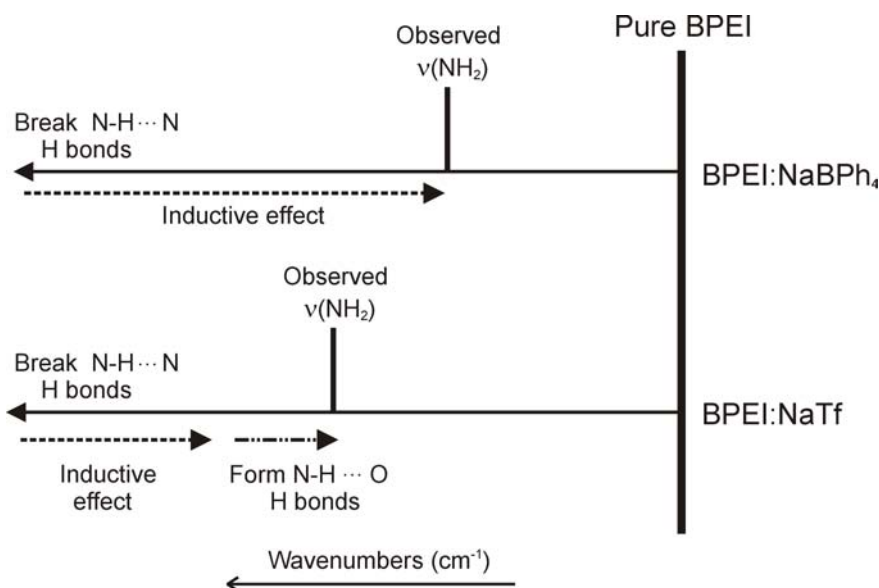


**Figure 5.16.** Schematic representation of hydrogen bonding and inductive effects on the  $\nu_s(\text{NH}_2)$  and  $\nu_{as}(\text{NH}_2)$  frequencies in BPEI:NaTf and BPEI:NaBPh<sub>4</sub> complexes.

The breaking of N–H...N hydrogen bonds by coordination with the cation occurs to the same extent in both complexes at a given composition as indicated by the left arrow for each complex which represents the accompanying frequency increase. The inductive effect of the sodium ion is larger in the BPEI:NaBPh<sub>4</sub> complex, which leads to a larger decrease in the NH stretching frequency. In the BPEI:NaTf complex, the replacement of N–H...N hydrogen bonds by weaker N–H...O hydrogen bonds leads to an additional small decrease in the N–H stretching frequency. However this additional

decrease is not sufficient to compensate for the significantly larger inductive decrease occurring in the BPEI:NaBPh<sub>4</sub> complex.

Finally, the addition of sodium tetraphenylborate shows that the CN stretch of the primary amines is more affected by coordination with the cation than the CN stretch of the secondary amines. This observation, along with previous studies suggests that the cation preferentially coordinates to the primary amine nitrogen rather than the secondary amine nitrogen.

## 5.5. REFERENCES

- (1) Colthup, N. B.; Daly, L. H.; Wiberley, S. E. *Introduction to Infrared and Raman Spectroscopy*, Third ed.; Academic Press, Inc.: San Diego, 1990.
- (2) Paul, J.-L.; Jegat, C.; Lassègues, J.-C. *Electrochim. Acta* **1992**, *37*, 1623.
- (3) Pimental, G. C.; McClellan, A. L. *The Hydrogen Bond*; W.H. Freeman: San Francisco, 1960.
- (4) Jeffrey, G. A. *An Introduction to Hydrogen Bonding*; Oxford University Press: New York, 1997.
- (5) Wolff, H.; Gamer, G. *J. Phys. Chem.* **1972**, *76*, 871.
- (6) Sharpe, A. N.; Walker, S. *J. Chem. Soc. (London)* **1961**, 2974.
- (7) Bonner, T. G.; Hancock, R. A. *Chem. Ind. - London* **1965**, *6*, 267.
- (8) Collins. *Chem. Ind. - London* **1957**, 704.
- (9) Jones, E. N.; Lautenberger, W. J.; Willermet, P. A.; Miller, J. G. *J. Am. Chem. Soc.* **1969**, *92*, 2946.
- (10) Harris, C. S.; Ratner, M. A.; Shriver, D. F. *Macromolecules* **1987**, *20*, 1778.
- (11) Stewart, J. E. *J. Chem. Phys.* **1959**, *30*, 1259.
- (12) Ansari, S. M.; Brodwin, M. *Solid State Ionics* **1985**, *17*, 101.
- (13) Shriver, D. F.; Papke, B. L.; Ratner, M. A.; Dupon, R. W.; Wong, T. T.; Brodwin, M. E. *Solid States Ionics* **1981**, *5*, 83.
- (14) York, S.; Frech, R.; Snow, A.; Glatzhofer, D. *Electrochim. Acta* **2001**, *46*, 1533.
- (15) York, S.; Boesch, S. E.; Wheeler, R. A.; Frech, R. *PhysChemComm.* **2002**, 99.

## 6. BRANCHED POLY(METHYLETHYLENIMINE)

Branched poly(methylethylenimine), BPMEI, is a methyl-substituted derivative of branched poly(ethylenimine), BPEI. There has been no previous study on BPMEI systems therefore a thorough investigation is necessary. Branched poly(methylethylenimine) was complexed with LiTf and investigated using infrared spectroscopy, differential scanning calorimetry (DSC), and complex impedance spectroscopy. Similar to the linear and branched PEI systems, there is a linear form of the methylated polymer, linear poly(methylethylenimine), LPMEI, that has been previously studied with LiTf and NaTf.<sup>1,2</sup> The interactions of LPMEI with these salts has been modeled by solutions of N,N,N',N',N''-pentamethyldiethylenetriamine (PMDETA) with the same salt.<sup>3,4</sup> Furthermore, strong similarities between the spectra of PMDETA, low molecular weight linear PMEI, and high molecular weight linear PMEI, and the recognition of similar spectral signatures in BPMEI significantly helps assignments in BPMEI systems.

### 6.1. THERMAL ANALYSIS

The glass transition temperature ( $T_g$ ) of BPMEI and BPMEI with various compositions of LiTf are reported as midpoint temperatures and summarized in Table 6.1, along with the  $T_g$  values for the LPMEI and LPMEI – LiTf complexes.<sup>1,2</sup> BPMEI and LPMEI are fully amorphous polymers that have very similar  $T_g$  values. When salt is added, the  $T_g$  rises in both systems to reach very similar values at a 20:1 composition. Above this salt concentration, the difference between the two systems starts to appear. In the branched polymer, the  $T_g$  rises more rapidly to reach +13°C at a 5:1 composition,

with a corresponding value of -14°C in the linear complex. Upon addition of salt, the coordination of the lithium cation to the nitrogen atoms hinders the flexibility of the polymer chains, therefore increasing the  $T_g$  values. In the branched polymer, the lithium – nitrogen coordination is stronger, and segmental motion must be reduced to a higher degree than in the linear form, especially at high salt concentrations. It should be noted that all spectroscopic measurements were made above the  $T_g$  values for all samples.

**Table 6.1.** Glass transition temperatures  $T_g$  (°C) (midpoints) of BPMEI and LPMEI with their LiTf complexes at various nitrogen:lithium ratios.

Composition N:M	BPMEI:LiTf	LPMEI:LiTf
Pure	-91	-93
30:1	-88	
20:1	-81	-79
15:1	-43	
10:1	-18	-60
5:1	13	-14

## 6.2. SPECTROSCOPIC ANALYSIS

### 6.2.1. Room temperature study

*Comparison of the spectroscopic features in BPMEI and LPMEI.* The infrared spectra of BPMEI and LPMEI are shown in Figure 6.1 in the 1000 to 1500  $\text{cm}^{-1}$  region, along with the infrared spectra of the low molecular weight PMEI (~550 MW) and pentamethyldiethylenetriamine (PMDETA), a low molecular weight model compound for the two linear PMEI polymers.<sup>3-5</sup>

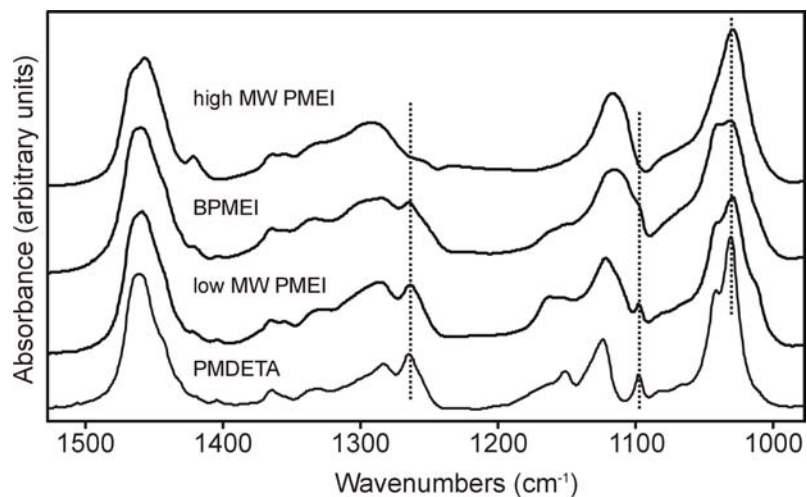


**Figure 6.1.** IR spectra of PMDETA, low MW PMEI, and high MW BPMEI and LPMEI in the 1000 – 1500  $\text{cm}^{-1}$  region.

Only a few, but nevertheless important differences can be noticed. The first dissimilarity lies in the band at  $1265 \text{ cm}^{-1}$ , present in the branched polymer, the low molecular weight PMEI, and PMDETA, but not in the high molecular weight linear form. In the region between 1000 and  $1200 \text{ cm}^{-1}$ , many more bands are present in BPMEI, low MW PMEI and PMDETA that are not present in LPMEI. In this region, there is a broad distribution of bands that are assigned to  $\text{CH}_2$  rocking and twisting, C-C and C-N stretching, and  $\text{CH}_3$  wagging motions. The C-C and C-N stretching motions play an important role below  $\sim 1070 \text{ cm}^{-1}$ , whereas the  $\text{CH}_2$  twisting and  $\text{CH}_3$  wagging motions are important above  $1070 \text{ cm}^{-1}$ .<sup>5,6</sup> For example, high MW LPMEI only has one band at  $1029 \text{ cm}^{-1}$ . In all the other systems, this band is shifted 1 to  $3 \text{ cm}^{-1}$  to higher frequencies, and the spectra contain an additional overlapping band around  $1042 \text{ cm}^{-1}$ . In BPMEI, both bands have similar intensities, while in low MW PMEI and PMDETA, the  $1042 \text{ cm}^{-1}$  band has a much smaller intensity compare to the lower frequency band. All those differences can be attributed to the presence of  $\text{N}-(\text{CH}_3)_2$  tertiary amine groups in the

branched polymer, which are not present in the high MW linear form. In the low MW polymer, the significant amount of end groups brings a substantial contribution from the vibrations of the N-(CH<sub>3</sub>)<sub>2</sub> tertiary amine groups. In PMDETA, the breadth of the bands is significantly smaller than in all the polymers, and is due to a more homogeneous distribution of the potential energy environment compared to that of highly disordered polymers.

The spectra of the four molecules in the conformation region (750 to 1000 cm<sup>-1</sup>) are presented in Figure 6.2. Modes in this region are comprised mainly of CH<sub>2</sub> rocking and C-N stretching motions based on computations of PMDETA.<sup>3,5</sup> In the 750 to 830 cm<sup>-1</sup> region, there is a broad distribution of bands in all the spectra. The band intensities and frequencies in the branched PMEI spectrum appear very similar to those of PMDETA; likewise, high MW PMEI and low MW PMEI have very similar band structure in this part of the spectrum. It seems that bands that are very weak in PMDETA and BPMEI have stronger intensities in high and low MW PMEI, and vice versa. In the region between 830 and 860 cm<sup>-1</sup>, two bands are present in all the spectra, except in the high MW LPMEI, where the two bands have significantly smaller intensities. The bands at 834 and 859 cm<sup>-1</sup> in PMEDTA markedly shift to higher frequencies as the chain length increases. In all the polymers, these bands have very similar intensities, and are closer in frequency: 844 and 859 cm<sup>-1</sup> in low MW PMEI, 843 and 858 cm<sup>-1</sup> in high MW PMEI, and 846 and 858 cm<sup>-1</sup> in BPMEI. Again, in PMDETA, the band structure is more resolved, and the conformations peaks more intense due to the homogeneity of the sample. In addition, the band at 938 cm<sup>-1</sup> in the BPMEI spectrum has similar bandwidth,

intensity, and asymmetry as the corresponding bands in the high and low MW PMEI, and PMDETA (939, 938, 937  $\text{cm}^{-1}$ , respectively).

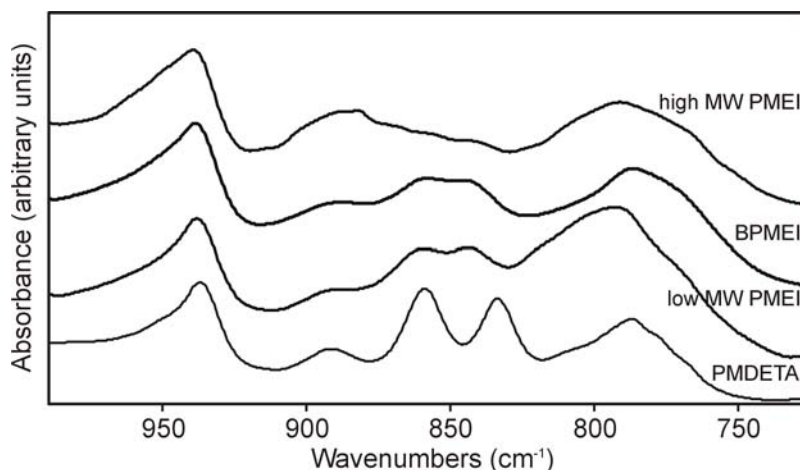


**Figure 6.2.** IR spectra of PMDETA, low MW PMEI, and high MW BPMEI and LPMEI in the 735 – 1000  $\text{cm}^{-1}$  region.

When comparing the different spectral regions of BPMEI, LPMEI, and low MW PMEI, it is quite clear that the low MW PMEI is a very good model for BPMEI. There are only very few dissimilarities between their spectra. The low MW PMEI has in average about 10 repeat units per chain, but a distribution of chain length occurs in the system. The presence of a significant number of  $\text{N}-(\text{CH}_3)_2$  tertiary amine end groups brings significant changes to the spectra, as seen when comparing with the high MW LPMEI, where the end groups are insignificant.

***BPMEI – LiTf and LPMEI – LiTf complexes.*** When LiTf is added to BPMEI and LPMEI, the changes that occur in the spectra are similar in the two hosts as illustrated in Figure 6.3. These changes include the disappearance of bands, the appearance of new bands, and the narrowing of bandwidths. For example, when LiTf is

added to BPMEI, two overlapping bands grow around 776 and 784  $\text{cm}^{-1}$ . In a similar manner, two predominant bands start to grow in LPMEI, with a few more small bands at higher frequencies. Another striking change that occurs with addition of LiTf is the decrease of the two BPMEI bands at 846 and 858  $\text{cm}^{-1}$ . A similar behavior occurs in the LPMEI system, but the effect is not as important because the corresponding bands at 843 and 858  $\text{cm}^{-1}$  have much lower intensities in the spectrum of the pure polymer. In the 900 – 1000  $\text{cm}^{-1}$  region, the bands are primarily a mixture of C-N and C-C stretching, and  $\text{CH}_2$  rocking motions (determined from PMDETA – LiTf calculations).<sup>5</sup> Upon addition of LiTf to BPMEI, a shoulder starts to grow on the high frequency side of the band at 939  $\text{cm}^{-1}$ . In contrast, when LiTf is added to LPMEI, no changes occur until the 5:1 composition, where a little band appears around 955  $\text{cm}^{-1}$ .

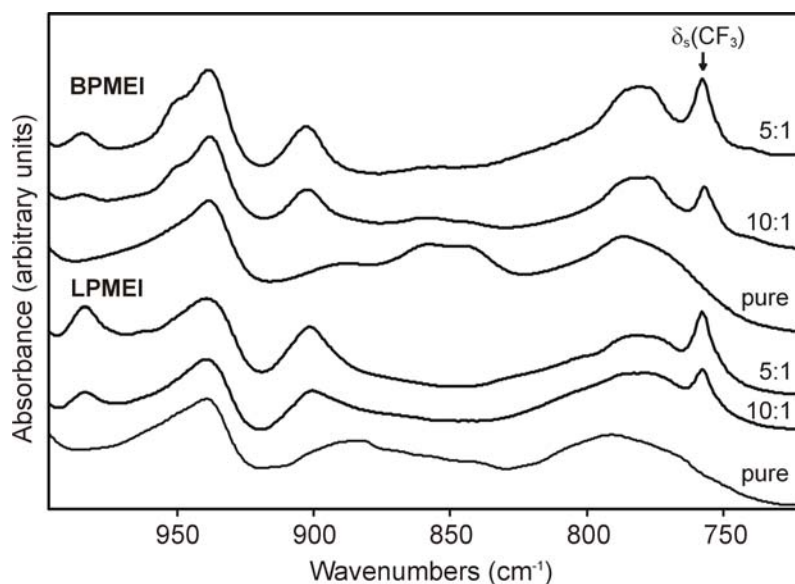


**Figure 6.3.** IR spectra of high MW BPMEI and LPMEI and their LiTf complexes ( $\text{N}:\text{Li}^+ = 10:1$  and  $5:1$ ) in the 735 – 1000  $\text{cm}^{-1}$  region.

Figure 6.4 shows the spectra of BPMEI and LPMEI complexed with LiTf in the 1000 – 1400  $\text{cm}^{-1}$  region. In the 1000 – 1200  $\text{cm}^{-1}$  region, the addition of salt alters the

nature of several polymer modes, as seen in the lower frequency region (Figure 6.3). In BPMEI and LPMEI, the intensity of the bands at 1115 and 1117  $\text{cm}^{-1}$ , respectively, significantly decreases. In LPMEI, a small band starts to grow at 1096  $\text{cm}^{-1}$  upon addition of LiTf, while the band at 1117  $\text{cm}^{-1}$  has almost disappeared in the 5:1 sample. In BPMEI – LiTf 5:1, only a small band remains at 1102  $\text{cm}^{-1}$ ; it is not clear if this band originates from the band at 1115  $\text{cm}^{-1}$ , from the low frequency shoulder at 1099  $\text{cm}^{-1}$ , or if it is a new band. The region from 1025 to 1050  $\text{cm}^{-1}$  is complicated by the presence of bands originating from the  $\text{SO}_3$  symmetric stretching vibration of the triflate ion.

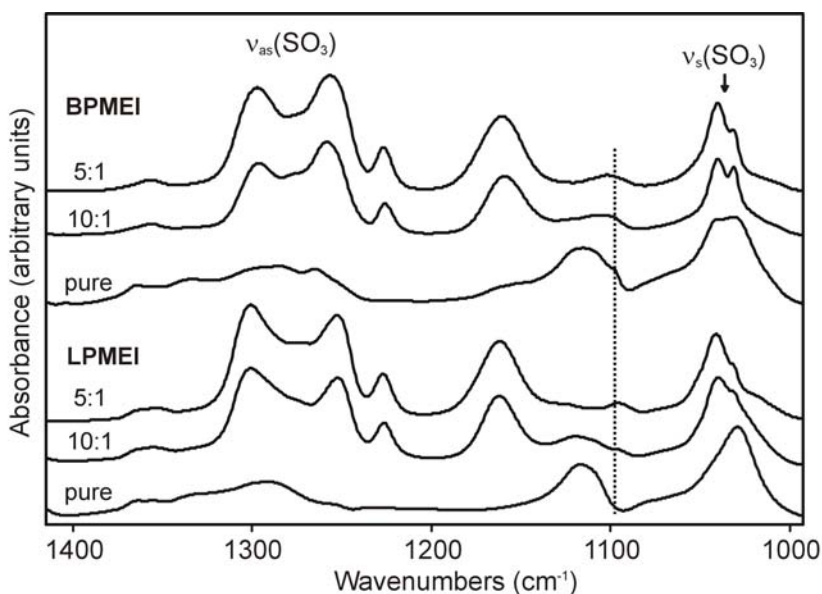


**Figure 6.4.** IR spectra of high MW BPMEI and LPMEI and their LiTf complexes ( $\text{N}:\text{Li}^+ = 10:1$  and  $5:1$ ) in the  $1000 - 1400 \text{ cm}^{-1}$  region.

***Ionic association region.*** In BPMEI - LiTf, the  $\nu_s(\text{SO}_3)$  band overlaps with BPMEI bands, which greatly complicates the deconvolution of this peak. On the other hand, the results from the  $\delta_s(\text{CF}_3)$  and the  $\nu_{as}(\text{SO}_3)$  regions are very clear; the data are summarized in Table 6.2. Based on the analysis of the  $\delta_s(\text{CF}_3)$  region, the contact ion pairs are the dominant species present at all salt concentrations. At low LiTf

compositions, contact ion pairs (756 – 758 cm<sup>-1</sup>) and “free” ions (752 cm<sup>-1</sup>) are present. When the salt composition reaches 5:1, aggregate species start to form, while the relative amount of “free” ions decreases. Also shown in the table is the splitting of the SO<sub>3</sub> antisymmetric stretching mode,  $\Delta v_{\text{as}}(\text{SO}_3)$ , which originates in the breaking of the two-fold degeneracy of the  $v_{\text{as}}(\text{SO}_3)$  mode through the lithium ion - triflate ion interactions (Figure 6.4). The increase in  $\Delta v_{\text{as}}(\text{SO}_3)$  reflects the growing importance of ion pair interactions with increasing salt concentration, and the accompanying decrease in the strength of the lithium ion - nitrogen atom interactions. Similar trends occur in the LPMEI – LiTf system (Table 6.3), except that the aggregate species appear at lower salt concentrations (15:1). Upon addition of salt, the relative amount of aggregate increases, while the relative amount of “free” and contact ion pair decreases. In the  $v_{\text{as}}(\text{SO}_3)$  region, the bands are split further than in the BPMEI system at all salt concentrations, in agreement with the higher degree of ionic association in LPMEI compared to BPMEI, and the stronger lithium – nitrogen coordination in the branched polymer.

**Table 6.2.** Band center frequencies (cm<sup>-1</sup>) in the  $\delta_s(\text{CF}_3)$  region and splitting of  $v_{\text{as}}(\text{SO}_3)$  for BPMEI:LiTf.

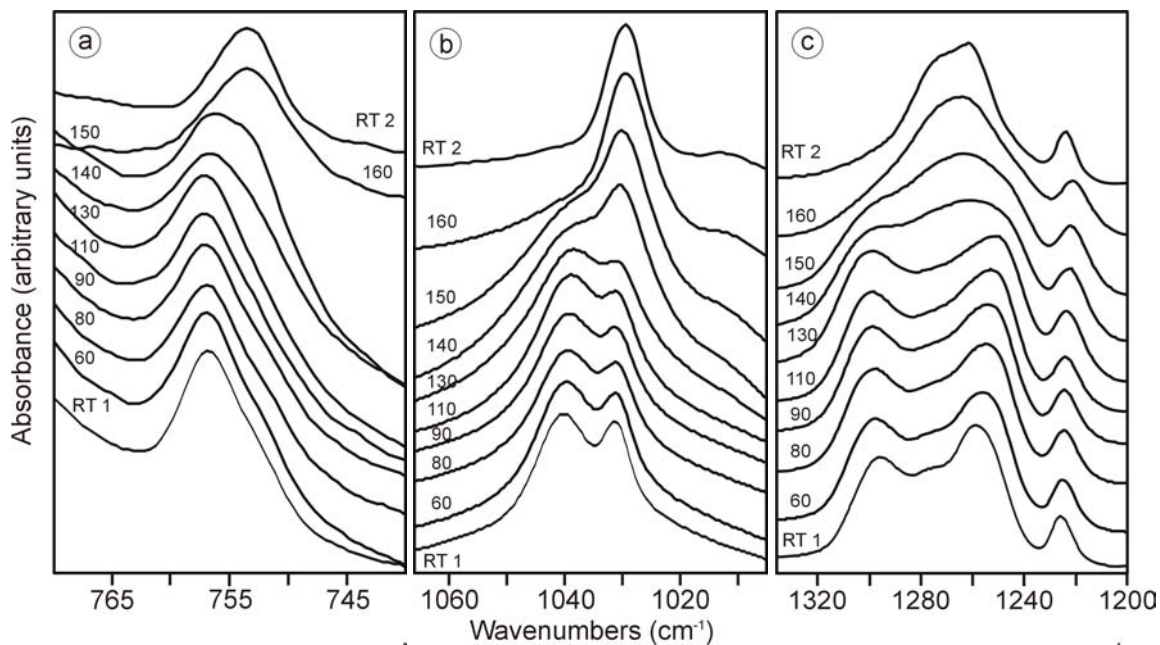
Composition	$\Delta v_{\text{as}}(\text{SO}_3)$	$\delta_s(\text{CF}_3)$		
		Aggregate	Pair	“Free”
20:1	35		756 (78%)	752 (22%)
10:1	37		757 (78%)	752 (22%)
5:1	40	762 (6%)	758 (81%)	752 (13%)

**Table 6.3.** Band center frequencies ( $\text{cm}^{-1}$ ) in the  $\delta_s(\text{CF}_3)$  region for LPMEI:LiTf.<sup>1</sup>

Composition	$\Delta\nu_{\text{as}}(\text{SO}_3)$	$\delta_s(\text{CF}_3)$		
		Aggregate	Pair	“Free”
20:1	46		757 (64%)	752 (36%)
15:1	48	762 (12%)	758 (61%)	752 (27%)
10:1	49	762 (14%)	758 (60%)	752 (26%)
5:1	49	761 (20%)	758 (56%)	752 (24%)

### 6.2.2. Temperature dependence study

There is a very interesting temperature effect that occurs in the infrared spectra of BPMEI – LiTf. These findings had previously been observed in the infrared spectra of LPMEI and poly(ethylethylenimine) (PEEI) complexed with LiTf.<sup>2</sup> In the first heating cycle, the temperature was raised at a rate of  $10^\circ\text{C}$  per hour until  $160^\circ\text{C}$ , while the spectra were recorded every  $10^\circ\text{C}$  increments. The sample was then cooled down to room temperature and left for about 24 hours. The heating cycle was then repeated. Figures 6.5a, 5b, and 5c illustrate the results of subsequent heating and cooling cycles on a 10:1 BPMEI – LiTf sample.



**Figures 6.5.** Temperature dependence IR spectra of BPMEI – LiTf 10:1 from room temperature to 160°C, and then back to room temperature; **a.** In the  $\delta_s(\text{CF}_3)$  region, **b.** In the  $\nu_s(\text{SO}_3)$  region, **c.** In the  $\nu_{as}(\text{SO}_3)$  region.

During the first heating cycle, the only difference between the room temperature spectrum and the spectrum at 160°C is the change in the ionic association of the triflate anion. In the  $\delta_s(\text{CF}_3)$  region, peak deconvolution established the presence of ion pair (757  $\text{cm}^{-1}$ , 78%) and “free” ions (752  $\text{cm}^{-1}$ , 22%) at room temperature (Table 6.2). At 160°C, the concentration in “free” ions is increased dramatically at the detriment of the contact ion pairs as seen in Figure 6.5a; unfortunately, curve fitting analysis did not converge. In the  $\nu_s(\text{SO}_3)$  region (Figure 6.5b), similar observations can be made, although peak deconvolution is not possible due to the presence of polymer bands. At room temperature, two peaks of similar intensities occur at 1040 and 1031  $\text{cm}^{-1}$ . When the sample reaches a temperature between 140 and 150°C, the band at 1040  $\text{cm}^{-1}$  decreases dramatically in intensity, while the other peak at 1031  $\text{cm}^{-1}$  remains unchanged.

The spectra of the  $\nu_{\text{as}}(\text{SO}_3)$  region, shown in Figure 6.5c, are consistent with the trends observed in the  $\delta_{\text{s}}(\text{CF}_3)$  and  $\nu_{\text{s}}(\text{SO}_3)$  regions. In the first room temperature spectrum, the strength of the lithium – triflate interaction is sufficient to break the double degeneracy of the mode and yield two main components at 1296 and 1259  $\text{cm}^{-1}$ . Upon increasing the temperature, the two large bands start to split further apart, to reach 1299 and 1251  $\text{cm}^{-1}$  at 130°C. When the temperature reaches 140°C, the two main bands start to merge closer together, and eventually, only one broad band remains centered at 1264  $\text{cm}^{-1}$  at 160°C. After the first heating cycle has been completed and the sample returned to room temperature for about 24 hours, a more defined band structure reappears to leave one band at 1262  $\text{cm}^{-1}$ , with a shoulder around 1273  $\text{cm}^{-1}$ .

The analysis of the triflate bands clearly shows that the strength of the cation – anion interactions has been greatly reduced by the thermal treatment. It is unexpected that none of the BPMEI bands are affected by the thermal cycling. Generally, a change of the nature of ion – ion interactions involves a change of the cation – polymer coordination, which results in changes of the polymer bands involving motions of the heteroatom to which the cation is coordinated. Temperature dependence studies on poly(ethylene oxide) and poly(propylene oxide) polymer electrolytes have shown that upon increasing the temperature, the ionic association shifts from “free” ions and contact ion pairs to the more associated species such as triple cations. Eventually, the salt precipitates out at increasing temperatures.<sup>7-11</sup>

To further this investigation, differential scanning calorimetry was performed on a BPMEI – LiTf 10:1 sample. The sample was cycled three times, with the first two cycles from room temperature to -70°C and then to 25°C. The next cycle was from 25 to 200°C,

then down to  $-70^{\circ}\text{C}$  and back to room temperature. In the first two heating periods, the glass transition temperature is observed at  $-18^{\circ}\text{C}$ . In the third cycle, upon heating the sample, an exothermic transition slowly appears starting around  $160^{\circ}\text{C}$ . In the following heating period, the glass transition temperature is at  $-11^{\circ}\text{C}$ . After the DSC experiment, part of the sample appeared slightly darker in color, and part of the sample appeared black. IR spectroscopy on the darkened material (avoiding the black material) revealed no changes compared to a sample that did not undergo the thermal treatment. IR spectroscopy on the black material showed a large band around  $1670\text{ cm}^{-1}$  and a decrease of the intensity of the polymer bands. The triflate bands in this material are located between those of the sample with no thermal treatment and the sample taken to  $160^{\circ}\text{C}$  in the IR. The appearance of the transition around  $160^{\circ}\text{C}$  probably comes from the degradation of the polymer host, leading to the formation of the black material.

### **6.3. IONIC CONDUCTIVITY**

First, the reproducibility of the conductivity data was checked by cycling the sample between room temperature and  $80^{\circ}\text{C}$  at least three times, collecting data at room temperature and  $80^{\circ}\text{C}$  only. Then data were collected in a heating cycle ranging from room temperature to  $160^{\circ}\text{C}$  in  $20^{\circ}\text{C}$  increments. Finally, measurements at room temperature and  $160^{\circ}\text{C}$  were repeated. No hysteresis was observed in the conductivity behavior. The resulting conductivity values for BPMEI with various composition of LiTf are plotted in Figure 6.6.

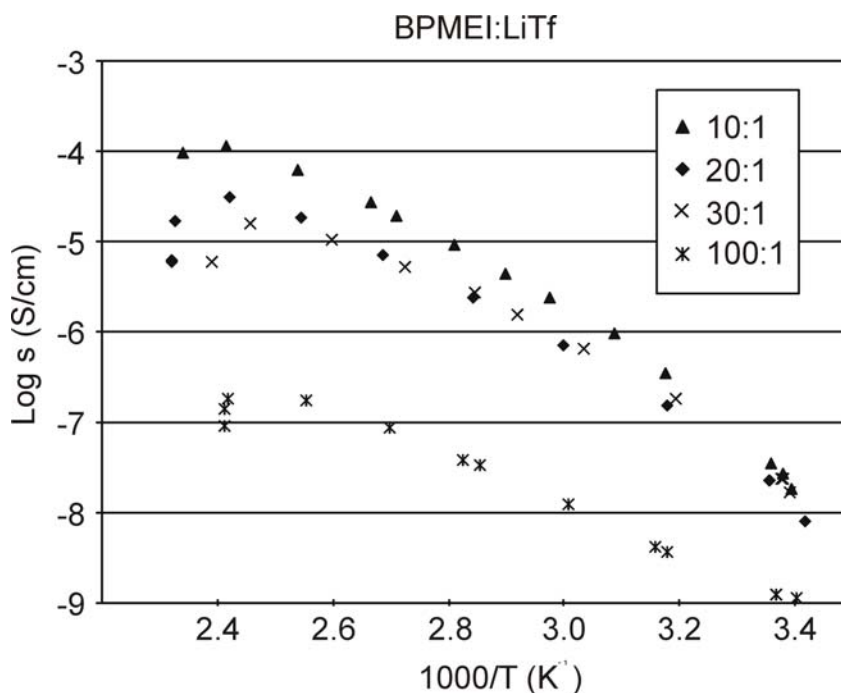


**Figure 6.6.** Temperature-dependent conductivity data of BPMEI at various compositions of LiTf.

The 10:1 composition shows the highest conductivity values at all temperatures. At this composition, contact ion pairs dominate the system, based on the curve-fitting analysis of the  $\delta_s(\text{CF}_3)$  region (Table 6.2). Surprisingly, the ionic conduction of the 20:1 composition is lower than that of the 10:1 composition, even though the ionic speciation is the same for both compositions, and the glass transition temperature is much higher in the 10:1 sample ( $-88^\circ\text{C}$  at a 20:1 vs.  $-18^\circ\text{C}$  at a 10:1 composition), which indicates a much stronger lithium - nitrogen coordination. Furthermore, for all salt compositions, the ionic conductivity suddenly drops when the temperature reaches about  $140^\circ\text{C}$ . This transition may be associated with the change in the ionic speciation of the 10:1 sample that starts to occur around  $140^\circ\text{C}$ , as described in a previous paragraph. It is possible that this drop of the ionic conductivity values with temperature corresponds with a degradation of the polymer host. As was found for the DSC sample, part of the sample

was black, and part of the sample was slightly darker in color. The IR spectra of the discolored part revealed no changes compare to a 10:1 sample that did not undergo any thermal treatment, while the IR spectra of the blackened material compared very well to the IR of the blackened material after the DSC treatment.

#### 6.4. CONCLUSIONS

PMDETA and low MW PMEI are better spectroscopic models for branched PMEI than for linear PMEI. In all the regions of the spectrum, the coincidence between the band frequencies is remarkable. The differences between the spectra of branched and linear PMEI results from the presence of  $N-(CH_3)_2$  terminal groups in BPMEI. These terminal groups are also present in PMDETA and low MW PMEI to a significant extent. Conversely, high MW PMEI has significantly longer chains and the number of end groups is negligible leading to very small contribution to the IR intensity.

In BPMEI - LiTf, the cation – nitrogen atom interaction is stronger than in LPMEI - LiTf, as seen by the more resolved band structure in the BPMEI – LiTf complexes compared to the LPMEI – LiTf complexes, and also because of the significantly higher glass transition temperature values for BPMEI – LiTf complexes. In BPMEI, the region of the links (or branching sites) provides a lot of coordinative sites that may facilitate the coordination of the cation. Moreover, if there are short side-chains connected to a long backbone chain the flexibility increases allowing the chains to adopt more conformations to coordinate to the cation.

In LPMEI, the ion – ion interactions are stronger than in BPMEI, as seen by the higher degree of ionic association in LPMEI, and also the larger splitting of the  $\nu_{as}(SO_3)$

mode. This may be simply due to the weaker cation – polymer interaction in the linear polymer, which is compensated by a stronger ion – ion interaction.

The temperature dependence data show that as the temperature increases, the nature of the ionic association shifts towards “free” ions, with no changes in the polymer backbone bands over the same temperature range. Differential scanning calorimetry data and conductivity data also show abrupt changes in the behavior of the electrolyte. These transitions may be related to a thermal decomposition of the polymer host at high temperatures.

## 6.5. REFERENCES

- (1) Sanders, R. A.; Snow, A. G.; Frech, R.; Glatzhofer, D. T. *Electrochim. Acta* **2003**, *48*, 2247.
- (2) Frech, R.; Giffin, G. A.; Castillo, F. Y.; Glatzhofer, D.; Eisenblatter, J. *Electrochim. acta* **2005**, *50*, 3963.
- (3) Sanders, R. A.; Frech, R.; Khan, M. A. *J. Phys. Chem. B* **2004**, *108*, 12729.
- (4) Sanders, R. A.; Boesch, S. E.; Snow, A. G.; Hu, L. R.; Frech, R.; Wheeler, R. A.; Glatzhofer, D. T. *Polym. Prepr.* **2003**, *44*, 996.
- (5) Sanders, R. A.; Boesch, S. E.; Snow, A. G.; Hu, L.; Frech, R.; Wheeler, R. A.; Glatzhofer, D. **To be submitted.**
- (6) Sanders, R. A.; Frech, R.; Khan, M. A. *J. Phys. Chem. B* **2003**, *107*, 8310.
- (7) Kakihana, M.; Schantz, S.; Torell, L. M. *Solid State Ionics* **1990**, *40/41*, 641.
- (8) Kakihana, M.; Shantz, S.; Torell, L. M. *J. Chem. Phys.* **1990**, *94*, 6271.
- (9) Sandner, B.; Tubke, J.; Wartwig, S.; Shashkov, S. *Solid State Ionics* **1996**, *83*, 87.
- (10) Greenbaum, S. G.; Pak, Y. S.; Wintersgill, M. C.; Fontanella, J. J. *Solid State Ionics* **1988**, *31*, 241.
- (11) Teeters, D.; Frech, R. *Solid State Ionics* **1986**, *18/19*, 271.